Dosimetric Properties and Radiation Hardness of the Storage Phosphor Europium Doped Potassium Chloride for Radiation Therapy Dosimetry

---

A dissertation presented
the faculty of the Graduate School
at the University of Missouri, Columbia

In partial fulfillment
of the requirements for the degree

Doctor of Philosophy

Joseph P. Driewer

H. Harold Li, PhD, Dissertation Supervisor
Sudarshan K. Loyalka, PhD, Academic Advisor

Columbia, MO, May 2011

The undersigned, appointed by the dean of the Graduate School, have examined the dissertation entitled

Dosimetric Properties and Radiation Hardness of the Storage Phosphor Europium Doped Potassium Chloride for Radiation Therapy Dosimetry

presented by Joseph P. Driewer, a candidate for the degree of doctor of philosophy, and hereby certify that, in their opinion, it is worthy of acceptance.

Professor H. Harold Li, Chair

Professor Sudarshan K. Loyalka

Professor Tushar K. Ghosh

Professor Ping Yu

Professor William H. Miller

Professor Mark A. Prelas

Professor Daniel A. Low

To my Ladies—

first to my beautiful bride,

Nicole,

and then to our four wonderful daughters,

Margaret, Isabelle, Lucille, and Lydia.

ACKNOWLEDGEMENTS

I am deeply grateful to my supervisor and advisor, Dr. Harold Li, for bringing me on board in his lab at the Washington University School of Medicine. I will always appreciate his guidance and abundant support during my studies as well as his vision for radiation physics research. I am confident that he will remain a trusted advisor during my future development.

Dr. Sudarshan Loyalka, Dr. William Miller, Dr. Tushar Ghosh, and Dr. Mark Prelas, all committee members, were extremely supportive during my years of study at the Nuclear Science and Engineering Institute of the University of Missouri. I sincerely thank them for giving a would-be philosopher a chance to find and pursue his real passion. I also thank Dr. Ping Yu (MU Physics) for his guidance as an outside committee member and Dr. Daniel Low for giving his full support to this project and maintaining his committee status, even from a distance (UCLA).

I have had the privilege of working with three fine postdoctoral researchers during this study: Dr. Zhaohui Han, Dr. Baozhou Sun, and Dr. Haijian Chen. I was able to lean on their practical and theoretical knowledge many times and I wish them all the best in their medical physics careers. In particular, I thank Dr. Chen for providing helpful comments on a draft of this work.

Dr. Buck Rogers, Dr. Girdhar Sharma, and Dr. Dinesh Thotala of the Washington University School of Medicine Department of Radiation Oncology Cancer Biology Division generously coordinated the use of and provided access to the ^{137}Cs irradiator used in this study. Dr. Andres Osvet performed the lifetime measurements at his lab in Erlangen, Germany.

This work has been supported in part by the Nuclear Science and Engineering Institute of the University of Missouri through a Graduate Assistance in Areas of National Need fellowship funded by the Department of Education and NIH Grant Nos. R21CA131690 and R01CA148853. So far, it has resulted in the publication of two papers, which will be

cited frequently throughout the study, and the submission of a third. Excerpts from the published papers were used with permission.

- Z. Han, J. P. Driewer, Y. Zheng, D. A. Low and H. H. Li, "Quantitative megavoltage radiation therapy dosimetry using the storage phosphor KCl:Eu^{2+}," Medical Physics 36, 3748-3757 (2009).

- Y. Zheng, Z. Han, J. P. Driewer, D. A. Low and H. H. Li, "Theoretical and empirical investigations of KCl:Eu^{2+} for nearly water-equivalent radiotherapy dosimetry," Medical Physics 37, 146-153 (2010).

- J. P. Driewer, *et al.*, "Radiation hardness of the storage phosphor europium doped potassium chloride for radiation therapy dosimetry," submitted to Medical Physics (2011).

Finally, during my first year in Dr. Li's lab in St. Louis I was commuting from Columbia, MO. Jason and Kella Dohring, Ed and Judy Koehler, and Jim and Linda Armbrecht generously opened their homes to me while I was traveling back and forth. Without them my first year would have been much more difficult. These families are models of hospitality and I am grateful to them. Ed Koehler also deserves a special thank you for helping adapt the graphics in figure 2.2.

Contents

List of Figures

List of Tables

Nomenclature

Symbol	Meaning
PSL	Photostimulated Luminescence
PL	Photoluminescence
TLD	Thermoluminescence Dosimetry
OSLD	Optically Stimulated Luminescence Dosimetry
CR	Computed Radiography
IP	Imaging Plate (a.k.a CR plate)
SPF/P	Storage Phosphor Film/Plate (a.k.a IP)
PVD	Physical Vapor Deposition
SSD	Source to Surface Distance
MC	Monte Carlo
Z	Atomic number
Z_{eff}	Effective atomic number
F-center	Electron trapped at an anion vacancy
F'-center	Two electrons trapped at an anion vacancy
F^+-center	Anion vacancy
H-center	An interstitial halogen bound to a lattice halogen by a hole, i.e., a diatomic halogen ion, e.g. Br_2^-, occupying a single halogen, e.g. Br^-, site
M-center	Two adjacent F-centers
V_k-center	A hole trapped by a halogen ion
W	Generation efficiency (eV/$h\nu$)

DOSIMETRIC PROPERTIES AND RADIATION HARDNESS OF THE STORAGE PHOSPHOR EUROPIUM DOPED POTASSIUM CHLORIDE FOR RADIATION THERAPY DOSIMETRY

Joseph P. Driewer

H. Harold Li, PhD, Dissertation Supervisor

ABSTRACT

This work establishes the photostimulable phosphor KCl:Eu^{2+} as a next generation radiation therapy dosimetry material. Prototype chip dosimeters 6-7 mm in diameter and 1 mm thick were fabricated in-house according to well-developed materials science processes. Dosimetric properties were studied with a laboratory optical reader after irradiation by a linear accelerator. KCl:Eu^{2+} exhibited a characterizable dose response after irradiation from 0 to 800 cGy. Twelve hours after irradiation, the photostimulated luminescence (PSL) signal stabilized to 0.1% signal decrease/h. Sensitivity was independent of dose rate from 15 to 1000 cGy/min and also independent of beam energy for both open x ray and megavoltage electron fields. Over-response to low-energy scattered photons was comparable to radiographic film and was reduced by sandwiching the dosimeters between 0.3 mm thick lead foils during irradiation.

KCl:Eu^{2+} exhibited strong radiation hardness up to 5000 Gy. An initially supralinear dose response became linear with dose history. After 60 Gy, measured data fit a linear model with $R = 0.999$ and an average deviation of 1.3% with a maximum of 3.5% over 100-700 cGy. Linearity did not change significantly up to 5000 Gy history. Sensitivity increased out to 3000 Gy history and then declined to 90% of zero-dose history value at 5000 Gy. The PSL stimulation curve peaked at 560 nm for fresh dosimeters and showed a slight red shift with dose history, possibly due to the creation of large aggregate trap centers. PSL emission remained peaked at 420 nm and agreed well with the photoluminescence (PL) emission spectrum of the europium activator in the material. Luminescence lifetime remained constant at 1.2 μs with dose. These results indicate that the PSL process of

irradiation, energy storage, excitation, energy transfer, and excitation and relaxation of the activator remains stable with dose histories up to 5000 Gy and that the material could be reused up to 2500 times at 2 Gy per use, as in, for example, patient-specific intensity modulated radiation therapy (IMRT) quality assurance.

It is also demonstrated from theory that reducing the thickness of KCl:Eu^{2+} maximizes the water-equivalence of the dose response. Monte Carlo (MC) simulations were performed using BEAMnrcMP and DOSXYZnrc for KCl:Eu^{2+} panels from 1 μm to 1 mm thick. The generation efficiency, W, of prototype KCl:Eu^{2+} was used to estimate the sensitivity of micron-thick dosimeters and determined by comparing the sensitivity of a 150 μm thick KCl:Eu^{2+} two dimensional (2D) panel to a commercial $BaFBr_{0.85}I_{0.15}$:Eu^{2+}-based phosphor with a known W. Dose information was read out on a custom built, high-speed 2D optical scanner. MC simulations demonstrate that micron-thick KCl:Eu^{2+} films have a nearly water-equivalent dose response. W of KCl:Eu^{2+} was determined to be 157 eV/$h\nu$ and sub-millimeter spatial resolution was achieved for films 150 μm thick. It was determined that micron-scale films would generate over $10,000$ photoelectrons at the PMT photocathode for detection and amplification for delivered doses as low as a one cGy dose-to-water. In experiments, PSL was routinely achieved for thin vapor-deposited KCl:Eu^{2+} panels less than 10 μm. Signal stability measurements of thin panels revealed challenges related to moisture protection of this material that may be mitigated through the application of protective coating technologies.

In conclusion, KCl:Eu^{2+} is demonstrated to have many desirable properties for radiation therapy dosimetry. Thin panel KCl:Eu^{2+} dosimeters of micron-scale thicknesses would provide a nearly water-equivalent dose response. The results of this study provide a practical and theoretical knowledge base that supports future KCl:Eu^{2+} dosimetry research.

Chapter 1

Introduction to the Study

1.1 Motivation

Multidimensional reusable dosimeters are extremely important for characterizing the complex dose distributions associated with modern radiation therapy techniques, such as intensity modulated radiation therapy (IMRT) [1, 2]. Dosimeters ideally suited for the clinical tasks of beam commissioning or dose validation quality assurance would have the following properties: 1) reusability, 2) high sensitivity, 3) multidimensionality/high spatial resolution, 4) water equivalence, 5) linear or characterizable response, 6) signal stability, and 7) the ability to be integrated into phantoms (cf. [3]). However, current clinical dosimeters lack one or more of the seven properties. Ionization chambers, for instance, the gold standard for benchmark dosimetry measurements, provide only a single, volume-averaged dose measurement. Although multidimensional ionization chamber arrays are in wide use, they are limited to coarse spatial resolution measurements. Radiographic and radiochromic films, which are capable of high resolution measurements and, in the case of radiochromic films, water-equivalence, are not reusable. Quantitative dosimetry with these films requires the acquisition of a sensitometric curve each time a dosimetric measurement is made. This practice, however, is based on the assumption that each individual film has the same response as others in the batch. Electronic portal imagers are quick and convenient but not

water equivalent and are suitable only for single plane measurements perpendicular to the beam axis. In fact, none of the dosimeters currently in clinical use are ideally suited for the complex tasks of commissioning and quality assurance.

A recent advancement in megavoltage beam dosimetry came when Olch evaluated commercial $BaFBr_{0.85}I_{0.15}:Eu^{2+}$-based computed radiography (CR) plates for 2D dosimetry [4]. Functionally, CR plates rely on a mechanism of photostimulated luminescence (PSL) to yield dose information [4–11]. Irradiation of the material produces electron-hole pairs that are stored in metastable energy traps. The spatial distribution of these trapped charge carriers forms a two-dimensional (2D) "latent image," whose information can be read out by stimulating the trapped charge carriers to recombine and release PSL photons proportional to the locally deposited dose. Charges remaining trapped after readout can be "erased" with a bright, broadband light and the material can be used again in the same manner. Importantly, since CR plates are reusable they allow the physicist to establish and monitor the long-term properties and response of the plates. Olch found that the $BaFBr_{0.85}I_{0.15}:Eu^{2+}$ storage phosphor plate had many of the desirable properties mentioned above [4]. However, because the material has high atomic number components, there was a strong photon energy dependence at large fields and depths. An alternative material having the desirable properties of CR plates but with a reduced effective atomic number is desirable for radiation therapy.

Nanto *et al.* first observed PSL emission from europium doped potassium chloride ($KCl:Eu^{2+}$) that was exposed by a diagnostic x ray beam [12]. The magnitude of the signal was approximately one tenth that of $BaFBr_{0.85}I_{0.15}:Eu^{2+}$, due in part to the lower effective atomic number of $KCl:Eu^{2+}$ (18 versus 49, respectively). The lower Z, however, makes the material conducive to radiation therapy dosimetry. Additionally, the much greater dose produced in therapy beams (cGy vs. μGy) compensates for the reduced sensitivity compared to $BaFBr_{0.85}I_{0.15}:Eu^{2+}$. Thus $KCl:Eu^{2+}$ has the potential to satisfy all seven desirable properties at the same time by combining a low effective atomic number with computed

radiography-related benefits, in this way advancing the state-of-the-art in radiation therapy dosimetry.

1.2 Dissertation Objective

While KCl:Eu^{2+} has significant potential to advance radiation therapy dosimetry, designing and developing a novel dosimeter is a challenging task. Consequently, once a sensitive material is selected, several proof-of-concept and systematic studies must follow before the device is put into clinical use. Therefore, the purpose of this dissertation is threefold: to present proof-of-concept data that demonstrates the applicability of KCl:Eu^{2+} for radiation therapy dosimetry; to systematically study the radiation hardness of the material, thereby establishing the extent of its reusability in megavoltage applications; and, finally, to present preliminary theoretical investigations of thin panel KCl:Eu^{2+} dosimeters. The results of this dissertation fully establish KCl:Eu^{2+} as a next generation radiation therapy dosimetry material and provide a practical and theoretical knowledge base for future research and development.

1.3 Outline

The dissertation is organized in the following manner. Chapter 2 surveys the literature of storage phosphors with an eye towards quantitative dosimetry. The proposed KCl:Eu^{2+} dosimeter is related to other phosphor materials and several current dosimeters. Chapter 3 surveys the experimental methodology used in this work. Chapter 4 presents principle data for KCl:Eu^{2+} that demonstrates proof-of-concept for radiation therapy applications [13]. Chapter 5 presents a systematic study of the radiation hardness of KCl:Eu^{2+}. Together, chapters 4 and 5 establish KCl:Eu^{2+} as a next generation dosimetry material. Chapter 6 then offers preliminary investigations of thin panel KCl:Eu^{2+} dosimeters that will be the focus of future research. Chapter 7 concludes the dissertation.

Chapter 2

Background and Significance

The purpose of this chapter is to survey the literature related to storage phosphors, thereby providing necessary background for understanding of the mechanism of photostimulated luminescence (PSL) in KCl:Eu^{2+} and for relating the current study to current clinical dosimeters and clinical needs. Irradiation produces electron-hole pairs in the KCl:Eu^{2+} material that are stored in metastable energy traps proportional to the locally deposited dose. The spatial distribution of these trapped charge carriers forms a "latent image," whose information can be read out by stimulating the trapped charge carriers to recombine near an activator and release PSL photons proportional to dose. The PSL process is complex, involving irradiation, energy storage, stimulation, energy transfer, and excitation and relaxation of an activator, and can be influence by materials processing parameters and radiation history. Scientific investigation into KCl:Eu^{2+} is necessary because existing clinical dosimeters fail to possess all the desirable features of radiation therapy dosimeters.

2.1 Introduction

2.1.1 Development of Photostimulable Phosphor Materials

Research into the application of photostimulable storage phosphors in diagnostic radiology began as early as 1975 [7], but gained momentum in the early 1980s with the development of

BaFBr:Eu^{2+} [14], which was shown to have high sensitivity and excellent optical properties. BaFBr:Eu^{2+} particles were mixed with organic binders and the computed radiography (CR) film, also known as the imaging plate (IP) or storage phosphor film (SPF), was introduced in shortly thereafter in 1983 [15]. Barium fluorohalide-based radiography systems developed rapidly and current commercial system specifications allow high resolution (50 μm) and high throughput (30-200 IPs/h) [6]. Due to high use, the American Association of Physicists in Medicine (AAPM) issued a technical report in 2006 on their acceptance and commissioning [6].

The standard IP, shown in figure 2.1a, consists of polycrystalline doped phosphor material particles (median grain size around 7 μm [16], 61% by volume [17]) in an organic binder on a polyethylene terephthalate (PET) substrate. Protective and/or light shielding back

(a) Traditional phosphor film.

(b) Dual side readout phosphor film.

(c) Structured, needle-shaped phosphor film.

Figure 2.1: Structures of storage phosphor films. The traditional storage phosphor film (a) consists of particles embedded in a binder coated on an opaque substrate. Recent advancements include dual side readout (b) and the structured, needle-shaped phosphor place (c). Figures adapted from [6].

layers may also be applied. During x ray irradiation, electrons and holes are generated in the IP in numbers proportional to the locally deposited dose. These electrons and holes are

stored in the phosphor in energy traps, such as F-centers and Eu^{2+}/V_k centers [8,9,18,19]. The spatial distribution of trapped charges forms a latent "image" of the dose that can be subsequently read out by scanning the IP in a point-by-point manner with a focused laser beam. During the scan, electrons recombine with holes in their neighborhood resulting in characteristic blue Eu^{2+} luminescence that is optically filtered from the stimulation light and detected with a photomultiplier tube (PMT). Data from the PMT is recorded and visualized on a computer. The "depth" of the scan, that is, the percentage of stored information read out at a given point, is related to the readout laser intensity. Residual latent image information is erased with a high intensity broadband light with minimal UV components in order to prevent re-trapping. Erasure allows the IP to be used multiple times, which is necessary for establishing and maintaining baseline performance.

The basic cycle of medical image formation with storage phosphors is illustrated in figure 2.2. Irradiation is followed by readout in a pixel-by-pixel or digital manner. After readout of stored information, the phosphor is optically annealed with a high intensity, broadband light and available for reuse.

The advantages of IPs for diagnostic radiology have been well documented. Authors have noted: a dynamic range of over 5 orders of magnitude, excellent linearity, no apparent limitation on dose rate, high efficiency, high spatial resolution, no wet chemical processing, digital readout, a low useful dose limit, and large detection areas [7,8,20–22] . Furthermore, the versatility of IPs have led to numerous applications, including autoradiography of weak beta and gamma emitters, such as ^{14}C, ^{3}H, and ^{195m}Pt, in mice [23] and agarose gel from electrophoresis [24], non destructive imaging with beta emitters [25], protein crystallography [26], 50 MeV proton beam dosimetry [27], neutron dosimetry [21, 28, 29], skin entrance dosimetry during interventional radiology [30], integral dosimetry around a cyclotron [31], and quality assurance of kV x ray tubes [32].

Recent advancements in CR have come through the development of dual side readout as in figure 2.1b [7], and, significantly, a binder-less needle-shaped CsBr active layer as in figure 2.1c and figure 2.3 [33–41]. The needle structure of the CsBr film creates microscopic

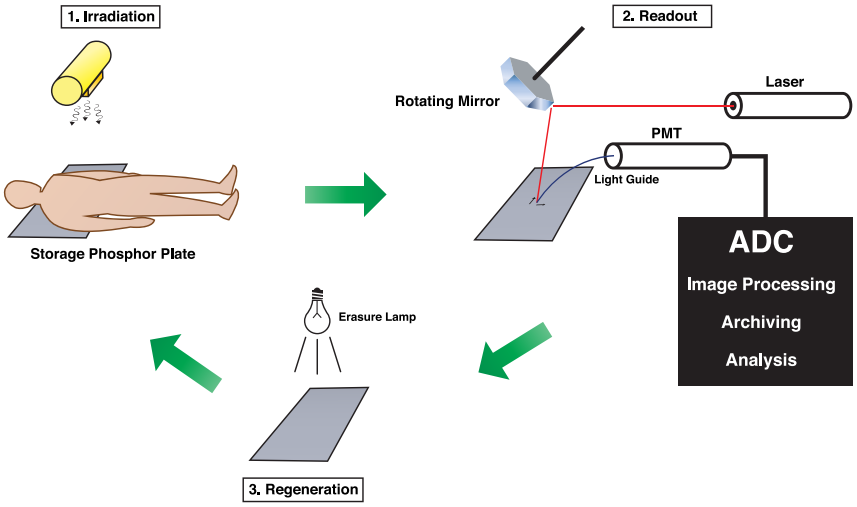

Figure 2.2: Basic cycle of medical image formation with storage phosphors, adapted from [8]. Irradiation produces a "latent image" in the phosphor layer that is readout in a pixel-by-pixel or digital manner. After readout of stored information, the phosphor is optically annealed with a high intensity, broadband light and available for reuse.

light guides that reduce light scattering in the film, improving resolution. The elimination of binder allows for a thicker, denser film, which increases sensitivity. As a result, the needle-films exhibit up to two times the detective quantum efficiency (DQE) of traditional particle and binder plates [35, 42].

2.1.2 Photostimulable Phosphor Dosimetry

High Z_{eff} Photostimulable Phosphor Dosimetry

The current gold standard material used in IPs is $BaFBr_{0.85}I_{0.15}$:Eu^{2+} [6, 7], but literature on IP dosimetry is limited. In 2005, Olch evaluated commercial $BaFBr_{0.85}I_{0.15}$:Eu^{2+} films (Agfa MD10) for megavoltage dosimetry and observed: 1) response uniformity across 30 cm within 1%, 2) a linear dose response between 6 cGy and 328 cGy (cf. [43]), 3) signal stability after 12 hours, and 4) response stability up to 10,000 cGy [4]. Olch concluding that a

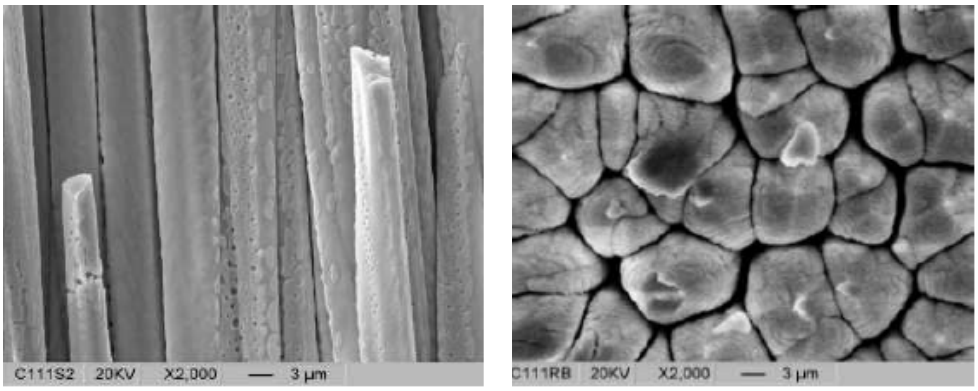

(a) Needle shaped CsBr side view. (b) Needle shaped CsBr top view.

Figure 2.3: Top and side view of needle shaped CsBr, reprinted from [34], with permission from Elsevier. Needles act as light guides to improve spatial resolution by reducing stimulation light and PSL scattering.

commercial IP made of $BaFBr_{0.85}I_{0.15}$:Eu^{2+} could potentially serve as a digital substitute for conventional film for absolute and relative dosimetry in radiation oncology clinics provided lead filtration was used. Lead filtration would be required because the high effective atomic number ($Z_{eff} = 49$) of commercial IPs enhances low-energy photon interactions in the film and enhances the dosimetric response for large fields and deep measurement planes.

In addition to Olch's study, Li *et al.* studied IP dosimetric response to megavoltage beams in order to determine the generation efficiency, W, of $BaFBr_{0.85}I_{0.15}$:Eu^{2+} for ^{60}Co and 6 MV beams [44]. W is the amount of energy that needs to be absorbed by the phosphor to produce one PSL photon. Within 16.6% experimental error, W was determined to be 190 eV for ^{60}Co and 160 eV for 6 MV, values that will serve as a basis of comparison for KCl:Eu^{2+}.

The high sensitivity of commercial IPs has led to other dosimetry applications. Ohuchi *et al.* used IP systems to characterize entrance skin doses during interventional radiology, reporting that the IP can accurately measure doses from 1 μGy to 10 Gy [30]. Ariga *et al.* reported that an IP system can estimate exposure doses from 3 μGy to 1.5 mGy within an uncertainty of $\pm$5% as required by the Japanese Industry Standard [32]. Gonzalez *et al.* investigated the dose response of a $BaFBr_{0.85}I_{0.15}$:Eu^{2+}-based IP to beta-particle reference

radiation fields used for calibrations at the National Institute of Standards and Technology. They reported a linear dose response down to 1 μGy in beta-particle beams with electron energies ranging from 200 KeV to 2 MeV emitted from Pm-147, Kr-85 and Sr-90.

These reports demonstrate that $BaFBr_{0.85}I_{0.15}:Eu^{2+}$ is highly sensitive to radiation. However, its high atomic number makes it undesirable for quantitative megavoltage radiotherapy x ray dosimetry.

Low Z_{eff} Photostimulable Phosphor Dosimetry

Nanto *et al.* published the first papers on $KCl:Eu^{2+}$ storage phosphors beginning in 1993 [12, 45, 46]. They report efficient room temperature PSL peaking at 420 nm when stimulated with 560 nm light. The 420 emission was assigned to the $4f^6 5d \rightarrow 4f^7$ ionic transition of Eu^{2+} due to an overlap with the photoluminescence peak of isolated Eu^{2+} (cf. [47]). Additionally, the luminescence lifetime of the 420 nm PSL was found to be about 1.6 μs, comparable to barium fluorohalides [11]. PSL intensity was proportional to UV (243 nm) and x ray dose, but sensitivity was found to be much lower than $BaFBr_{0.85}I_{0.15}:Eu^{2+}$ [48,49]. The reduced effective Z of $KCl:Eu^{2+}$ compared to $BaFBr_{0.85}I_{0.15}:Eu^{2+}$, 18 versus 49, respectively, is responsible for the decreased sensitivity due to the photoelectric mass coefficient dependence on Z^3. However, the greater dose utilized in radiation therapy procedures than in diagnostic imaging procedures—cGy versus μGy—compensates for the reduced sensitivity.

$KCl:Eu^{2+}$dose information may also be read by thermal stimulation. In 1994 Aceves *et al.* studied the thermoluminescent response to UV and x rays at room temperature [50]. Thermoluminescence (TL) glow curve structure was similar, but differed in intensity, for both UV and x rays and the response was linear in the mGy range. Meléndrez *et al.* also observed a linear dose response for single crystal $KCl:Eu^{2+}$ for all types of radiation [51]. They report excellent long term stability of the signal (i.e., after an initially rapid decay period of a few minutes) of about 50% signal loss over a period of 45 days [51, 52].

The first published work on evaporated KCl:Eu^{2+} thin films appeared in 2007 when Aceves *et al.* studied the TL and PSL properties of KCl:Eu^{2+} thermally evaporated onto glass substrates and exposed by 20 kV x ray, 546 keV $\bar{\beta}$ energy from ^{90}Sr, and 5 kV electron energy from an SEM [53]. Final film thickness was estimated to be about 5 micron and the microstructure resembled overlapping foils. TL glow curve structure was ascribed to F-type centers produced by irradiation. PSL was found to have F-aggregated luminescence. This study indicates the versatility in form factor for KCl:Eu^{2+} dosimeters, which can be used in either pellet or 2D forms.

2.1.3 Summary

In summary, a material that has all the beneficial properties of CR—e.g., reusability, high spatial resolution, wide dose response—with a lower effective atomic number, such as KCl:Eu^{2+}, is desirable and would potentially meet radiation therapy requirements. Yet since research into photostimulable phosphors for quantitative megavoltage dosimetry is limited, there is a need for proof-of-concept and systematic investigations into the dose response of KCl:Eu^{2+} so that the material can be confidently applied in radiation therapy.

2.2 Nature of Photostimulated Luminescence

From the above discussion, a low-Z storage phosphor material is desirable. In order to better understand the mechanism of photostimulated luminescence and possible ramifications for dosimetry applications, the following literature review is presented.

The literature suggests that two types of storage centers exist in storage phosphors [8,54]. Electrons are stored in x-ray generated F-centers and variants. An F-center is a halide vacancy occupied by an electron [55]. Similarity between the photostimulation spectrum and F-center absorption bands identifies the photostimulable electron traps as F-centers, e.g., F(Cl^-)-centers. The position of the stimulation peak is determined by the width of the potential well for the F-center electron, which is influenced by the lattice constant. The

shape of the stimulation spectrum is in the form of a broad, resonance peak, rather than a sharp edge, which is partly accounted for by the fact that centers are strongly coupled to the lattice and may radiate energy by phonon emission. Holes are trapped at or near impurity sites called activators. Traps may be stable at room temperature for many hours. The nature and generation of the trap centers, as well as the transport of trapped charge upon photostimulation, are points of contention and discussed below.

2.2.1 Takahashi Theory

Takahashi *et al.*, in studies of of single crystal and powdered europium-doped barium fluorohalides, BaFX:Eu^{2+} (X=Cl, Br), observed weak red luminescence due to Eu^{3+} in addition to Eu^{2+} of material prepared in an oxidizing atmosphere [5, 11, 14]. When irradiated by a N_2-laser (3.7 eV, 337 nm), the intensity of Eu^{2+} was seen to decrease while Eu^{3+} simultaneously increased. After stimulation, the intensities returned to their original level. Additionally, under PSL conditions, the stimulation spectrum, the photoconductivity spectrum, the absorption spectrum, and the electron spin resonance (ESR) fading spectrum corresponded with one another.

To explain the results, Takahashi *et al.* [5] supposed that upon upon x ray irradiation, Eu^{2+} is partially ionized to the 3+ valence state. Liberated electrons migrate via the conduction band to existing F^+ defects (a halogen ion vacancy) thus forming F-centers. Under subsequent excitation by visible light, the trapped electrons are raised to an excited state and subsequently thermally excited to the conduction band. In the conduction band, they are free to migrate back to Eu^{3+} ions where a reduction to Eu^{2+} takes place under the emission of 3.2 eV light. This model, which has come to be known as the "bimolecular" recombination model because the recombination rate is proportional to the number of electrons and number of Eu^{3+} ions, is diagramed in figure 2.4 [14].

The Takahashi model assumes the existence of F^+ centers in the lattice prior to irradiation and electronic diffusion occurring through the conduction band. Due to band transport, no spatial correlation between electron traps and hole traps is assumed.

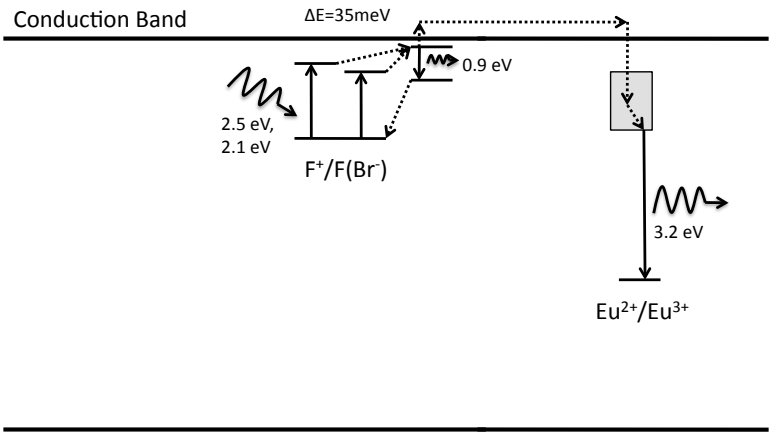

Figure 2.4: Band model of Takahashi PSL mechanism for $BaFBr_{0.85}I_{0.15}$:Eu^{2+} phosphors, after [14] and [56]. Upon x ray irradiation, Eu^{2+} is partially ionized to the 3+ valence state. Liberated electrons migrate via the conduction band to existing F^+ defects (a halogen ion vacancy) thus forming F-centers. Under subsequent excitation by visible light, the trapped electrons are raised to an excited state and subsequently thermally excited to the conduction band, where they migrate back to Eu^{3+} ions, resulting in a reduction to Eu^{2+} takes place under the emission of 3.2 eV light.

2.2.2 Itoh/von Seggern Theory

von Seggern *et al.* wrote rate equations describing the bimolecular PSL x irradiation and readout process and determined that the model would lead to a quadratic increase in stimulated photon emission rate with dose during optical readout [57] . However, they observed a linear increase in experiments, as well as efficient PSL down to liquid helium temperatures and a temperature independence of luminescence lifetime [57]. At low temperatures, the thermal energy (35 meV) required to raise an electron out of the relaxed excited state (RES) of the F-center and into the conduction band is lacking and only a tunneling model can explain the efficient PSL. Tunneling has a higher probability of occurrence with shorter distances, which introduces the idea of spatial correlation of trapped charges and activators. Thus von Seggern *et al.* proposed a "monomolecular" recombination model in which PSL is mediated through a "photostimulated luminescence complex (PSLC)", namely an F-center

in close proximity to a recombination center [56, 57], which is created during irradiation. PSL occurs when electrons are stimulated from F-centers to tunnel to trapped holes, which, upon *e-h* recombination transfer energy resonantly to Eu^{2+} yielding the characteristic blue (420 nm) luminescence. As initially proposed, the recombination center was thought to be either Eu^{3+} or an Eu^{2+}/hole complex.

Rüter *et al.* expanded on this idea by offering a theory of x ray induced PSLC production [58] based on work by Itoh in the alkali halides [59]. Upon irradiation, free excitons are created. Excitons then de-excite in the neighborhood of a lattice distortion introduced by Eu^{2+} and become self-trapped at either a V_k centers or a $halogen_2^-$ molecular ions. After transition states, F-centers (halogen vacancies with bound electrons) and H-centers (an interstitial halogen bound to lattice halogen by a hole) are formed [59]. Thus Rüter *et al.* proposed an Eu^{2+} and *F*-*H* pair recombination center [58].

The Itoh/von Seggern model may be schematically illustrated as in equation 2.1 [8], and diagramed as in figure 2.5 [56]:

$$\begin{aligned} h\upsilon &\rightarrow e^- + h \\ e^- + h &\rightarrow F + H \\ F + H &\rightarrow F + Eu^{2+}/H \end{aligned} \tag{2.1}$$

Experimental results have supported the model. Hangleiter *et al.* argued from electron paramagnetic resonance (EPR) data that no Eu^{3+} is created upon room temperature irradiation [60]. Koschnick *et al.* observed partial spatial proximity between electron-hole traps and Eu^{2+} by detecting cross relaxations of electrons through optically detected EPR [61]. Thoms *et al.* argued for spatial correlation of F-centers and recombination centers from temperature dependent PSL yield studies [56]. This group found that the fraction of correlated photostimulable centers was about 23%, with the remaining 77% being uncorrelated [56]. Chen *et al.* also offered evidence of energy transfer between e-h recombination and Eu^{2+} through PL and PSL emission studies before and after irradiation [62].

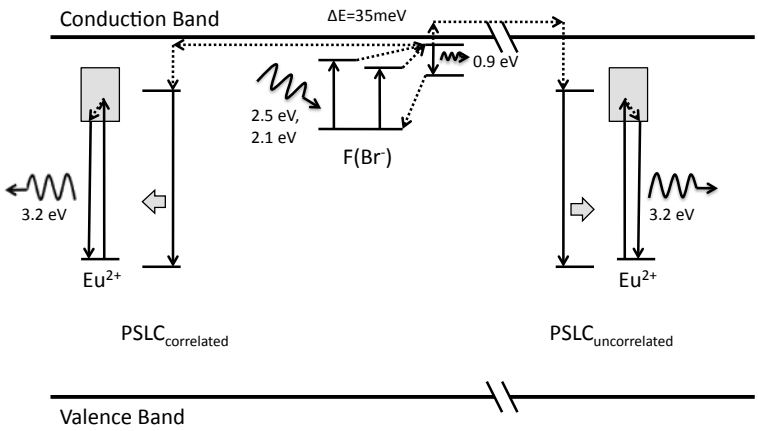

Figure 2.5: Band model of Itoh/von Seggern PSL mechanism for $BaFBr_{0.85}I_{0.15}:Eu^{2+}$ phosphors, after [56]. Irradiation produces a "photostimulated luminescence complex (PSLC)", namely an F-center in close proximity to a recombination center. Upon stimulation, electrons are stimulated from the F-centers to tunnel to a trapped hole or are thermally released to the conduction band. In either case, upon *e-h* recombination, energy is transferred resonantly to Eu^{2+} yielding the characteristic blue (420 nm) luminescence.

Iwabuchi *et al.*, however, refuted the PSLC model and offered evidence in favor of Takahashi's bimolecular kinetic model, based primarily on observation of PSC [18]. The PSC can be explained without resorting to conduction band diffusion, however. Harrison *et al.*, for example, introduced the idea of optically stimulated diffusion of trapped charges on 2D sub-lattices in the $BaFBr_{0.85}I_{0.15}:Eu^{2+}$, which can explain the observed overlap in PSC and PSL spectra [63].

2.2.3 Summary

In view of these findings, there is a greater ability to explain the experimental evidence given the more complex PSLC model of photostimulated luminescence. A band model for PSL in $KCl:Eu^{2+}$ can now be generated (figure 2.6; after [56] and [64], cf. [65]). From the radiation therapy physicist user's perspective, this model is important for several reasons. First, PSL should be linearly proportional to dose because the number of created centers

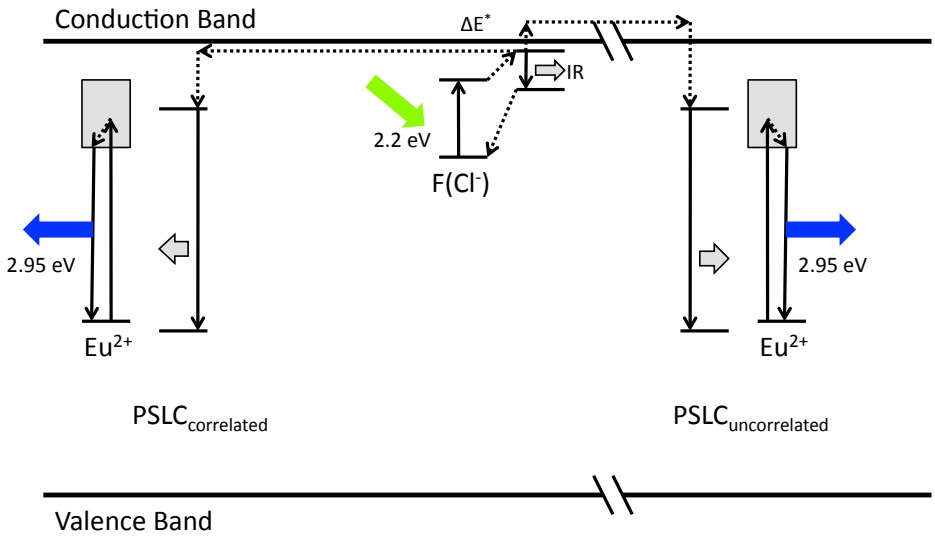

Figure 2.6: Band model of Itoh/von Seggern mechanism for KCl:Eu^{2+} phosphors (after [56] and [64], cf. [65]). *Activation energy determined from temperature dependent PSL studies.

is proportional to dose. Second, the PSL process is complex, involving irradiation, storage, excitation, recombination, energy transfer, and relaxation. Consequently, there are several factors that may influence the PSL signal. These include (after [66]):

1. Competing traps
2. Thermal stimulation from shallow traps
3. Re-trapping at a PSL-active trap
4. Stimulation from multiple trapping levels
5. Recombination at multiple recombination levels
6. Photo-transfer of charges from deep to PSL or shallow traps

2.3 Performance Issues

2.3.1 Sensitivity

Due to the divalent nature of the Eu^{2+} ion in the monovalent host lattice, a neighboring charge compensating mechanism is required to guarantee charge neutrality. Oxygen can act as the charge compensation ion residing on a chlorine site in the vicinity of a divalent Eu^{2+} ion [67, 68]. In fact, reports show PSL sensitivity increases in CsBr:Eu^{2+} crystals after annealing in air [36, 37]. Initially it was thought that the PSL increase could be attributed to the formation of $CsEuBr_3$ and/or Cs_4EuBr_6 precipitations [38]. Hesse *et al.*, however, determined through detailed x ray diffraction studies that precipitations of $CsEuBr_3$ degrade in normal atmosphere to phases containing trivalent europium and thus they are PSL inactive [67].

Alternatively, O^{2-} is thought to form a dipole with Eu^{2+} which acts to increase charge separation of the electron-hole pairs created during ionizing radiation, leading to more efficient hole trapping [40]. A recent report has also suggested that room-temperature hydration of CsBr:Eu^{2+} for 60 minutes in 99% relative humidity increased the PSL intensity by a factor of 25 [68]. In this case, the increase was attributed to the incorporation of H_2O molecules into the lattice which enhanced the trapping efficiency of preexisting (Eu^{2+}–O^{2-})-dipoles.

2.3.2 Radiation Hardness

Recent investigations have demonstrated the complex and material-dependent effects of cumulative dose on various solid-state dosimeters that are designed for multiple uses. Jursinic, in a study of Al_2O_3:C, which is used in optically stimulated luminescence dosimetry (OSLD) radiation badges [69,70], observed an initial decrease in sensitivity followed by an increase in sensitivity and increase in linearity after doses of 60 Gy [71]. After 1000 Gy, the sensitivity leveled out and a linear response dominated. Jursinic suggested that Al_2O_3:C dosimeters

could be used for accurate radiation therapy dosimetry if the sensitivity and extent of supralinearity were established for each dosimeter in use [71].

Zimmerman *et al.* have reported that CsBr:Eu^{2+} retains only 20% of its initial PSL yield after accumulated doses of 20 Gy, which decreases to 10% after 100 Gy [72]. It was suggested that the major cause of this loss of sensitivity is the creation of large defect centers such as M_{Eu}, an agglomeration of two adjacent F-centers that is stable at room temperature near an activator site. Within such an agglomeration in the lattice, Eu^{2+} can easily change sites and form larger precipitations, second phases, or aggregations that are responsible for luminescence quenching. As Zimmerman *et al.* [72] note, thermally activated aggregation of Eu^{2+} was studied in several alkali halides by Savel'el *et al.* in 1974 [73]. Due to differing crystal parameters, this aggregation may occur at different rates due to the variability in the elastic deformation caused by the substitution of the impurity cation for the host cation. For example, aggregation occurs at room temperature for CsBr:Eu^{2+} very quickly but has been reported to be controlled in RbBr:Eu^{2+} [74].

Recently, Zimmerman *et al.* have shown that co-doping with Li improves the radiation hardness of CsBr:Eu^{2+}, with the phosphor retaining about 50% of it's initial PSL yield with an accumulated dose of 20 Gy (vs. 20% for the non co-doped case) [39]. They proposed that Li ions distributed in the lattice suppressed the formation of F centers, which is an intermediate step in the formation of M-centers. In the proposed model, an F center electron is donated to another F center, forming a F^+ center (anion vacancy) and an F' center. The centers move toward each other through Coulombic attraction and form an M center [39]. Li then suppresses the formation of F centers so strongly that the formation of F' centers and M centers becomes unlikely. Unfortunately, co-doping also reduces the production of F-centers compared to non-doped samples [39], thus reducing the amount of stored x ray energy.

2.3.3 Signal Stability

Ohuchi *et al.* studied effects of ambient temperature on $BaFBr_{0.85}I_{0.15}:Eu^{2+}$ signal stability and argued that, following irradiation, signal fading is related to thermal assisted de-trapping of electrons and holes [31, 75]. Their group undertook a series of annealing experiments at various temperatures in an effort to identify trapping levels.

Nanto *et al.* [48] and Douguchi *et al.* [76] reported that in addition to ambient temperature, fading is related to crystallinity of the phosphor, irradiation energy, doping concentration, and humidity. The results they reported are limited to the first 60 minutes post-irradiation for x ray irradiation energies up to 40 kV. KBr:Eu (to 0.01%) showed no fading over 60 minutes post-irradiation while KCl:Eu seemed to stabilize after 30 minutes [76].

The influence of humidity on signal stability may be mitigated by carefully designed protective layers. In an early design, a thick glass protective layer encapsulating nitrogen gas and the phosphor layer was used to minimize fading of $RbCl:Tl^{+}$ [77]. Under this design, the $RbCl:Tl^{+}$ storage phosphor retained 70% of its initial PSL intensity after 12 hours and maintained initial signal stability characteristics for over 500 days. Recently, modern protective coating technologies have been introduced in order to protect CsBr needle-shaped phosphor films from ambient humidity [78]. These reports provide confidence that adequate protective layers can be applied to $KCl:Eu^{2+}$ in future applications.

2.3.4 Generation Efficiency

The generation efficiency, W, is defined as the mean radiation energy that must be absorbed by the phosphor to produce a PSL photon. W was determined to be 160 eV in $BaFBr_{0.85}I_{0.15}:Eu^{2+}$ in a 6 MV beam by Li *et al.* for a Fuji HRIII plate with a thickness of 170 μm [44]. This figure of merit can be used to determine W in $KCl:Eu^{2+}$ by a substitution method (see chapter 6).

2.4 Comparison to Other Dosimeters

The question arises as to why scientific investigation into a new dosimetry material is necessary when other devices are commercially available and widely used. Consequently, it is beneficial to compare and contrast KCl:Eu^{2+} with other dosimeters.

2.4.1 Ion Chamber Arrays

The gold standard dosimeter in radiation oncology is the ionization chamber. Arrays of chambers, such as the PTW 2D-ARRAY (PTW-Freiburg, Germany) or MatriXX (Scanditronix Wellhofer, Germany) are useful for coarse spatial resolution (i.e., >7mm) planar measurements, but may be problematic for high spatial frequency dose distributions, e.g., where dose gradients fall between adjacent chambers [79]. Processing techniques have been developed for dose verification whereby the expected array response, generated from the convolution of the lateral chamber response function with the calculated dose, is compared to the measured array values [80–82]. While these techniques may be suitable for routine quality assurance, it could be argued that they are not suitable for commissioning measurements. Furthermore, care must be taken to avoid anisotropic chamber response (e.g., differing collection efficiencies of the array chambers if the beam passes through the underside of the array as in arc therapy measurements) [83] and situations that create electronic disequilibrium in the chamber volumes [84]. Therefore, an alternative, high spatial resolution, two dimensional dosimeter is desirable for radiation therapy practice.

2.4.2 Radiographic and Radiochromic Film

Radiographic films have a longstanding research history into their dosimetric use. Current generation films, such as Kodak XV and EDR2, are used in radiotherapy clinics for both routine and complex quality assurance [85–92]. Film is in widespread use due to its high spatial resolution (limited by the optical densitometer aperture), easy integration into many geometric phantoms, low cost, and the provision a permanent record. However, the dosi-

metric response is a function of field size, depth, photon beam energy, processor conditions, and scanner performance [93]. While it may be possible to mitigate low energy photon dependence with lead filters [94], this practice is not suitable for commissioning studies. Furthermore, film processors are being phased out as clinics move towards digital imaging and maintaining them will become increasingly problematic.

Radiochromic films, such as EBT and EBT2 (International Specialty Products, Wayne, NJ), are also in wide use [95–97]. Purportedly tissue-equivalent over a wide dose range, they may be handled in daylight and do not require chemical processing [98]. However, self-development over time has been reported, as well sensitivity to environmental conditions, polarization of light, film orientation, and artifacts from the scanning densitometer [95, 99, 100]. Significantly, Zeidan *et al.* recently reported an OD sensitivity threshold corresponding to a low dose limit of 25 cGy [100] using a 48 bit color scanner, which limits applicability in low dose regions. Additionally, Hartmann, in a study of EBT2 film, reported pixel-to-pixel inhomogeneities of $\pm$ 3.7% and uncertainties in dosimetric response of $\pm$ 6% [101] when using net optical densities.

Because both radiographic and radiochromic films are fundamentally single-use detectors, they cannot be reliably calibrated. Quantitative dosimetry with single-use films requires the acquisition of a sensitometric curve each time a dosimetric measurement is made, but this practice is based on the assumption that each individual film has the same response as others in the batch, and, for radiographic film, that the processor remains stable between developed films. The KCl:Eu^{2+} dosimeter proposed in this study is similar to film in that it will have high spatial resolution but different in that it is reusable, which allows a physicist or engineer to monitor the response of the dosimeter long term.

2.4.3 Semiconductor Arrays

External Portal Imaging Device (EPID) technologies have also been used for dose validation quality assurance [102–104]. While early EPIDs were scintillation/camera systems [105], current generation devices are generally multilayered, consisting of a scintillation layer in

combination with an array of a-Si photodiodes. Current generation EPIDs are high resolution, approximately linear devices [106]. However, they are not water-equivalent and not useful for measurements inside phantoms that mimic patient geometries. Therefore, a quantitative 2D dosimeter that is able to be placed within a phantom remains needed in radiation therapy quality assurance.

2.4.4 Gels and Radiogenic Polymers

3D dosimetry is made possible by solid volumes that are sensitive to radiation. Both ferrous sulphate, a.k.a. Fricke, solutions stabilized by a gel matrix and radiosensitive polymer gels have been investigated [107–110]. Dose information is read out by optical CT, x ray CT, or MRI/NMR. The advantage of gel dosimetry is that it provides true 3D, water-equivalent dose distribution measurements. Yet significant challenges remain. Dose information in Fricke dosimeters is not stable due to diffusion of the Fe^{3+} ion in the gel, which is effected by temperature, concentration, and gel composition [107]. Polymer gel dosimeters have advanced significantly [108], but dosimetric properties are still based on a non-reversible chemical reaction, which implies that the system is not reusable. Consequently, while a true 3D system is desirable for dosimetry, a convenient, reusable multidimensional dosimeter remains a desirable device.

2.4.5 TLDs

Thermoluminescent materials, such as LiF or CaF_2, are widely used in personal dosimetry and radiation therapy QA. Dose information is integrated over the irradiation period and then read out by heating the material to temperatures up to 500 °C and measuring thermally stimulated luminescence. These materials are capable of a wide range of measurable dose (mR to 10^5 R) and have proven to be stable [111]. Thermal stimulation results in the depletion of the entirety of trapped charge carriers, which essentially zeros the signal. In contrast, optical stimulation is more flexible in that it allows multiple readouts by weakening the stimulation power. Additionally, optical dosimeters lend themselves to rapid point-by-

point scanning and rapid zeroing of dose in high-dose RT applications. TLDs are not suitable for point-by-point scanning, which is the main long-term goal of this research.

2.4.6 OSLDs

Aluminum oxide, or Al_2O_3:C, dosimeters are common in the nuclear and health physics industries and research into this material has been widely reported [69,71,112,113]. In medical practice, Al_2O_3:C has primarily been used as a passive, *in vivo* dosimeter and for quality assurance [69]. A promising development for optically stimulated dosimeters occurred on June 1, 2010, when the Radiologic Physics Center (http://rpc.mdanderson.org/rpc) switched to OSLD technology from TLD technology for remote dosimetry audits. A large concern for Al_2O_3:C, however, is the length of the luminescence lifetime, which has been reported to be hundreds of milliseconds to seconds at room temperature [69,114]. This sets a limit on readout speed in high speed 2D dosimetry systems and creates the potential for high pixel cross-talk during readout. Furthermore, reported data indicates that thick film Al_2O_3:C dosimeters (300 μm) still over-respond 15.5% at 5 cm from a 20×20 cm^2 field edge and 20 cm depth for a 6 MV beam and 20.2% for an 18 MV beam [115].

2.4.7 Summary

A multidimensional, reusable, water-equivalent dosimeter that fits into geometric phantoms is a critical need for both the IMRT QA process and machine commissioning. The available dosimeters are either not reusable (e.g. radiochromic film), not water-equivalent (e.g. portal imagers), or lack high spatial resolution (e.g. ionization chamber arrays, TLDs, OSLDs). KCl:Eu^{2+} presents an exciting opportunity to advance the state-of-the-art in radiation dosimetry.

2.5 Conclusion

Photostimulable phosphor technologies have been applied successfully in a number of cases. In radiation therapy applications, a lower Z phosphor is desirable in order to maximize the water-equivalence of the dose response. In this way KCl:Eu^{2+} presents an exciting opportunity to advance the state-of-the-art in radiation dosimetry as the first ever low Z, reusable, high spatial resolution dosimeter, overcoming limitations of existing dosimeters and meeting clinical needs.

Based on this literature review, the response of KCl:Eu^{2+} can be understood using a PSLC schema. In this schema the PSL process is complex, involving irradiation, energy storage, stimulation, energy transfer, excitation, and relaxation. PSL yield is intimately related to materials chemistry and microstructure, which are, in turn, a function of a number of materials processing parameters and radiation history. Consequently, a careful examination of the process used in fabricating KCl:Eu^{2+} dosimeters as well as a systematic investigation of their response to cumulated dose is in order. These properties require scientific exploration before there will be any future development of this novel dosimeter for every-day, quantitative use.

Chapter 3

Experimental Methodology

The purpose of this chapter is to clarify the experimental methodology used in this work. KCl:Eu^{2+} storage phosphor powders were synthesized using well-developed materials science methods. Raw materials were milled in a planetary ball mill or mortar and pestle and particle sizes were selected with manual sieves. SEM was used to evaluate powder quality. Powders were then mixed and homogenized in a planetary ball mill or mixer mill and either pressed into pellet form or used as sources for tape casting or physical vapor deposition (PVD). Dose information was readout on point or two dimensional (2D) experimental optical setups. For pellet measurements, optical stimulation power was reduced to allow for multiple readings, including removing the dosimeter and remounting. Readings were corrected, averaged, and the standard error was taken as the experimental uncertainty.

3.1 Sample Preparation

Sample preparation can be broken down into groups: powder processing, pellet processing, tape casting, and physical vapor deposition (PVD). These steps are described below. Detailed powdering and pelleting procedures used in later studies are documented in appendix A.

3.1.1 Powder Processing

Dehydration

Raw materials consisted of both high purity (99.997%) and reagent grade KCl and $EuCl_3 \cdot 6H_2O$ (99.99%). Since KCl is hygroscopic, raw materials were dried 24 hours in a laboratory oven at 125 °C before use and were stored in vacuum or chemical desiccators at room temperature when not in use.

Particle Comminution

A planetary ball miller (Retsch PM100) was used for particle comminution. Two sizes of jars were available, 25 ml and 50 ml, both lined with agate. Dry milling was performed with 10 mm diameter agate balls as the milling aid. No dispersants were used during milling. Note that in order to achieve ultra-fine particles, e.g., under 25 micron, wet grinding with organic solvents and smaller milling balls may be necessary. Due to the small amount of dopant that was added to the bulk KCl in this study, europium precursors were ground by hand with mortar and pestle.

Particle Classification

A representative sample of KCl particles after milling is shown in figure 3.1 obtained from scanning electron microscopy (JEOL JSM-7001FLV). A wide distribution of particle sizes is evident which necessitates classification. Gross manual classification was performed by sieving with standard 8" testing sieves. Current protocol calls for sieving with numbers 250 (=63 μm), 325 (= 45 μm), and 500 (= 25 μm) stainless steel mesh sieves.

Particle Mixing

KCl and europium precursor of appropriate sizes were added together to the correct mol percent of europium. These materials were mixed via one of two methods: 1) in the ball miller with 2-3 milling balls set to medium speeds, or 2) in a vial filled to 70-80% volume

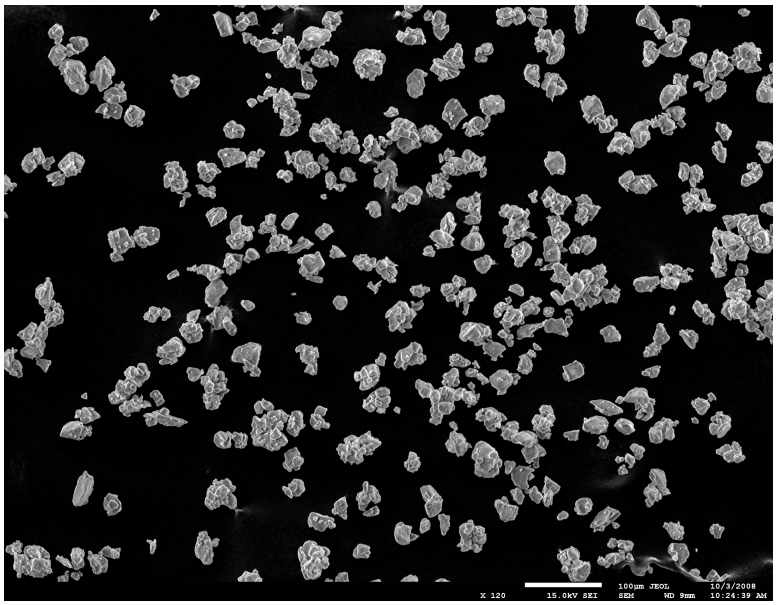

(a) KCl:Eu^{2+} particles broad field of view (scale = 100 μm).

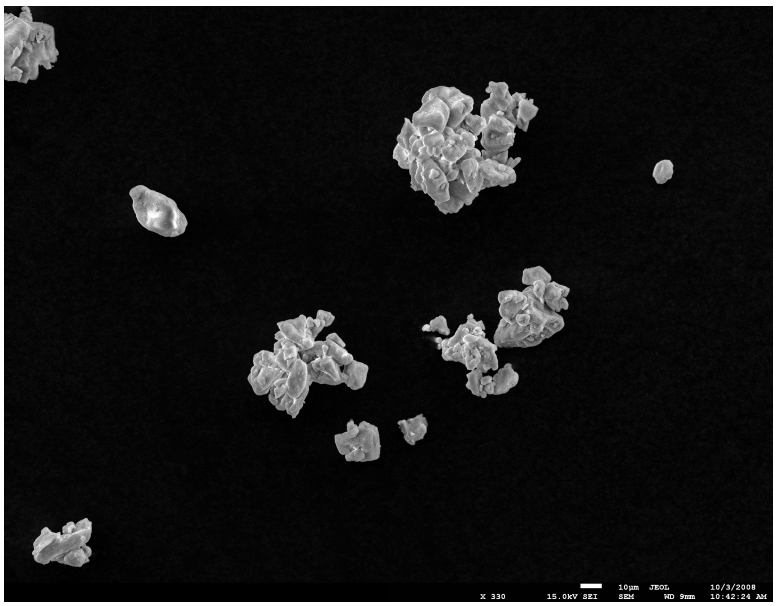

(b) KCl:Eu^{2+} particles narrow field of view (scale = 10 μm).

Figure 3.1: KCl:Eu^{2+} particles broad and narrow field of view. The milling process produces a wide distribution of particle sizes that necessitates particle classification.

and placed in a mixer mill (Turbula® T2F mixer) set to medium speeds. It was found that the mixer mill did not improve pellet-to-pellet consistency over mixing with the ball miller (figure 3.2) for non-preheated powders (see section 3.1.1). Therefore the ball miller may be used both for particle size reduction and particle mixing.

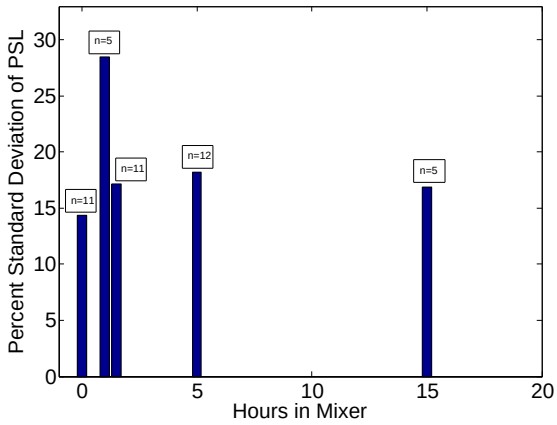

Figure 3.2: Influence of mixer mill time on chip-to-chip homogeneity. The standard deviation of chip response to absorbed doses of 200 cGy verses mixer mill (i.e., Turbula) time was computed as a measure of chip-to-chip homogeneity. Zero hours represents standard practice of mixing in the ball miller with 3 milling balls at 300 rpm (i.e., no Turbula). It was found that the the mixer mill did not significantly improve uniformity of response.

Particle Preheating

Through the course of experimentation it was found that proceeding with powder pressing and sintering immediately after mixing would result in pellets with various degrees of greying, as shown in figure 3.3. From observation, this reaction begins near 450 °C, demonstrated by the series of pictures in figure 3.4. It was hypothesized that the increased surface area of the powders created an opportunity for moisture and other contaminates to adsorb onto the surface of the particle and become incorporated into pressed pellet form with minimal chance to escape. It was found that heating the mixed powders to 350 °C in

Figure 3.3: Contaminated chip dosimeters. It is hypothesized that increased surface area of particle processing creates an opportunity for moisture and other contaminates to adsorb onto the particle surface, which become trapped during pressing. Heating mixed powders in air at 350 °C improves pellet response homogeneity and eliminates greying (cf. figure 3.6).

air for 2 h produced pellets with no visible discoloration, regardless of the cleanliness of the process tube during sintering. Furthermore, when powder was preheated to 350 °C prior to pressing and stored in a vacuum at 10^{-7} torr, the standard deviation of chip factors was measured to be between 4-6% of the average response of fresh dosimeters (cf. figure 3.2).

3.1.2 Pellet Processing

Powder Pressing

Mixed powders, preheated and non preheated, were pressed isostatically with either of two laboratory presses (MTI Corporation, model 24T, Richmond, CA; or Carver Inc., model 4350L, Wabash, IN) in either a 7 mm carbon steel die (MTI Corporation) or a 6.3 mm evacuable stainless steel die (Carver Inc.). Pressing dies were initially cleaned and rinsed three times with water, followed by a surfactant cleaning solution and multiple rinses with tap water. An ethanol rinse served as the final step. After each press it was necessary to remove residual material from the walls of the die sleeve and anvils. Consequently, the die was cleaned with water and a tube brush and blown dry after each press.

To achieve high applied loads with the carbon steel die, for example, 10 T, it is necessary to increase the load very slowly, for example 100 lbs per minute after 2 T. Increasing the load rapidly can result in cracked pellets. Likewise, when preparing to extract a pressed pellet,

(a) Pressed Pellets.

(b) $\theta = 300°\text{C}$.

(c) $\theta = 375°\text{C}$.

(d) $\theta = 425°\text{C}$.

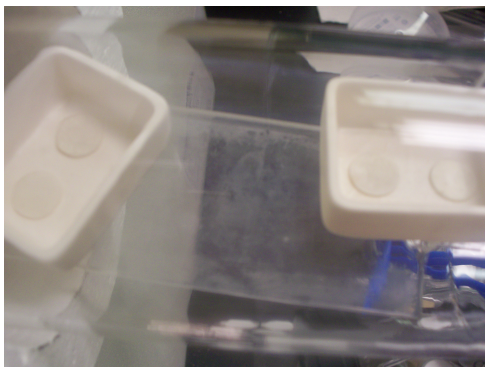

(e) $\theta = 460°\text{C}$.

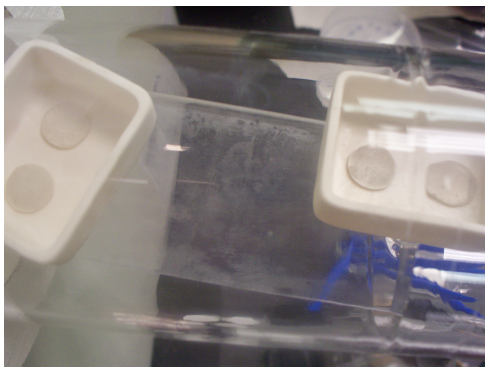

(f) $\theta = 500°\text{C}$.

Figure 3.4: Temperature dependent contamination process, shown from pictures taken through the furnace process tube at various temperatures. Sintering pressed pellets made from non preheated powder results in dosimeters of various shades of grey. From observation, this reaction begins near $\theta = 450°\text{C}$.

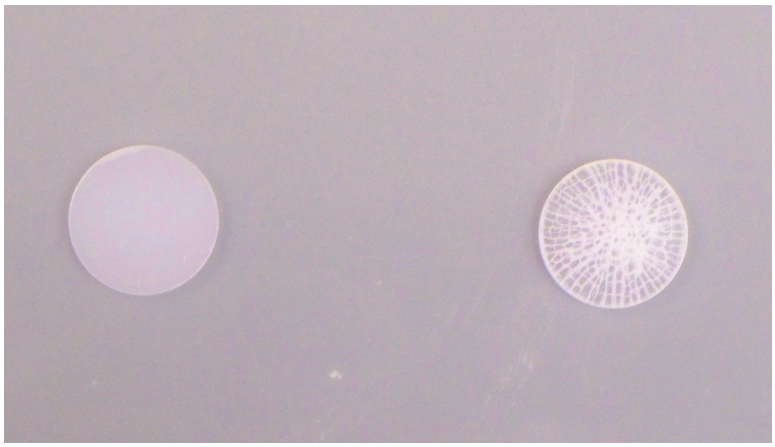

Figure 3.5: Effect of heating powder prior to pressing. On the left, a pellet made from powder preheated to 710 °C; on the right, a pellet from non-heated powder. Heating the powder prior to pressing leads to higher quality pressed pellets.

the load must be released very slowly to avoid rapid expansion of the pellet and cracking. Interestingly, heating the powder prior to pressing resulted in higher quality pressing, which is shown in figure 3.5.

To mitigate moisture damage, pressed pellets were wrapped in plastic film, for example, polyethylene, taped closed, and transported in metal foil bags with a desiccator capsule during experimentation.

Pellet Sintering

Pellets (or powders) were loaded into an Al_2O_3 crucible and placed in a quartz tube (Quartz Scientific, Fairport Harbor, OH) and furnace (Thermo Fisher Scientific Inc., Lindberg/Blue M furnace, Waltham, MA). The pellets were heated to a preset temperature in the center of the tube furnace and kept for a period of time. After synthesis, the mixture was allowed to cool to 300 °C naturally in the center of the furnace, after which they were pulled to the end of the process tube for a rapid cooling to room temperature. Figure 3.6 shows a picture of sintered pellets, along with a custom holder for readout.

During sintering of pressed pellets, a reduction in surface energy drives the coalescence of particles along particle boundaries. As sintering progresses, void spaces, i.e., pores,

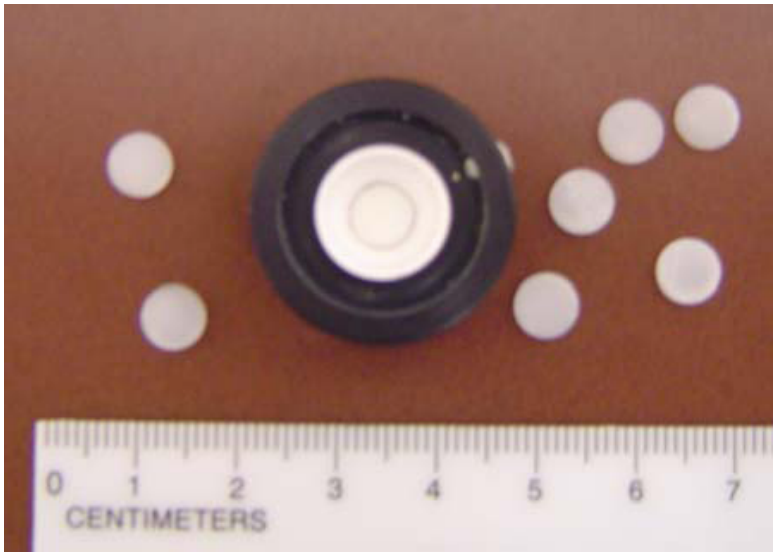

Figure 3.6: Chip dosimeters [13]. Dosimeters are 7 mm in diameter and 1 mm thick KCl:Eu^{2+}. Also shown is a holder which attaches a single dosimeter to the integrating sphere during readout.

become smaller and overall mechanical strength improves [116]. Thus binder additives are not necessary for pressed KCl:Eu^{2+} pellets.

It was also noticed that some material evaporates during sintering and deposits on the quartz tube around the location of the samples. Some devitrification of the quartz was also noted, due to the presence of the high temperature and alkaline environment but it was thought not to interfere with materials processing.

Pellet Annealing

Post-synthesis annealing procedures occurred in the laboratory furnace and oven (Binder Inc., Great River, NY). Pellets were heated in air after sintering at temperatures of 100-300 °C in order to compare the sensitivity to pellets that were not annealed.

3.1.3 Tape Casting

Tape casting, also known as doctor blading or knife casting, is a well-known method of laying down thin films greater than about 25 micron in thickness [117]. On laboratory-scale systems, the slurry, or slip, is poured into the casting head and a scraping blade, or doctor,

is drawn along a substrate just above a surface to remove excess material from the surface being coated. Uniform dried films of sub-millimeter thickness can be easily achieved. The adjustable parameters include the gap height, reservoir depth, speed of motion, viscosity of the slip, and the shape of blade.

The tape casting device shown in figure 3.7 was designed and constructed for prototyping purposes. A linear slide (Velmex, MA6000 series Unislide, Bloomfield, NY) fitted with a custom aluminum pusher-bar was utilized to move the casting head. The slide was positioned parallel to a 12"x18" vacuum plate (Paul N. Gardner Company, Inc., Pompano Beach, FL) under a fume hood. The weight of the slide and the vacuum plate was sufficient to prevent relative motion of the two devices during casting. The fume hood vacuum line was connected to the vacuum plate. Seven mil polyethylene substrates (DuPont Melenix 454, KRS Plastics, Tabor City, NC) served as the substrates for this study. The linear slide

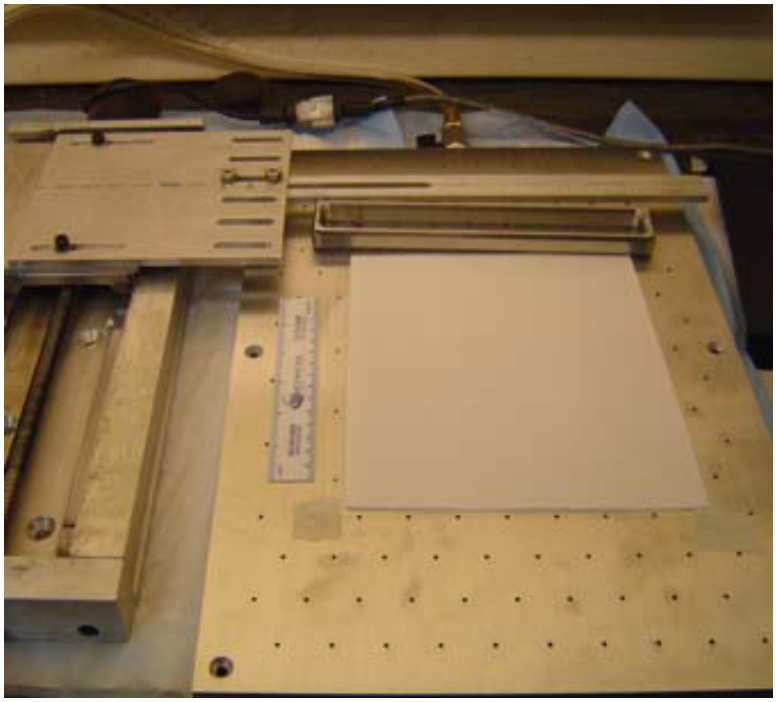

Figure 3.7: Designed tape casting device with custom casting head and sample KCl:Eu^{2+} film. A linear slide fit with a custom aluminum pusher-bar moves the casting head at defined speeds along PET substrates fixed to a 12"x18" vacuum plate.

was controlled by a stepper motor controller (Velmex, VMX) equipped with a thumb wheel for selecting one of four programs. The controller had sufficient memory for a maximum of four programs. Programs were written in a text editor and transmitted to the controller via an RS-232 cable.

Commercial casting machines are capable of 12-15 in draw downs and have speeds adjustable to 0.1 in/sec. The system described above allows more flexibility in programming the casting (e.g., controlling speed and acceleration of the blade) and is much less expensive. It has the disadvantage that, at any one given time, one of only three casting programs may be selected (one program is for zeroing the device) and the usable length of the draw is roughly 7 in. A longer range of motion on the slide would increase the tape casting draw.

A thorough study on tape casting the commercial phosphor $BaFBr_{0.85}I_{0.15}:Eu^{2+}$ was reported by Li, *et al.* [16]. From this study, four basic ingredients in a casting recipe emerge: phosphor powder, a liquid vehicle, a binder, and a dispersant. De-foamers and plasticizers are also often added to achieve an optimal dried tape but were not used in this study.

3.1.4 Physical Vapor Deposition

Theoretical considerations (see section 6.1) suggest that a $KCl:Eu^{2+}$ film with a thickness on the order of a few microns would maximize the water-equivalence of the response and provide excellent signal even for doses as low as a few cGy. It is very difficult to obtain films on the order of a few microns using a traditional tape casting method. Such a method would require significant investment in particle comminution, selection, and processing technologies. However, it may be possible to follow a recent advancement in CR technology developed by AGFA, the vapor deposited binderless $CsBr:Eu^{2+}$ storage phosphor film [33–35]. Under correct conditions of temperature and pressure, $KCl:Eu^{2+}$ material will thermally evaporate from a source producing a vapor flux that can be used to grow homogeneous $KCl:Eu^{2+}$ panel dosimeters.

The advantages of PVD are numerous. High purity films can be obtained from high purity evaporation sources. Volatile contaminates can be eliminated by vacuum preheating with the deposition shutter closed. Thickness can also be easily controlled, ranging from tens of angstroms to microns [118].

In this study, KCl:Eu^{2+} was deposited on a substrate of borosilicate glass (e.g., laboratory slides) with a physical vapor deposition system (Kurt J. Lesker, Nano38, Clairton, PA) (see figure 3.8). During evaporation, the substrate was rotated in order to maximize

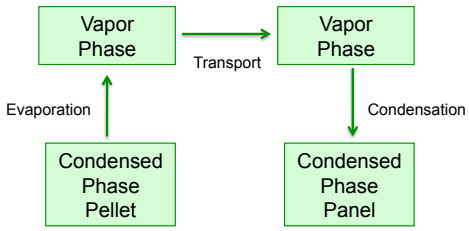

(a) PVD flowchart.

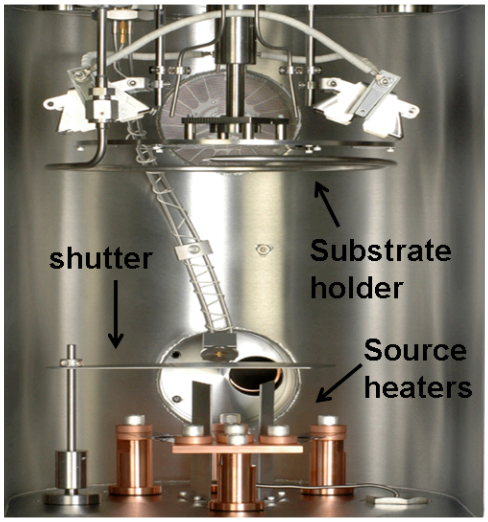

(b) Nano38 chamber*.

Figure 3.8: Physical vapor deposition flowchart and chamber. Raw materials, i.e., source charges, are processed and placed into evaporation boats inside the chamber. After the chamber is pumped down to 10^{-6} torr, source charges are resistively heated to supply energy for evaporation onto substrates. *Courtesy Kurt J. Lesker Company.

film homogeneity. The distance from the source to the substrate was fixed at 8 inches in the current system. The substrate holder had an optional heating element with a maximum achievable temperature of 300 °C. Raw materials were placed in evaporation source holders, i.e. tungsten or tantalum boats or aluminum oxide crucibles, which were restively heated under vacuum, for example 10^{-6} torr. Deposition rate was controlled by a PID controller, which adjusted current through the thermal sources upon receiving feedback from a deposition rate monitor. Thought not tested in this study, inert processing gasses, such as N_2 or Argon may be fed into the process chamber in order to aid film homogeneity.

3.2 Irradiation

The x ray beams used in this study had nominal energies of 6, 10, and 18 MV. Electron beams had nominal energies of 6, 9, 12, 16, and 20 MeV. The beams were generated by either a Varian 23EX, Varian Trilogy (Varian Medical Systems, Palo Alto, CA), or an Elekta Precise (Elekta, Norcross, GA) linear accelerator, calibrated according to the American Association of Physicists in Medicine's TG-51 protocol [119]. The dosimeter plane was oriented perpendicular to the beam central axis for all irradiations. The nominal dose rate was 600 MU/min unless otherwise noted.

For dose escalations greater than 300 Gy, a high dose rate ^{137}Cs irradiator (J. L. Shepherd and Associates, Mark I Model 25, San Fernando, CA) was utilized. Based on factory

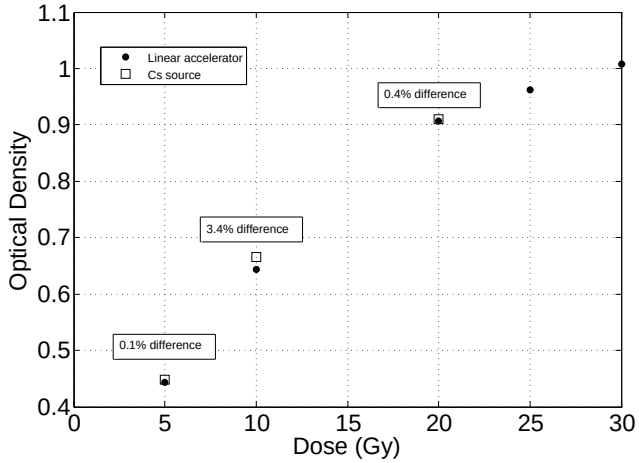

Figure 3.9: Verification of ^{137}Cs dose. 2 cm × 3 cm pieces of radiochromic film were exposed by a 6 MV beam of a linear accelerator and a high dose rate ^{137}Cs source to the same dose. Films were read on a manual densitometer. Results were found to be comparable for both sources.

calibrations and isodose curves, the dose rate to water was 10.7 Gy/min, corrected for decay to the time of irradiation. Dosimeters were mounted on a styrofoam block that was cut to place the dosimeters near the center of the irradiation chamber. During irradiation, the block was rotated to mitigate any inverse-square distance dependence of dose delivery to individual chips. An isodose plot for the irradiation chamber, accounting for rotation along

the central axis of the chamber, is included in appendix B. Dosimetry for the irradiation position at the center of the chamber was verified with 2 × 3 cm^2 pieces of radiochromic film (EBT2, International Specialty Products, Wayne, NJ) irradiated to the same dose in both the ^{137}Cs irradiator and a calibrated linear accelerator. Optical densities were read on a manual densitometer (Digital Densitometer II, Victoreen) and compared. Results shown in figure 3.9 give confidence in the ^{137}Cs irradiator dose delivery.

3.3 PSL Readout

3.3.1 Pellet Dosimeter Readout

The basic optical set up for detecting PSL is diagramed in figure 3.10. Straightforward, continuous-wave luminescence was applied for stimulation [13]. The stimulation power was supplied by either a 100 W quartz tungsten-halogen lamp (Newport, Stratford, CT), 150 W UV enhanced Xe lamp (Newport), or a 5mW, 594 nm He-Ne laser (Melles Griot, Covina, CA). The stimulation wavelength was selected by a motorized monochromator (Cornerstone 130, Newport) with a grating of 1200 lines/mm. The monochromator had an integrated shutter that was controlled through a GPIB interface and used to switch the stimulation light on and off. The stimulation light was chopped with an optical chopper (Model SR540, Stanford Research System, Sunnyvale, CA) in order to provide a reference signal to a lock-in amplifier for phase sensitive detection. The stimulation light was focused by a series of lenses and directed to an integrating, or Ulbricht, sphere with multiple ports (LabSphere, North Sutton, NH) to which samples were mounted. A photomultiplier tube (PMT, Hamamatsu, Bridgewater, NJ) collected and amplified the PSL signals. The gain on the PMT was controlled by a DC power source (Model PS310, Stanford Research Systems) that supplied a high voltage up to 1.25 kV. Optical glass filters, e.g., BG3 and BG39, were used between the integrating sphere port and the PMT tube as necessary to separate out the stimulating light. PMT output current was converted to voltage that was measured by a dual-channel lock-in amplifier (Model SR830, Stanford Research Systems). The system was controlled

through a GPIB interface. LabVIEW and Matlab programs automated the data collection and processing.

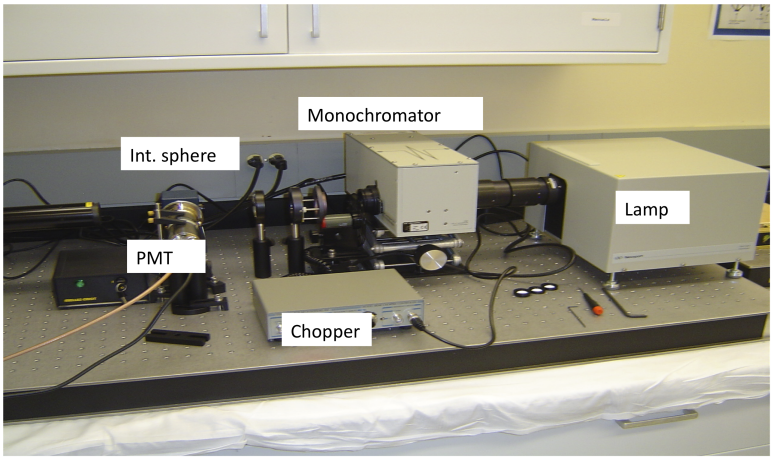

Figure 3.10: Readout system [13]. Photostimulated luminescence signals are collected by an integrating sphere and detected by a photomultiplier tube. The stimulation source is either a yellow He-Ne laser (left), a quartz tungsten halogen lamp (right), or a UV enhanced Xe arc lamp, coupled with a monochromator for stimulation wavelength selection.

Prior to irradiation, dosimeters were optically bleached with a high intensity lamp to mitigate the influence of self dose or environmental dose. For chip-style measurements, dosimeters were mounted either on a port opposite the stimulating light or directly in line with the stimulating light. A typical reading involved opening the shutter, waiting 1 s for the signal to stabilize, and then taking 10 consecutive measurements at a time interval of 100 ms. The mean of the 10 measurements was recorded as a reading.

PSL simulation and emission spectra were obtained by scanning the monochromator over a certain wavelength range in 1 nm increments while the PSL signals were collected through a narrow bandpass filter. The stimulation spectra were then corrected for the diffraction efficiency of the grating and the simulation power as a function of wavelength, as measured by a silicon photodiode (Model FDS100-CAL, Thorlabs, Newton, NJ). To obtain the emission spectra, a 5 mW, 594 nm He-Ne laser was used in place of the halogen lamp for stimulation. The laser power was attenuated with neutral density filters to minimize the amount of signal loss during scanning. The monochromator was placed between the

integrating sphere and the PMT, which was fit with a bandpass filters. The emission spectrum was obtained by scanning the monochromator over a certain wavelength range while the stimulation light was applied.

3.3.2 Panel Dosimeter Readout

For 2-D scanner measurements, a precision tilter that holds the SPP in place was fit to a 2-D array of linear slides positioned in-line with the laser light as shown in figure 3.11 and figure 3.12. The plate was scanned in front of the laser, which was turned on for a line scan and blocked when the slides moved to the next row. Spatial resolution was determined by the range of travel between pulses that triggered data acquisition.

3.4 Uncertainty and Error Handling

The major sources of experimental uncertainty were the positioning error of dosimeters during readout and the stability of the stimulation lamp. Measurements were found to be sensitive to the mounting of the dosimeters on the integrating sphere. From an estimate of repeated readings, the uncertainty related to mounting is 2-3%. The long term fluctuation of the stimulation power was also detected to be up to 2% during 24 h monitored by a Si photodiode. For all chip-style measurements, each dosimeter was read two or three times, including removing the dosimeter from the integrating sphere port and remounting. The readings were corrected for partial depletion, averaged, and corrected for chip factor. The standard error of repeated readings was taken as the experimental uncertainty [120].

The background signals consist of a DC component and a random noise signal. The DC signal was largely due to the leakage of the ambient light, e.g. from a computer monitor, luminescence centers generated by cosmic radiation and the bleaching lamp, as well as the PMT dark current. This DC signal can be as large as a few percent of the total signal, depending on the dose and stimulation power and can be removed by subtraction. The background noise, which is thermal and electronic in origin, ultimately defines the minimum

detectable limit. For a typical dose of 200 cGy, a signal-to-noise ratio of greater than 250 can be readily achieved.

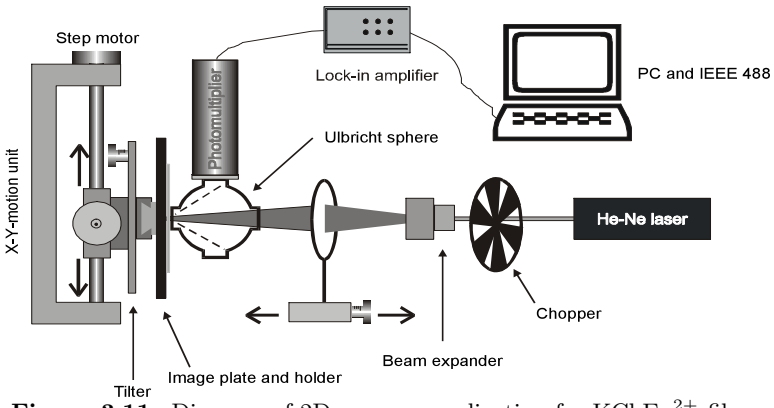

Figure 3.11: Diagram of 2D scanner application for KCl:Eu^{2+} films.

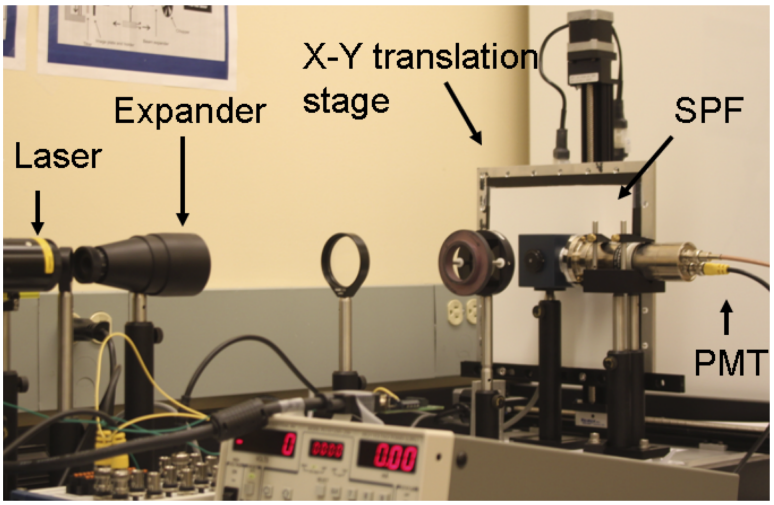

Figure 3.12: Photograph of 2D scanner application. The current setup is capable of providing sub-millimeter spatial resolution and a sub 20 minute scan time for a 17×17 cm^2 scan area. Data is simultaneously sampled from the signal generating PMT and a reference diode (not shown) in order to correct for laser power fluctuation. Laser spot size is controlled by a precision micrometer and is typically 0.1 mm.

Chapter 4

Principle Data and Process Improvement

This chapter presents preliminary results of KCl:Eu^{2+} applied to quantitative dosimetry. The readout system developed in chapter 3 was confirmed for PSL measurements with commercial $BaFBr_{0.85}I_{0.15}$:Eu^{2+} dosimeters. Then prototype pellet KCl:Eu^{2+} dosimeters were fabricated in house and read out on the same optical system. KCl:Eu^{2+} dose response was characterizable after irradiation from 0 to 800 cGy. The photostimulated luminescence (PSL) signal stabilized to 0.1% decrease/h after 12 h. Sensitivity was independent of dose rate from 15 to 1000 cGy/min and also independent of beam energy for either open x ray or megavoltage electron fields. Over-response to low-energy scattered photons was comparable to radiographic film, e.g., Kodak XV. Maximum PSL sensitivity occurred when KCl:Eu^{2+} pellets were sintered at 710 °C. Annealing the sintered chips at temperatures from 100 to 350 °C did not improve sensitivity and below 200 °C had a negative impact. Sensitivity increased with doping concentration but began to level after 0.25 %mol, likely due to concentration quenching. In summary, this data establishes KCl:Eu^{2+} as a promising radiation therapy dosimetry material and further motivates the radiation hardness study in chapter 5.

4.1 Benchmarking

4.1.1 Materials and Methods

Dosimeters and Phantom

Two thicknesses of $BaFBr_{0.85}I_{0.15}:Eu^{2+}$ were studied, 300 μm (Agfa MD10, Eastman Kodak, Rochester, NY) and 50 μm (research sample), in order to examine irradiation and readout processes. Cylindrical dosimeters 7 mm diameter were cut from 2D dosimeters with a hole punch. Solid water (SW-457, Gammex RMI, Middleton, WI) plates, with areas of 40×40 cm^2, were stacked to yield desired thicknesses for the phantom. A 5 mm thick slab with a linear array of holes machined 7.5 mm in diameter and 2 mm in depth served to host the dosimeters during irradiation. Central axis measurements were acquired in the following studies, thus the dosimeters were placed at the center hole. Prior to irradiation, the dosimeters were optically bleached (annealed) for 5 s using a 500 W tungsten-halogen lamp.

Irradiations

The x ray beams used in the following tests had a nominal energy of 6 MV (Varian 23EX). The dosimeter plane was oriented perpendicular to the beam central axis for all irradiations. The nominal dose rate was 600 MU/min. Due to the limited availability of accelerators, and to provide consistent experimental conditions, the irradiations were performed during the evenings. The irradiated dosimeters were kept in the dark at room temperature and read on the next day after a fixed delay time of 16 hours between irradiation and readout.

Readout

Chips were read using the optical setup illustrated in figure 3.10. Before each irradiation session, the dosimeters were irradiated to 200 cGy in an open field in order to determine

the relative sensitivity or response normalization (i.e., "chip-factor") of each dosimeter. Background signals were measured by placing unirradiated dosimeters on the integrating sphere.

Measurements

The following tests were conducted:

1. Dose Response. The material's response to absorbed dose was determined by taking a sensitometric curve over the dose range of 140 cGy to 380 cGy at a depth of 10 cm and a field size of 10×10 cm^2.

2. Energy Dependence. Field size and depth measurements were performed to determine the relative sensitivity of the material to altered fluence spectra. As the field size and depth increase, the ratio of low-energy scattered photons to primary photons in the beam also increases. Thus detectors that are oversensitive to low-energy photons will tend to overestimate the dose at the portal center. These data are indicative of the effect of using a single dose response calibration curve for measurements with multiple effective field sizes and multiple depths.

The dosimeters were irradiated at isocenter to 200 cGy (SAD = 100 cm) at four depths (5 cm to 20 cm) for each of five square field sizes (5×5 cm^2 to 25×25 cm^2). The ratio of the measured dose using the calibration/sensitometric curve (see above) to the dose measured at the calibration point was used to indicate the magnitude of dose measurement error.

For comparison, sensitometric and field size and depth measurements were repeated using Kodak XV radiographic films. The effective atomic number for these films is 43 (vs. 49 for $BaFBr_{0.85}I_{0.15}$:Eu^{2+}). Because of the shallow dose range of XV film, doses were scaled down to around 30 cGy. A non-irradiated but processed film was used as a background measurement. The films were processed using a diagnostic quality film processor (Kodak RP X-Omat Processor, Eastman Kodak Co., Rochester, NY) and the optical densities (ODs) were measured using a calibrated manual densitometer (Digital Densitometer II,

Victoreen). Only films from the same box were used for each measurement session and the OD measurement was taken at the field center.

3. Spectroscopic Data. In order to test the scanning features of the readout system, stimulation and emission spectra were obtained for $BaFBr_{0.85}I_{0.15}$:$Eu^{2+}$and the results compared to published data. The stimulation spectra were obtained by scanning the monochromator between 475 nm and 750 nm in 1 nm increments while the PSL signals from the 300 μm commercial phosphor samples were collected through a narrow bandpass filter (FB390-10, Newport). Since stimulation power can vary as a function of wavelength and diffraction efficiency of the monochromator's grading, the spectra were corrected based on measurements with a calibrated silicon photodiode (Model FDS-100-CAL, Thor Labs, Newton, NJ). The emission spectrum was obtained by scanning the monochromator from 350 nm to 450 nm with a 1 nm step.

4.1.2 Results

Sensitivity

Figure 4.1 shows a linear response to dose for a 6 MV beam over the range 140-380 cGy, for both the thick and thin $BaFBr_{0.85}I_{0.15}$:Eu^{2+} dosimeters. The 300 μm chip data fit the line $y = 9.2 * 10^{-5}x + 6 * 10^{-5}$ and the 50 μm data fit the line $y = 2.4 * 10^{-5}x - 1.5 * 10^{-5}$.

Figure 4.2 shows XV film response to dose from a 6 MV beam. The film sat overnight prior to readout on the digital densitometer. The data fit the line $y = 0.023x + 0.076$.

Field Size and Depth Dependence

Sensitometric data were then used to to generate data on the energy response of both $BaFBr_{0.85}I_{0.15}$:Eu^{2+} and XV film. Figure 4.3(a) and figure 4.3(b) show the dosimeters' response to increasing field sizes and depths. The results were normalized to the calibration conditions, i.e., at a depth of 10 cm in a 10×10 cm^2 field. A maximum over-response of 82% was observed for the thick chips and 118% for the thin chips in the largest field and depth (25x25 cm^2 and 20 cm, respectively) used in this study. The composition of the thin

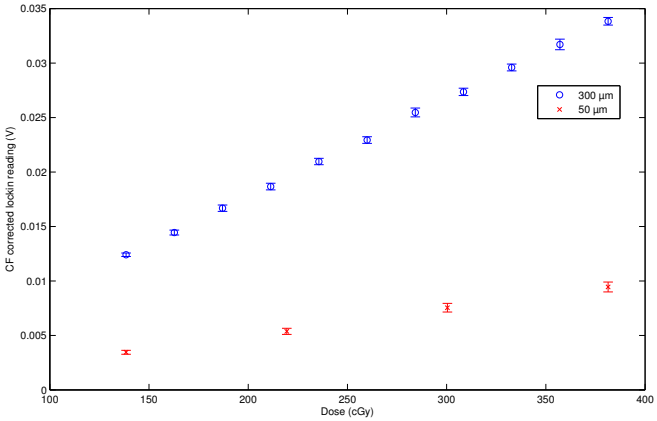

Figure 4.1: $BaFBr_{0.85}I_{0.15}:Eu^{2+}$ dosimeters' response to x ray dose from a 6 MV beam. Readout was 16 hours after irradiation. Response over this dose region is linear, with the 300 μm data fitting the line $y = 9.2 * 10^{-5}x + 6 * 10^{-5}$ and the 50 μm data fitting the line $y = 2.4 * 10^{-5}x - 1.5 * 10^{-5}$. Error bars represent the standard error of repeated measurements.

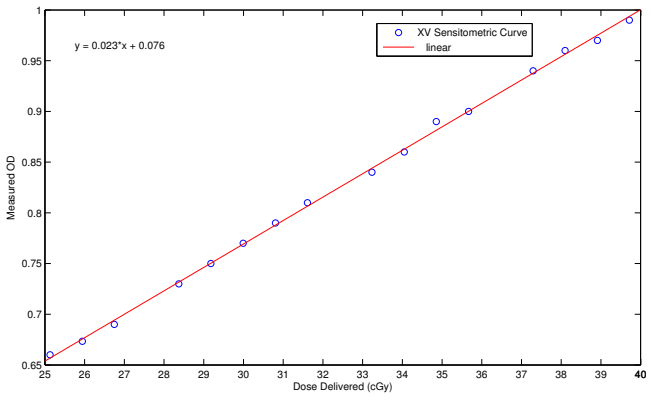

Figure 4.2: XV film response to 6 MV x ray dose. Response over this dose region is linear, with the data fitting the line $y = 0.023x + 0.076$.

chips was unknown (but was thought to be similar to $BaFBr_{0.85}I_{0.15}$:Eu^{2+}), which made direct comparison of the two chips difficult; however, reducing the thickness to 50 μm did not improve the over-response.

Interestingly, XV film showed a significantly improved low-energy photon response, as indicated by figure 4.4, even though the sensitive layer consists of AgBr which has an effective atomic number of 43. A maximum over-response of 8% was observed for largest field and depth (25x25 cm^2 and 20 cm, respectively) used in this study.

Spectra

Figure 4.5 shows the stimulation and emission spectra for a 300 μm commercial phosphor sample. When stimulated, the $BaFBr_{0.85}I_{0.15}$:Eu^{2+}dosimeter emits intense PSL centered at 398 nm. The maximum stimulation efficiency occurs at 600 nm (the peak of the stimulation spectrum). These findings agree with previously published reports.

4.1.3 Discussion

Based on the literature review in chapter 2, a linear response to absorbed dose was expected for $BaFBr_{0.85}I_{0.15}$:Eu^{2+}. Additionally, a strong over-response to low energy photons was expected since the material has a relatively high effective atomic number. However, XV film, with an effective atomic number of 43, had a much reduced over-response compared to the commercial phosphor. It will be argued in chapter 6 that this observation can be attributed to the difference in the thickness of the active layer in the two materials.

The readout system developed in chapter 3 is well suited for PSL measurements as the data collected for $BaFBr_{0.85}I_{0.15}$:Eu^{2+} agrees with published data. The system is flexible enough to allow for single point measurements or automated scanning.

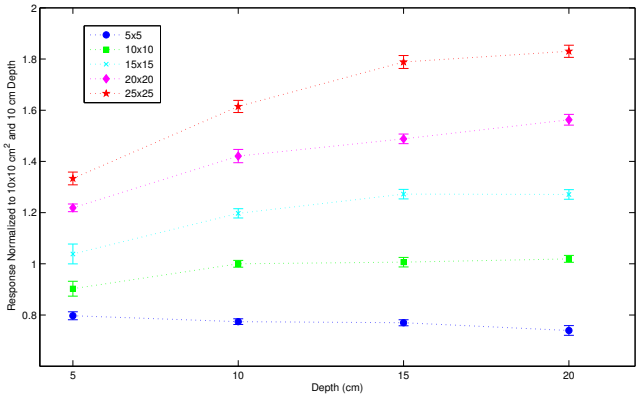

(a) 300 μm $BaFBr_{0.85}I_{0.15}$:Eu^{2+} chips.

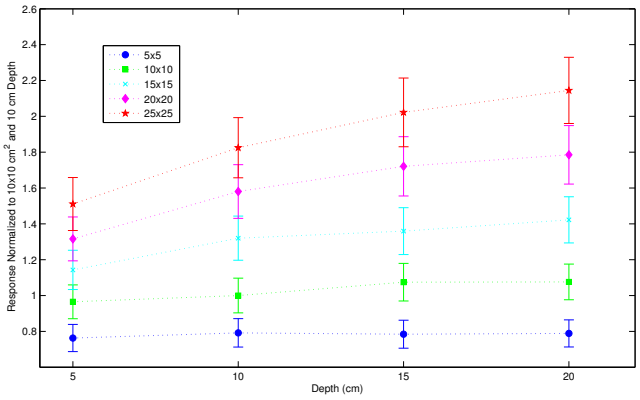

(b) 50 μm BaFBr chips.

Figure 4.3: The relative sensitivity of $BaFBr_{0.85}I_{0.15}$:Eu^{2+} dosimeters as a function of field size and depth. The results are normalized to the calibration conditions, i.e., at a depth of 10 cm in a 10×10 cm^2 field. As the field size and depth increase, the dosimeters' sensitivities increase due to the increase in the scatter-to-primary ratio. As a result, a maximum over-response of 82% was observed for the thick chips and 118% for the thin chips in the largest field and depth (25×25 cm^2 and 20 cm, respectively) used in this study. Error bars represent the standard error of repeated measurements.

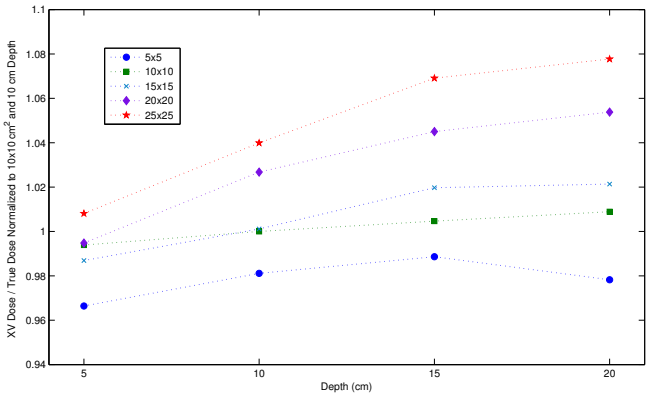

Figure 4.4: The relative sensitivity of XV film dosimeters as a function of field size and depth. The results are normalized to the calibration conditions, i.e., at a depth of 10 cm in a 10×10 cm^2 field. As the field size and depth increase, the film sensitivity increase due to the increase in the scatter-to-primary ratio. As a result, a maximum over-response of 8% was observed for largest field and depth (25×25 cm^2 and 20 cm, respectively) used in this study. An over-response of 82% was observed for a $BaFBr_{0.85}I_{0.15}:Eu^{2+}$ commercial plate.

4.2 Pellet KCl:Eu^{2+} Dosimeters

Based on the previous section, the readout system is appropriate for PSL measurements. In this section, KCl:Eu^{2+} dosimeters were fabricated for proof-of-concept measurements.

4.2.1 Materials and Methods

Dosimeters and Phantom

Cylindrical KCl:Eu^{2+} dosimeters, 7 mm in diameter and 1 mm thick, shown in figure 3.6, were fabricated according to the methodology presented in chapter 3. In this case, raw materials of KCl and $EuCl_3 \cdot 6H_2O$ were mixed thoroughly in a planetary ball mill and the resulting polycrystalline powders were pressed (i.e., without preheating) at an average force of 6 T for 10 minutes. The chips were sintered in a tube furnace in air for 3 hours at 710 °C. This was followed by a cooling down period to 300 °C and a rapid cooling to room temperature. The irradiation phantom was described in section 4.1.1. The dosimeters were optically annealed prior to irradiation.

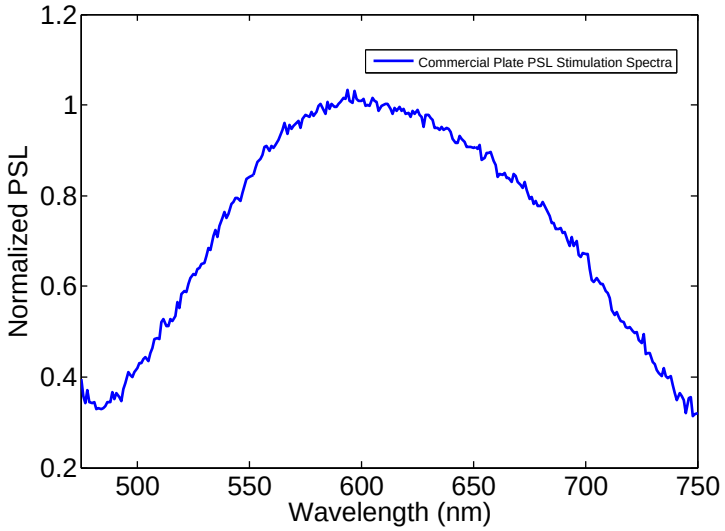

(a) $BaFBr_{0.85}I_{0.15}:Eu^{2+}$ PSL stimulation spectra.

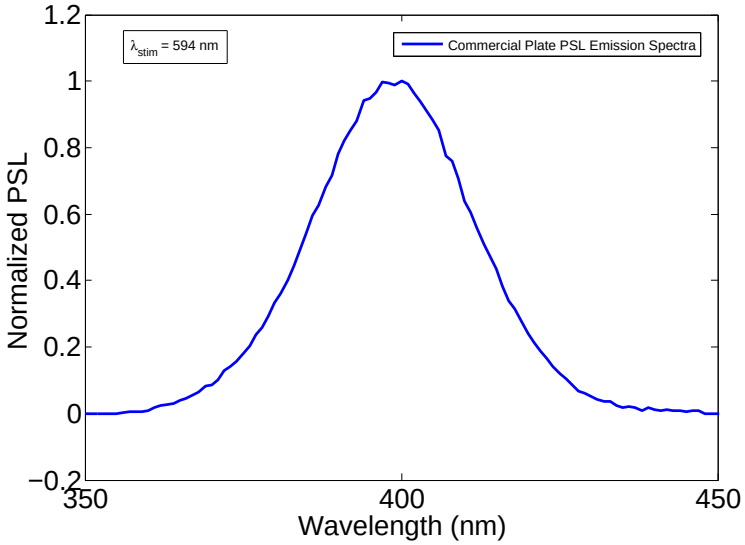

(b) $BaFBr_{0.85}I_{0.15}:Eu^{2+}$ CR PSL emission spectra.

Figure 4.5: Stimulation and emission spectra of $BaFBr_{0.85}I_{0.15}:Eu^{2+}$dosimeters. When stimulated, the $BaFBr_{0.85}I_{0.15}:Eu^{2+}$dosimeter emits intense PSL centered at 390 nm. The maximum stimulation efficiency occurs at 600 nm (the peak of the stimulation spectrum).

Irradiation

The x ray beams used in this study had nominal energies of 6, 10, and 18 MV. Electron beams had nominal energies of 6, 9, 12, 16, and 20 MeV. The beams were generated by a Varian 23EX (Varian Medical Systems, Palo Alto, CA) or an Elekta Precise (Elekta, Norcross, GA) linear accelerator. The nominal dose rate was 600 MU/min unless otherwise noted.

Readout

The dosimeters were read using the setup illustrated in figure 3.10. The stimulation power was supplied by a 100 W quartz tungsten-halogen lamp (Newport, Stratford, CT). The stimulation wavelength of 600 nm was selected using a motorized monochromator (Cornerstone 130, Newport) and interface as described in section 3.3.1.

Measurements

Dosimeter readout was examined through the following tests:

1. Stimulation and emission spectra. The stimulation spectra were obtained by scanning the monochromator between 450 nm and 700 nm in 1 nm increments while the PSL signals were collected through a narrow bandpass filter (FB420-10, Newport) and correcting the measured data for stimulation power as a function of wavelength (cf. section 4.1.1). The emission spectrum was obtained by scanning the monochromator from 300 nm to 540 nm with a 0.5 nm step.

2. Readout signal depletion. A KCl:Eu^{2+} dosimeter stores dose information in the form of trapped electrons and holes formed during ionizing irradiation. Dose information can be read out repeatedly by multiple stimulations using the current setup; however, each subsequent reading will have slightly decreased signal strength due to partial depletion of the trapped electrons by previous readouts. The readout signal loss was measured by taking 30 consecutive readings at an interval of 10 s on a single dosimeter 13 hours after irradiation.

3. Signal stability. From chapter 2, an important characteristic of a storage phosphor

is the signal decrease over time. To measure this property, KCl:Eu^{2+} dosimeters were irradiated by a dose of 200 cGy and read repeatedly for 24 hours, beginning immediately after irradiation. Each reading was corrected for the reading signal depletion as measured above.

In general, a fixed time delay between irradiation and readout was used to minimize errors associated with variable signal fading. In order to measure the impact of fading, a batch of 8 dosimeters was exposed to a 6 MV beam up to 400 cGy and read at delay times of 20, 44 and 68 hours. The results were normalized to the readings at 100 cGy and compared.

The following dosimetric tests were conducted:

1. Radiation hardness. Three dosimeters were first irradiated with 0, 100, and 200 Gy by a 6 MV beam. These dosimeters were subsequently bleached, irradiated to 200 cGy, and read.

2. Dose response. 12 dosimeters were irradiated individually up to 800 cGy with a source-to-surface distance (SSD) of 90 cm, depth of 10 cm and field size of 20×20 cm^2 using 6, 10, and 18 MV beams.

3. Beam energy dependence. For megavoltage x ray beams, dosimeters were irradiated using 6, 10, and 18 MV photons at an SSD of 90 cm, a depth of 10 cm and a field size of 20×20 cm^2. For the electron beams, the dosimeters were irradiated using 6, 9, 12, 16, and 20 MeV electron beams with the dosimeters placed at the respective depths of maximum dose (d_{max}).

4. Dose rate dependence. The dose rate dependence was investigated using a 6 MV beam. The dosimeters were placed at d_{max} (1.5 cm) with a field size of 10×10 cm^2 and an SSD of 100 cm. Nominal dose rates of 100, 200, 300, 400, 500, and 600 cGy/min (based on the same number of MU/min) were delivered by changing the accelerator repetition rate. A lower dose rate of 15 cGy/min was achieved by irradiating the dosimeter underneath fully closed multileaf collimators (MLCs). A dose rate of 16.5 cGy/min was achieved at an SSD

of 424.5 cm. A higher dose rate of 1000 cGy/min was achieved by reducing the SSD to 77 cm. At each dose rate, a dose of 100 cGy was delivered to the dosimeter.

5. Field size and depth dependence. Similar to section 4.1.1, the dosimeters were irradiated at isocenter to 200 cGy (SAD = 100 cm) at four depths (5 cm to 20 cm) for each of five square field sizes (5×5 cm^2 to 25×25 cm^2). A sensitometric curve for the dose range of 170 cGy to 250 cGy was obtained at a depth of 10 cm and a field size of 10×10 cm^2 and the magnitude of the dose measurement error relative to calibration conditions was computed.

6. Field size and depth dependence with low-energy photon filters. As stated in section 2.1.2, lead filtration can remove residual energy dependence by preferentially removing low energy photons from the incident spectrum. The above field size and depth dependence measurements were repeated with two 0.3-mm-thick lead foils sandwiching the dosimeters, separated by 6 mm solid water material upstream and 3 mm downstream.

4.2.2 Results

Stimulation and Emission Spectra

Figure 4.6 shows the emission and stimulation spectra of KCl:Eu^{2+}dosimeters after x ray irradiation. The PSL emission peak was broad band centered at 420 nm when stimulated with a yellow (594 nm) Ne-Ne laser. This peak corresponds to the emission band of F-centers. The maximum stimulation efficiency occurred at 570 nm, which was subsequently selected as the readout wavelength in studies presented below. These findings are consistent with previously published reports [12, 45, 46].

Readout Signal Depletion

Figure 4.7 shows the results of 30 consecutive readings taken at 10 s intervals 13 hours after irradiation. The signal decrease was due to partial depletion of trapped electrons. A linear fit to the readings gives a slope of -0.0027, indicating that each reading depleted approximately 0.27% of trapped electrons using light from the monochromator. Note that

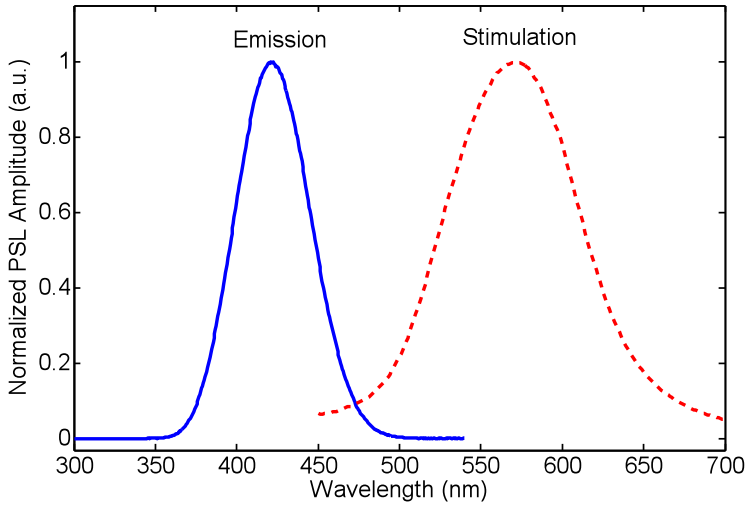

Figure 4.6: Stimulation and emission spectra of KCl:Eu^{2+}dosimeters, from [13] with permission throughout. When stimulated, the KCl:Eu^{2+}dosimeter emits intense PSL centered at 420 nm. The maximum stimulation efficiency occurs at 570 nm (the peak of the stimulation spectrum).

a smaller readout depth can be achieved by attenuating the stimulation light with gray filters. However, this would come at the expense of signal strength.

Signal Stability

Characteristic signal stability curves are shown in figure 4.8. The curve was corrected for readout signal depletion of 0.27% per readout. 63% of the signal remained after 12 h, after which the dosimeter stabilized to 0.1%decrease/h. The relatively fast fading during the first few hours could be due to shallow charge traps in the forbidden band, which are thermally emptied. This is consistent with the finding that the PSL remains almost the same after wait times of 20, 44, or 68 hours (figure 4.10(b)).

Also shown in figure 4.8 is the signal stability curve for a commercial Agfa MD10 CR plate. The stimulation wavelength was 620 nm, corresponding to the maximum stimulation efficiency for $BaFBr_{0.85}I_{0.15}$:Eu^{2+}. Based on 30 consecutive readings, a depletion rate of 0.07% was obtained, which was taken into account in the fading curve. After 12 hours, the

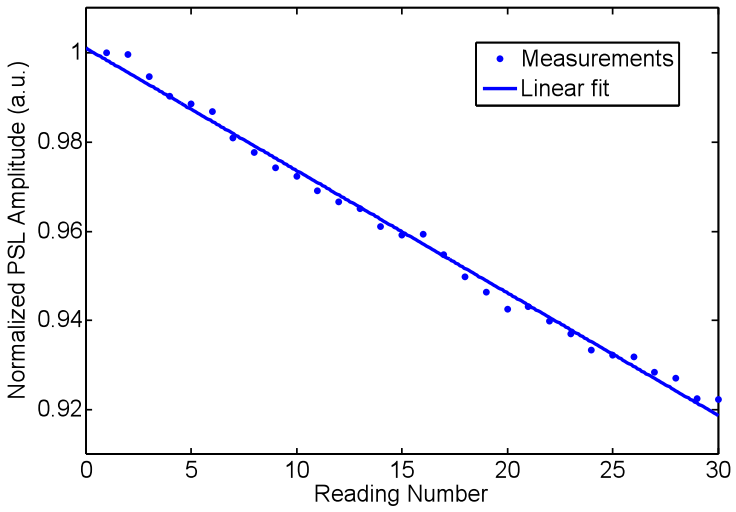

Figure 4.7: Readout loss due to partial depletion of trapped electrons after repeated readings [13]. A KCl:Eu^{2+}dosimeter was kept in the dark for 13 hours after x ray irradiation. Thirty consecutive readings were then made at a 10 s interval. A linear fit to the data indicated a depletion of approximately 0.27% of trapped electrons using light from the monochromator. A smaller readout depth can be achieved by attenuating the stimulation light with gray filters.

KCl:Eu^{2+}dosimeters have slower fading rates than $BaFBr_{0.85}I_{0.15}$:Eu^{2+}.

Radiation Hardness

As shown in figure 4.9, there was no significant change in the stimulation spectrum after irradiation to 100 and 200 Gy, compared to a fresh dosimeter. This indicates that the lattice of the dosimeter remained nearly intact after irradiation to 200 Gy. The slight red shift with higher dose history could be due to an increased creation of M(Cl^-) centers, the aggregate of two neighboring chlorine ion vacancies occupied by two electrons [72]. A 15% loss in sensitivity was observed for an accumulated dose of 50 Gy. Little further loss was detected up to 200 Gy.

Dose Response

KCl:Eu^{2+}dose response to 6 and 18 MV beams is show in figure 4.10(a). The two curves agreed with each other within 2%. Similar to TLDs, the material exhibited a supralinear

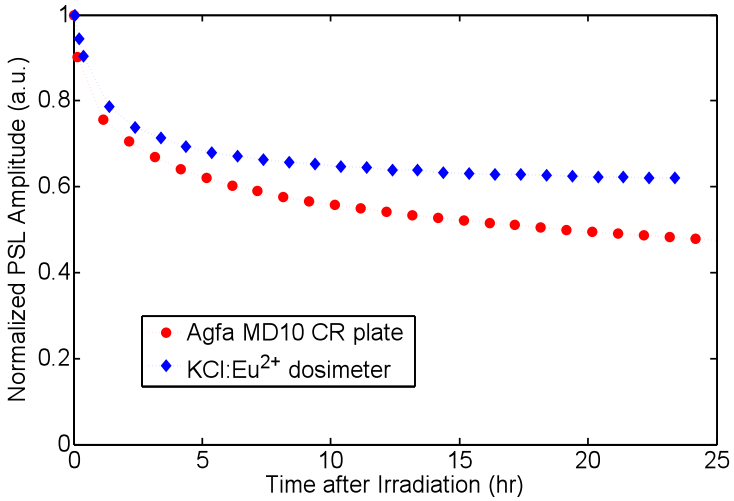

Figure 4.8: Signal stability over time [13]. The fading of KCl:Eu^{2+}(diamonds) consists of an initially rapid component followed by a slower component. The signal eventually reaches a rate of 0.1%/hour. 63% of the signal remains after 12 h. For comparison, the fading of a commercial plate, the Agfa MD10 CR, is also shown (circles). KCl:Eu^{2+}dosimeters exhibit reduced signal fading characteristics.

response to dose [111]. Figure 4.10(b) shows the measurements, normalized to the readings at 100 cGy, for a batch of eight dosimeters exposed to the 6 MV beam up to 400 cGy and read at different delay times of 20, 44, and 68 h. As the delay time increased, the PSL signal decreased following the fading curve (figure 4.8); however, the normalized curves agreed with each other within the experimental uncertainty, indicating no delay time effect. Therefore, absolute doses can be deduced from readings at any time provided the signal stability curve is known.

Beam Energy Dependence

The sensitivity dependence on nominal incident beam energy is summarized in figure 4.11. Within a measurement uncertainty of ±2.5%, the KCl:Eu^{2+} dosimeters showed no energy dependence for either open field x rays or megavoltage electrons commonly available from a multi-modality linear accelerator.

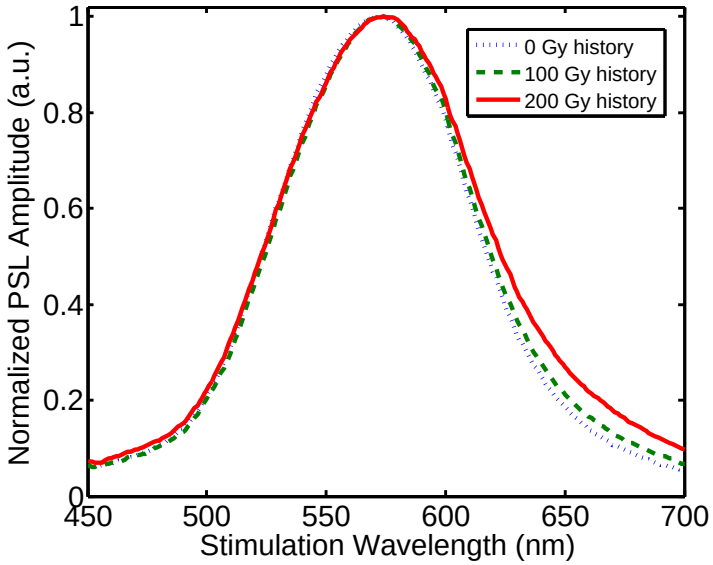

Figure 4.9: Radiation hardness up to 200 Gy [13]. Three KCl:Eu^{2+}dosimeters were given 0, 100, and 200 Gy, respectively, from a 6 MV beam. They were subsequently bleached, irradiated to 200 cGy, and read. No significant change in the stimulation spectra is observed, indicating that KCl:Eu^{2+}has satisfactory radiation resistance.

Dose Rate Dependence

Figure 4.12 summarizes the sensitivity variations of KCl:Eu^{2+} dosimeters as a function of dose rate after irradiation by a 6 MV beam. There was no variation in sensitivity for dose rates ranging from 15 cGy/min (underneath a fully closed MLC) to 1000 cGy/min (at an SSD of 77 cm) within a measurement uncertainty of $\pm 2.5\%$.

Field Size and Depth Dependence

The effective atomic number for KCl:Eu^{2+} material is 18 (since the amount of europium is on the order of ppm it has a negligible contribution to the effective Z). Due to the Z^3-dependence of the photoelectric mass attenuation coefficient, an over-response to low-energy scattered photons was expected for KCl:Eu^{2+} dosimeters. As a result, a maximum over-response of 12% was observed in the largest field and depth (25×25 cm^2 and 20 cm, respectively) used in this study. This was substantially reduced from the commercial phos-

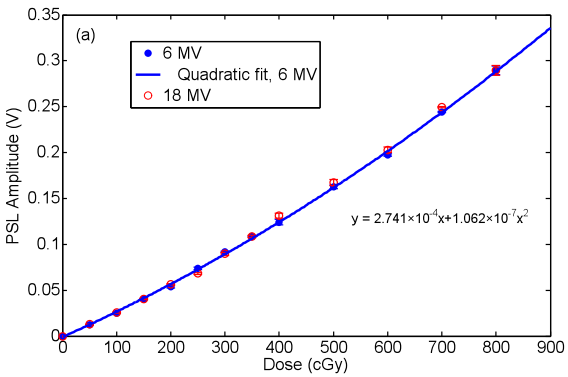

(a) KCl:Eu^{2+}response to dose from 6 and 18 MV beams.

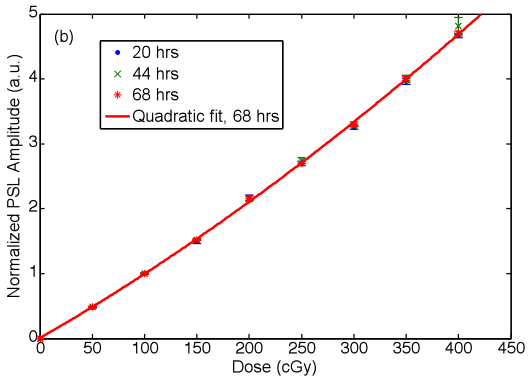

(b) KCl:Eu^{2+}dose response from 6 MV beam with readout delay.

Figure 4.10: Response of KCl:Eu^{2+}dosimeters to absorbed dose [13]. (a) Readout was made 20 h after irradiation. The dose response shows supralinear behavior, which can be fit with a second order polynomial. The response is independent of beam energy to within 2%. (b) Readout was made at different delay times after irradiation by a 6 MV beam. The normalized response shows no dependence on delay time. Error bars represent the standard error of repeated measurements.

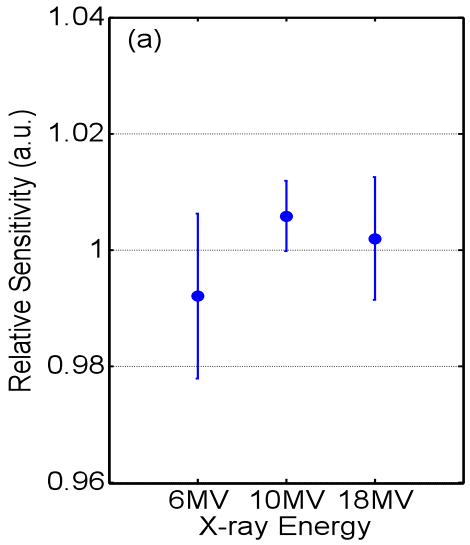

(a) KCl:Eu^{2+}response to dose from 6 and 18 MV beams.

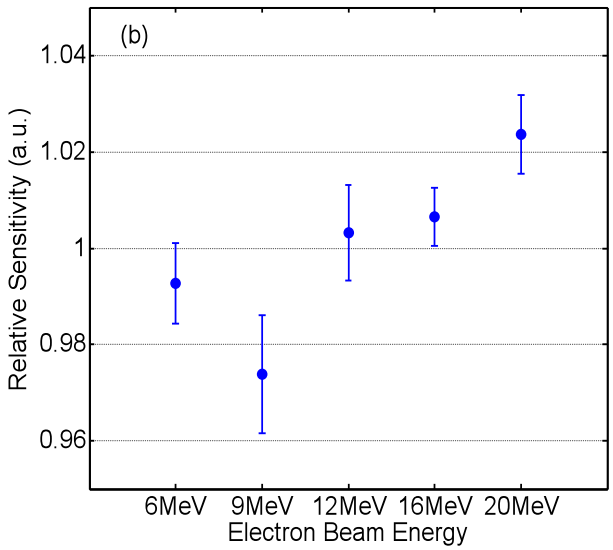

(b) KCl:Eu^{2+}response to dose from common electron beams.

Figure 4.11: KCl:Eu^{2+} dosimeter relative sensitivity versus beam mode and energy [13]. The sensitivities are normalized to their respective average values. For both x ray [4.11(a)] and electron [4.11(b)] beams commonly available from a multi-modality linear accelerator, the dosimeter's sensitivity is independent of the beam energy within ±2.5%. Error bars represent the standard error of repeated measurements.

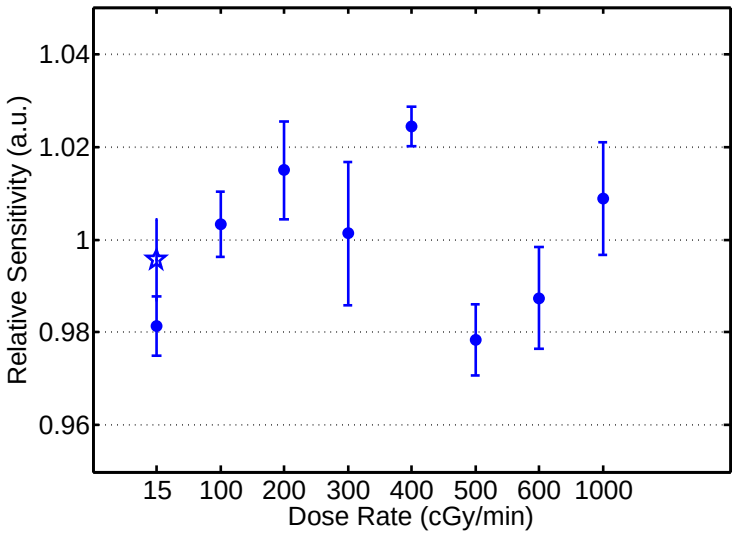

Figure 4.12: KCl:Eu^{2+} dosimeter relative sensitivity as a function of dose rate for a 6 MV x ray beam [13]. The sensitivities are normalized to their average value for all dose rates. The lowest dose rate of 15 cGy/min was achieved underneath a fully closed MLC. A dose rate of 16.5 cGy/min (star) was achieved at an SSD of 424.5 cm. The largest dose rate was achieved at an SSD of 77 cm. Within ±2.5%, the dosimeter's sensitivity shows dose rate independence from 15 cGy/min to 1000 cGy/min. Error bars represent the standard error of repeated measurements.

phor case, where as much as 82% over-response was observed (data shown in section 4.1.2). Inclusion of 0.3 mm lead foils sandwiching the dosimeters removed the over-response but introduced a depth dependence, which is shown in figure 4.14.

4.2.3 Discussion

As chapter 2 suggested, there is a need in radiation therapy for a reusable, multidimensional, water-equivalent dosimeter for beam commissioning and dose delivery validation quality assurance. Commercial computed radiography technology provides a significant avenue for advancement. Applying $BaFBr_{0.85}I_{0.15}$:Eu^{2+} CR material directly to dosimetry is not suitable, however, due to its high effective atomic number (see section 4.1.2).

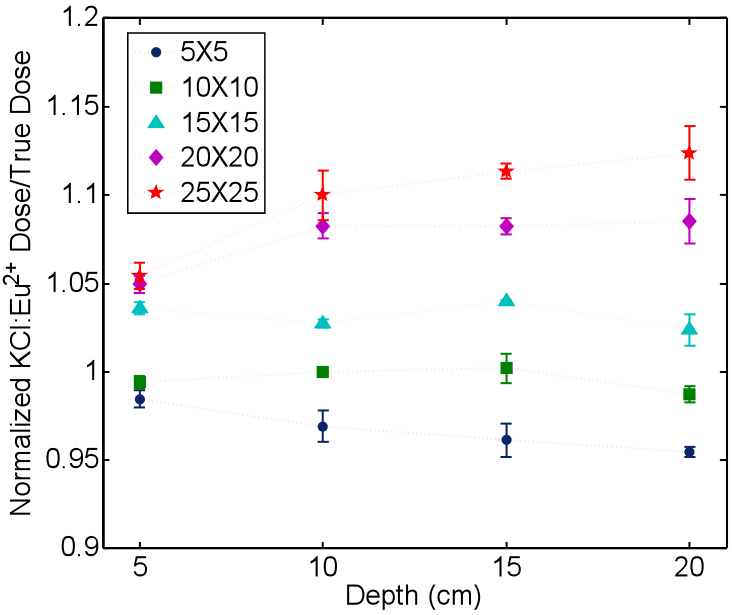

Figure 4.13: The relative sensitivity of KCl:Eu^{2+} dosimeters as a function of field size and depth [13]. The results were normalized to the calibration conditions, i.e., at a depth of 10 cm in a 10×10 cm^2 field. As the field size and depth increase, the dosimeters sensitivities increase due to the increase in the scatter-to-primary ratio. As a result, a maximum over-response of 12% was observed in the largest field and depth (25×25 cm^2 and 20 cm, respectively) used in this study. This represents a significant reduction from a value of 82% observed (data shown in appendix 4.1.2) for an Agfa MD10 CR plate at the same conditions. Error bars represent the standard error of repeated measurements.

The data presented here suggest KCl:Eu^{2+} is conducive to radiation therapy dosimetry. Since KCl:Eu^{2+} has a substantially reduced effective atomic number compared to the commercial phosphor, a reduction in over-response to low energy photons was expected. However, XV film exhibited a reduced over-response compared to KCl:Eu^{2+}, even though it has a significantly higher atomic number (Z_{eff} = 43). It will be argued in chapter 6 that these results are likely due to the thickness of the active layer in each dosimeter. In brief, energy dependence in a dosimeter is largely due to low energy photon interactions in the sensitive volume of the material. XV film's active layer is on the order of 0.2 μm, which reduces the probability of photon interactions in this layer. Reducing the thickness also increases the probability that low energy secondary electrons created by interactions

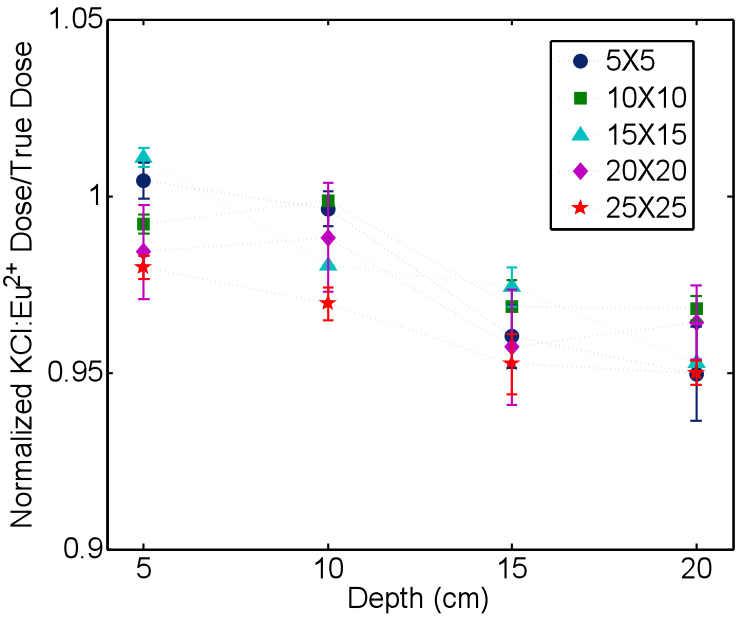

Figure 4.14: The relative sensitivity of KCl:Eu^{2+} dosimeters as a function of field size and depth in the presence of low-energy photon filters [13]. 0.3 mm lead foils sandwiching the dosimeters removed the over-response at large fields and depths. For all the field sizes the dosimeters show weak depth dependence with an approximately 2% variation from 5 cm to 20 cm. Error bars represent the standard error of repeated measurements.

in the sensitive volume will deposit a fraction of their energy outside of that volume, thus reducing the measurable energy dependent artifact.

The KCl:Eu^{2+} PSL signal stabilized to 0.1% decrease per hour 12 hours after irradiation, suggesting a convenient workflow for clinical practice. The fast fading during the first few hours after irradiation may be due to shallower electron or hole traps in the forbidden band, which is consistent with the finding that the PSL signal remains almost the same for different readout delay times. Further research would involve identifying these trapping levels through thermoluminescence or photoluminescence studies and potentially improving the fading rate though better crystal processing.

The material also had sufficient radiation hardness that allowed it to be reusable. The crystal lattice stayed nearly intact after irradiation to 200 Gy, indicating that the material could be reused up to 100 times at 2 Gy per use, as in, for example, patient specific

quality assurance. Further systematic studies are necessary to fully understand the effects of cumulated dose on the material.

4.3 Improvement of Pellet Processing

From the above data it is clear that KCl:Eu^{2+} dosimeters have many desirable properties. Further understanding of the influence of materials processing parameters is necessary for efficient and productive development of this novel material. The following investigations were carried out in order to investigate the relationship between the sensitivity of the KCl:Eu^{2+} storage phosphor and materials processing.

4.3.1 Sensitivity with Sintering Temperature

The melting point of KCl is 770 °C. While the liquid phase is favorable for ionic diffusion during sintering, operating at temperatures above the melting point may lead to uncontrolled evaporation and an uncertain stoichiometry. Higher temperatures may also mean that more europium is reduced from the 3+ valence state to the 2+ state. A series of samples were prepared to investigate the optimal sintering temperature window in terms of sensitivity and the results are show in figure 4.15. The maximum PSL output occurred at 710 °C, the highest sintering temperature used in this study.

4.3.2 Sensitivity with Annealing Temperature

As seen in chapter 2, an annealing treatment was shown to improve the sensitivity of CsBr:Eu^{2+} samples. A series of samples were prepared to investigate the optimal annealing temperature window in terms of sensitivity and the results are show in figure 4.16. PSL amplitude remained unchanged for annealing temperatures ranging from 200-350 °C but was observed to be reduced at temperatures below 200 °C.

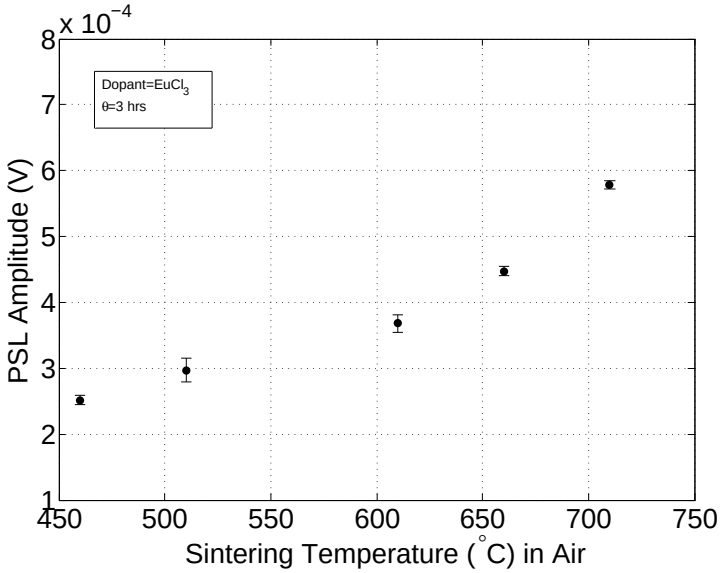

Figure 4.15: PSL vs. sintering temperature in air. Several batches of chips were pressed at 2200 lbs force and heated for three hours in air at various temperature. PSL was measured 17.5 hours after irradiation to 200 cGy. The maximum PSL output occurs at 710 °C, the highest sintering temperature used in this study. Error bars represent the standard error of repeated measurements.

4.3.3 Sensitivity with Doping Concentration

After x-ray irradiation, free electrons will be stored in anion vacancies to form F-centers while holes will be trapped at Eu^{2+} activator ions. Sufficient europium activators are necessary in order to capture adequate holes, thus producing light during readout. However, at high europium concentration, luminescence or concentration quenching may occur, leading to a decreased PSL. A series of samples with varying europium concentrations were prepared to investigate sensitivity variation with doping concentration. After 0.25 mol%, PSL amplitude began to level, likely due to concentration quenching.

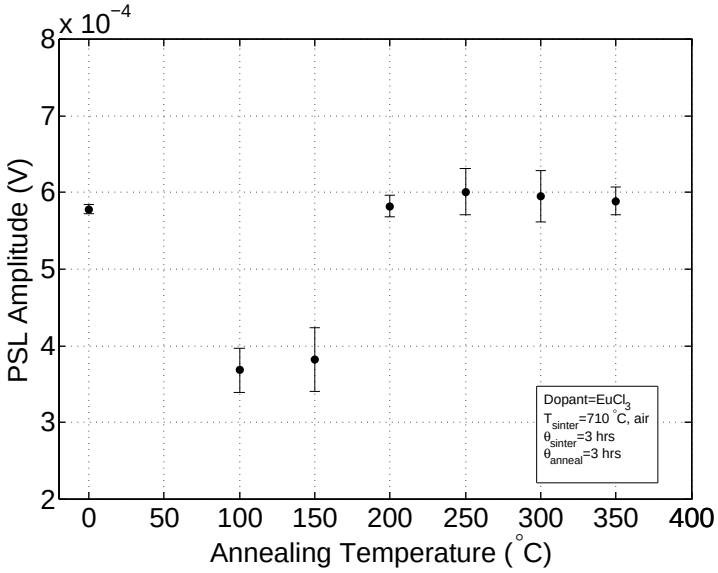

Figure 4.16: PSL vs. annealing temperature in air. Several batches of chips were pressed at 2200 lbs force and heated for three hours in air at 710 °C. An annealing treatment for 3 hours at various temperatures in air followed. PSL was measured 17.5 hours after irradiation to 200 cGy. PSL amplitude remains unchanged for annealing temperatures ranging from 200-350 °C. Error bars represent the standard error of repeated measurements.

4.4 Conclusion

The above results demonstrate that the readout systems developed for this study are well suited to photostimulated luminescence measurements. The disadvantage of using $BaFBr_{0.85}I_{0.15}$:Eu^{2+} in radiation therapy dosimetry is evident in figure 4.3(a) in a strong low energy photon dependence. Comparing the $BaFBr_{0.85}I_{0.15}$:Eu^{2+} and XV film data suggests that the thickness of the active layer plays a significant role in energy dependence, a topic that will be explored in chapter 6.

This chapter supports the proof-of-concept of a KCl:Eu^{2+} dosimetry system. PSL near 420 nm was generated through irradiation and subsequent stimulation near 570 nm. The signal stabilized 12 hours after irradiation to 0.1% loss/h and stability was improved compared to $BaFBr_{0.85}I_{0.15}$:Eu^{2+} at this time. The material had a characterizable dose response

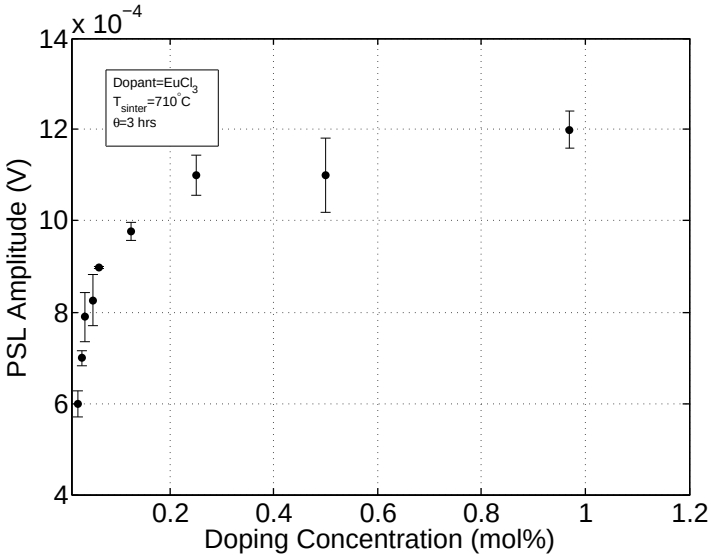

Figure 4.17: PSL vs. doping concentration. Several batches of chips were pressed at 2200 lbs force and heated for three hours in air at 710 °C. PSL was measured 17.5 hours after irradiation to 200 cGy. PSL amplitude began to level near 0.25 mol%, likely due to concentration quenching. Error bars represent the standard error of repeated measurements.

but also an energy dependence artifact comparable to conventional film. Since the atomic number of KCl:Eu^{2+} is substantially reduced from the commercial phosphor (Z_{eff}=18 compared to 49), the artifact was substantially reduced. The material was reusable up to at least 200 Gy and showed no dependence on nominal dose rate from 15 to 1000 cGy/min or nominal beam energy from 6 to 18 MV x ray or 6 to 20 MeV electron beams.

The maximum sensitivity occurred when pellet dosimeters were sintered at 710 °C. Annealing these sintered chips at temperatures from 100 to 350 °C did not improve sensitivity and below 200 °C had a negative impact. Sensitivity was improved by increasing the doping concentration but reducing the doping concentration is desirable in order to minimize the cost of raw materials.

Chapter 5

The Radiation Hardness of KCl:Eu^{2+}

An important property of a reusable dosimeter is its radiation hardness, that is, its ability to retain its dosimetric merits after irradiation. While chapter 4 reported promising experimental results for KCl:Eu^{2+}, a systematic study of radiation hardness was necessary to fully establish KCl:Eu^{2+} as a next generation dosimetry material. The present chapter offers the first systematic investigation into the radiation hardness of KCl:Eu^{2+}. Macroscopic properties, such as sensitivity, dose response linearity, and signal stability, were explored using a laboratory-scale PSL readout system. Since phosphor performance is linked to changes in the charge storage centers and the activator environment within the host lattice [8], spectroscopic and temporal measurements were carried out to explore potential changes at the microscopic level.

An initially supralinear dose response in KCl:Eu^{2+} became linear over the range of 100 to 700 cGy after cumulated doses of 60 Gy. Linearity did not change significantly in the 5000 Gy dose history spanned in this study. Sensitivity increased to 3000 Gy history and then declined to 90% of its zero-dose history value at 5000 Gy. Annealing high dose history chips results in a return of supralinearity and a recovery of sensitivity. The PSL stimulation curve peaked at 560 nm for fresh dosimeters and showed a slight red shift with dose history,

possibly due to the creation of large aggregate trap centers. PSL emission remained peaked at 420 nm and agreed well with the photoluminescence emission (PL) spectrum of the europium activator in the material. Luminescence lifetime remained constant at 1.2 μs with dose. These results indicate that the PSL process of irradiation, energy storage, excitation, energy transfer, and excitation and relaxation of the activator remains stable with dose histories up to 5000 Gy and that the material could be reused up to 2500 times at 2 Gy per use, as in, for example, patient-specific quality assurance.

5.1 Introduction

As identified in chapter 2, recent investigations have demonstrated complex and material-dependent effects of cumulative dose on various solid-state devices. Jursinic reported changes in the dose response of Al_2O_3:C as a function of cumulated dose [71]. Additionally, a rapid loss of signal with cumulated dose has been reported in CsBr:Eu^{2+} [72]. These reports suggest that a thorough radiation hardness study is necessary to fully establish KCl:Eu^{2+} as a next generation dosimetry material.

5.2 Materials and Methods

5.2.1 Dosimeters and Phantom

KCl:Eu^{2+} dosimeters were fabricated according to the methodology described in chapter 3. In this case, high purity KCl (99.9975%) particles (45-63 micron) and reagent grade $EuCl_3 \cdot 6H_2O$ (99.99%) particles ($<$ 25 micron, 0.05% mole europium) were mixed. Mixed powders were dried at 350 °C in a furnace for two hours, cooled, and pressed at 2200 lbs force in a hydraulic press (Carver Inc., Wabash, IN) using an evacuable pressing die to 6 mm in diameter and 1 mm thick. The pellets were sintered at 710 °C for three hours in air and allowed to cool naturally to 300 °C followed by a rapid cooling to room temperature. Dosimeters were either coated with a commercial-grade conformal coating [78] or wrapped in plastic wrap, e.g. polyethylene, to mitigate the adverse effects of moisture on the material.

The plastic was removed for PL measurements in order to eliminate blue luminescence due to stimulation of the plastic material by UV light.

As in section 4.1.1, 40×40 cm^2 water-equivalent sheets (SW-457, Gammex RMI, Middleton, WI) were utilized as phantom material. The dosimeters were held in place in a 0.5 cm thick slab machined with a linear array of holes 7.5 mm in diameter and 2 mm depth across the center. Prior to irradiation, the dosimeters were optically annealed to background signal levels using a 500 W tungsten-halogen lamp.

5.2.2 Optical Setup

Photostimulated luminescence was read on the optical system described in chapter 3.

5.2.3 Dosimetric Properties

Irradiations

A 6 MV (nominal) x ray beam, generated by a Varian Trilogy (Varian Medical Systems, Palo Alto, CA) was used for irradiation to doses up to 300 Gy. Escalating doses greater than 300 Gy were delivered with a high dose rate ^{137}Cs source (J. L. Shepherd and Associates, Mark I Model 25, San Fernando, CA). The calibrated dose rate to water was 10.7 Gy/min, corrected for decay to the time of irradiation. Dosimeters were mounted on a styrofoam block in the center of the chamber (as specified in section 3.2).

Dosimetric Measurements

The following tests were conducted to examine the radiation hardness of the KCl:Eu^{2+} material:

1. Sensitivity with cumulated dose. A KCl:Eu^{2+} dosimeter was irradiated to 200 cGy in a 6 MV beam at 100 cm SSD, 1.5 cm depth, and a 10×10 cm^2 field to establish its zero-dose history response. The dosimeter was then bleached and given doses of 500, 1000,

2000, 3000, 4000, and 5000 Gy. After each escalating dose, the dosimeter was bleached to zero, given 200 cGy, and the sensitivity with cumulated dose compared to the baseline value.

2. Dose response linearity with cumulated dose up to 200 Gy. Dosimeters were irradiated individually up to 700 cGy with an SSD of 100 cm, depth of 4 cm, and a field size of 10×10 cm^2 using a 6 MV beam. After reading the dosimetric information, the dosimeters were bleached, given escalating doses, and bleached again. The sensitometric data were then re-acquired. This process was repeated for several dose levels up to 200 Gy.

3. Dose response with cumulated dose up to 5000 Gy. To determine whether there were any changes in linearity at high dose histories, sensitometric curves with points at 100, 300, and 500 cGy were taken with histories from 2 to 5000 Gy. For doses greater than 300 Gy, the ^{137}Cs irradiator was used to give the escalating doses.

4. Response reset with annealing procedure. Three chips with greater than 5000 Gy dose history were annealed at 710 °C in air for three hours. A sensitometric curve was obtained and this curve compared to dosimeters with 2 Gy and 5000 Gy dose history without an annealing procedure.

5. Signal stability with cumulated dose. The signal stability of dosimeters with various dose histories was monitored during the course of the experiments using the procedure explained in section 4.2. This procedure calls for probing the signal at various times after irradiation, in this case every hour, and correcting the data for readout signal loss. Simulation power was reduced through the use of neutral density filters with a total optical density of 3 and applied for 1.5 seconds in order to reduce the readout loss to 0.15% per reading. A linear fit was made to data points collected 13 hours or more after irradiation. The slope of the fitted curve provided an estimate of the signal stability. Results are reported along with the uncertainty of the slope estimate, given that there was 1-2% measurement point uncertainty due to electronic noise and laser power fluctuation. Note that adding a

reference detector could partially mitigate this uncertainty, but it was not necessary for the purpose of this study.

5.2.4 Spectroscopic Measurements

In order to investigate whether high dose alters the properties of the charge storage center and Eu^{2+} activator in the KCl host lattice, the following measurements were carried out:

1. PSL stimulation spectra with cumulated dose. PSL stimulation spectra of dosimeters with dose histories up to 5000 Gy were obtained by inserting the monochromator into the light path between the Xe source and the sample and scanning between 450 and 700 nm in 1 nm increments.

2. PSL emission spectra with cumulated dose. PSL emission spectra were obtained by inserting the monochromator into the PSL light path between the integrating sphere and the PMT, which was fitted with bandpass filters, and scanning between 390 to 470 nm in 1 nm increments. A 5 mW, 594 nm yellow He-Ne laser (Melles Griot, Covina, CA) served as the stimulation source. Laser power was attenuated with neutral density filters in order to minimize signal loss during scanning. Corrections for spectral response of the PMT and signal depletion during scanning were found to be insignificant.

3. PL emission spectra with dose. Broadband UV stimulation light was selected from Xe arc lamp emission by a combination of short pass filters (Edmunds Optics). UV optics directed the simulation light to an input on the integrating sphere directly opposite sample. The monochromator was again placed between the integrating sphere and the PMT, which was fitted with bandpass filters and scanned between 400 to 500 nm in 1 nm increments. Background leakage through optical filters was collected and subtracted from measurements.

4. Luminescence lifetime with dose. The luminescence lifetime is defined as the time it takes to reduce PL intensity by a factor of e and is determined by the lifetime of the excited state of the Eu^{2+} activator ion in the surrounding host lattice [7]. This figure of merit can be an indicator of microstructural changes occurring around the activator site. A 308 nm pulsed (30 ns) excimer laser was used as an excitation source [36]. PL intensity was

collected at 420 nm following excitation and plotted on a log scale for dosimeters irradiated from 0 (i.e., a fresh dosimeter) to 5000 Gy histories.

5.3 Results

5.3.1 Dosimetric Measurements

Sensitivity with Cumulated Dose

Figure 5.1 shows the average sensitivity of a KCl:Eu^{2+} dosimeter at various dose histories relative to its baseline (zero dose history) value. An increase in sensitivity up to 3000 Gy was observed, followed by a decline to 90% at 5000 Gy.

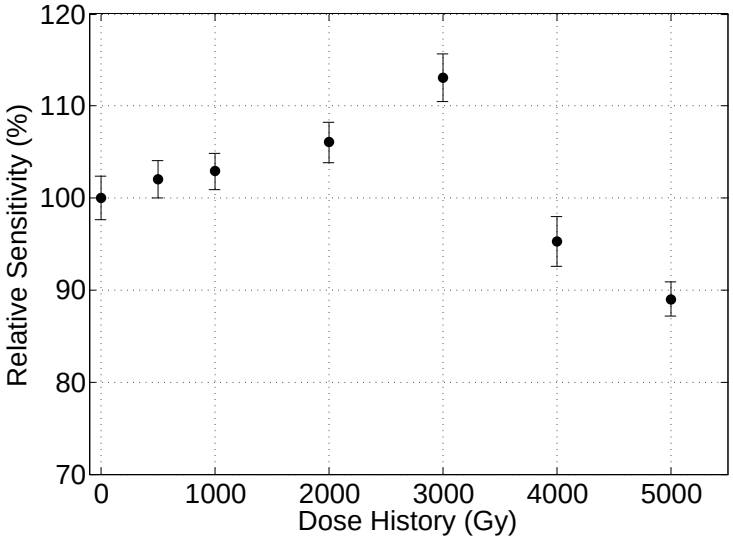

Figure 5.1: Sensitivity with cumulated dose. A KCl:Eu^{2+} dosimeter was given 200 cGy to establish its zero dose history sensitivity, then given a series of escalating doses. At several dose histories, 200 cGy was given and the PSL collected and compared to the fresh value. Sensitivity increased to 3000 Gy history and then declined to 90% of its zero-dose history value at 5000 Gy. Error bars represent the standard error of repeated measurements.

Dose Response Linearity

Figure 5.2 shows how the sensitometric curve changes with dose history (additional dose histories similar and not shown). At low dose history, a supralinear response over the range of 100-700 cGy is evident. As dose accrues, the magnitude of the supralinearity decreases and the curve becomes more linear. After 64 Gy history, measured data fit a linear model with R = 0.999 and an average deviation of 1.3% with a maximum of 3.5% over the full dose range, shown in the inset to figure 5.2, which is within the experimental uncertainty of the measurements. While there is residual supralinearity present over a dose range as large as 600 cGy, the effect can be minimized if the dosimeter is calibrated over a shorter range of interest. For example, the maximum deviation is less than 2% over a range of 100 to 400 cGy after 64 Gy accumulated dose. As shown in figure 5.3, the shape of the normalized sensitivity curves changes very little with cumulated dose up to 5000 Gy (additional dose histories not shown).

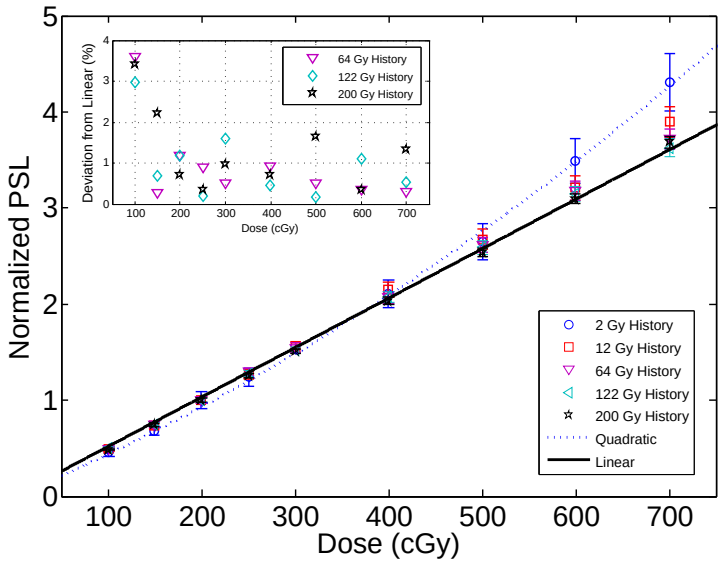

Figure 5.2: Response with cumulated dose up to 200 Gy. Dose response curves at various dose histories were obtained and plotted, normalized to 200 cGy. The dose response initially shows supralinear behavior but becomes more linear with dose history. The inset displays the percent deviation of the measured data from a linear model. Error bars represent the standard error of repeated measurements.

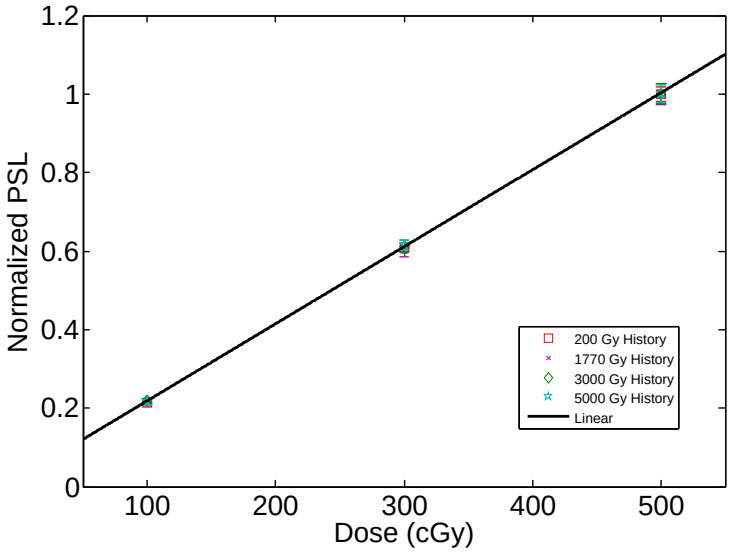

Figure 5.3: Response with cumulated dose up to 5000 Gy. Dose response curves at various dose histories were obtained and plotted, normalized to 300 cGy. A linear dose response holds up to 5000 Gy. Error bars represent the standard error of repeated measurements.

Dose Response Reset

Chips irradiated to greater than 5000 Gy were annealed at 710 °C for three hours. Within 3%, the supralinear response returns to its original, zero dose history shape, which is shown in figure 5.4. Furthermore, it was found that after annealing the average chip sensitivity returned to value expected for fresh, non-irradiated dosimeters.

Signal Stability

An important property of a storage phosphor is the long-term stability of the information stored in the phosphor. It is known that the PSL signal decreases with time, typically consisting of a fast component immediately after irradiation and a slower component afterwards [7]. Signal stability was monitored in this study with accumulated dose and results are presented in Table 5.1. Signal stability did not deviate from low dose values outside experimental uncertainty.

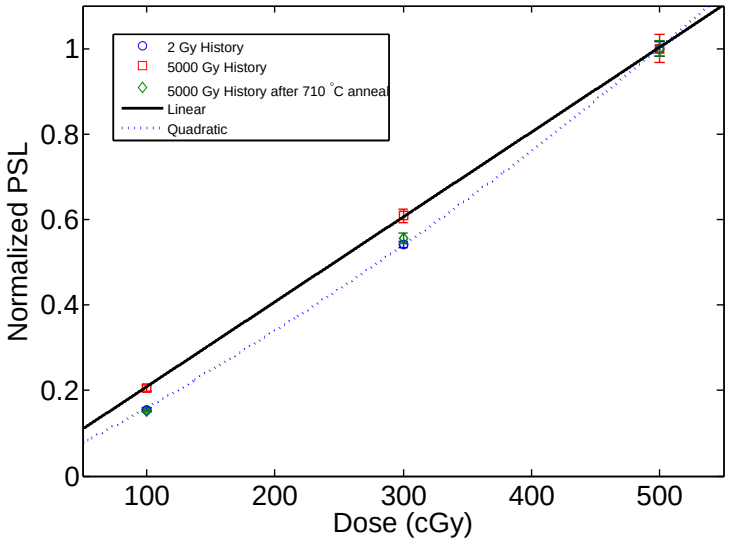

Figure 5.4: Reset of sensitivity curve with annealing procedure. Chips with 5000 Gy dose history were annealed in a laboratory furnace at 710 °C for 3 hours in air. Dose response at points of 100, 300, and 500 cGy were obtained and compared with chips with no annealing procedure. After annealing, the dose response returns to the supralinear behavior. Error bars represent the standard error of repeated measurements.

5.3.2 Spectroscopic and Temporal Measurements

PSL Stimulation Spectra with Cumulated Dose

Figure 5.5 shows that the shape of the stimulation curve remained almost unchanged with dose. The slight red shift with dose could be due to the creation of aggregate trap centers, such as M(Cl-).

PSL Emission Spectra with Cumulated Dose

Fresh KCl:Eu^{2+} dosimeters emit intense photostimulated luminescence centered at 420 nm following stimulation. It was observed that the peak of the PSL emission spectrum remained near its fresh dosimeter peak with dose histories up to 5000 Gy (figure 5.6).

Table 5.1: Signal stability with cumulated dose. Dosimeters were irradiated to several dose levels and the signal stability 13 hours after irradiation was examined according to a procedure described in Han *et al.* [13]. Signal stability remains largely unchanged after irradiation to greater than 5000 Gy history.

Dose History (Gy)	Signal Stability (% decrease per h)
0	0.24±0.04
144	0.17±0.06
630	0.13±0.06
1770	0.13±0.03
3000	0.14±0.05
5000	0.16±0.08

PL Spectra and Luminescence Lifetime

As shown in figure 5.7, there is a slight broadening (3.5 nm) and peak shift (2 nm) of the PL spectra at high doses; however, in general, the spectra for the different excitation processes (i.e., PL and PSL) agreed well. This data suggests that Eu^{2+} cation acts as the luminescence center in the PSL process via $4f_6 5d_1 \rightarrow 4f_7$ ($^8S_{7/2}$) transition. The close agreement between the PSL spectra (figure 5.6) and the PL spectra suggests that Eu^{2+} is acting as the photostimulated luminescence center at all dose histories. The combined data also suggest that little changes in the vicinity of the activator have occurred with dose and that the energy transfer mechanism to Eu^{2+} is robust even after high accumulated dose. Figure 5.8 shows the photoluminescence lifetime with dose history up to 5000 Gy did not deviate from its fresh value, approximately 1.2 μs, outside the experimental uncertainty, consistent with previous findings [45]. According to Zheng *et al.* [121], a luminescence time of the order of one microsecond per pixel allows a readout time within a few seconds for a 20×20 cm^2 panel with 0.5×0.5 mm^2 pixels.

Collectively, these findings, when considered with the recovery of sensitivity after high temperature annealing, suggest that the sensitivity loss with dose may be largely due to recoverable radiation-induced perturbations in the lattice, such as local lattice distortions, that act as luminescence killers.

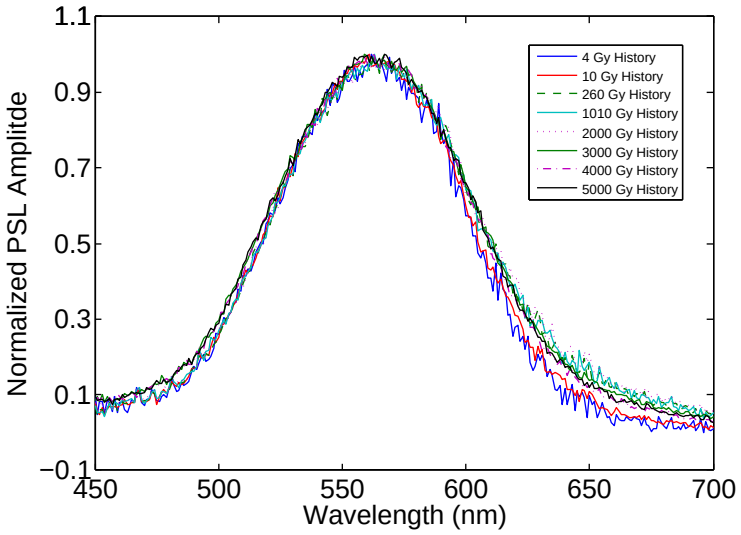

Figure 5.5: PSL stimulation spectra with cumulated dose. Stimulation wavelength was varied while collecting PSL at 420 nm (see text). The maximum stimulation efficiency for photostimulated luminescence remains constant at 560 nm with cumulated dose.

5.4 Discussion

As seen in chapter 2, PSL in KCl:Eu^{2+} is a complex process that can be influenced by a number of variables, including irradiation. It has been suggested [39] that a major cause of radiation damage in alkali halide storage phosphors is the creation of large defect centers, for example, M_{Eu}-centers (i.e., two adjacent anion vacancies each occupied by an electron in the neighborhood of an Eu^{2+}). Within such a structure, Eu^{2+} ions can easily change sites causing an agglomeration of europium ions and concentration quenching. The results of this study, however, suggest that agglomeration is controlled in a KCl:Eu^{2+} system to at least 5000 Gy dose history. Furthermore, the observed level of radiation hardness of KCl:Eu^{2+} allows the physicist to establish and monitor dosimeter performance characteristics and represents a factor of 25 increase in reusability compared to data in section 4.2.2.

A gradual increase in sensitivity for KCl:Eu^{2+} with dose history to 3000 Gy was observed (figure 5.1), a phenomenon also reported for Al_2O_3:C [71]. In this case, however, it is hypothesized that the increase in sensitivity is due to a combination of an increase in trapping

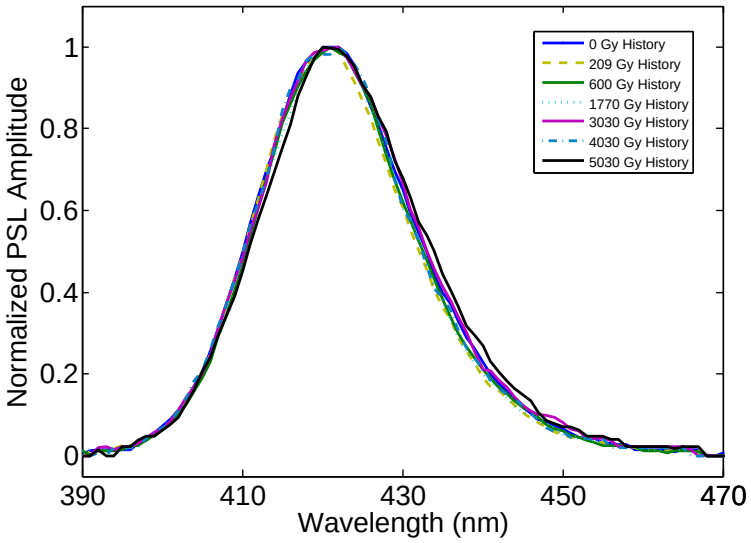

Figure 5.6: PSL emission spectra with cumulated dose. KCl:Eu^{2+} dosimeters were stimulated while varying the collection wavelength (see text). The dosimeters emit intense photostimulated luminescence centered at 420 nm, which remains constant with dose history.

efficiency in photosimulable energy bands and migration of trapped charge species into photostimulable complexes after optical annealing. In addition to preexisting vacancies [5, 14], according to Itoh irradiation produces vacancies occupied by electrons (F-centers) and interstitial halogen atoms bound to lattice halogens by holes [59]. Photostimulation at F-center bands releases stored electrons to produce PSL, but radiation-induced lattice changes remain. During very high escalating doses and subsequent optical annealing, more centers could be created and emptied, resulting in an increase in the number of storage centers for electrons and holes. Charge carriers generated during later irradiations may then have a higher probability of being trapped in photostimulable centers, thus increasing sensitivity. Additionally, charges or defects remaining after optical annealing to background levels could migrate in the dark at room temperature to form photostimulable complexes, leading to an observed increase in sensitivity [63, 71]. Since the literature related to KCl:Eu^{2+} dosimetry is limited, however, further investigations into the nature of sensitivity change with dose history are needed, as well as a detailed understanding of the optical annealing process.

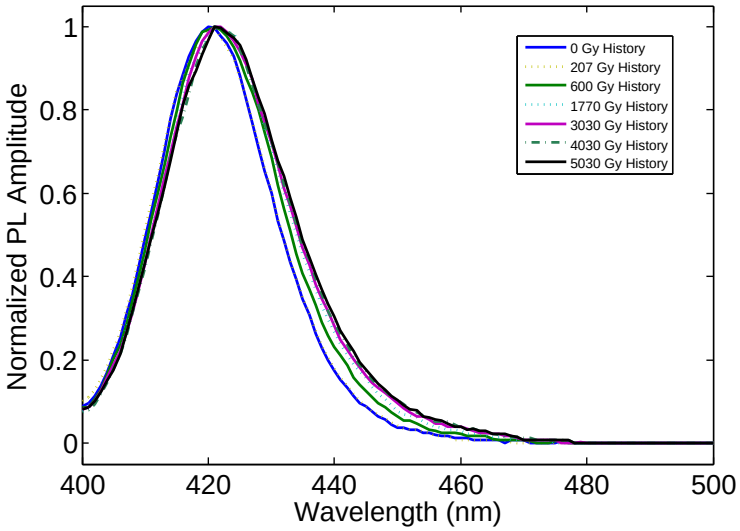

Figure 5.7: PL spectra with cumulated dose. Broad-band UV light was used to simulated the KCl:Eu^{2+} dosimeters to emit photoluminescence. The peak of the photoluminescence spectrum remains nearly constant at 420 nm, indicating that little changes in the vicinity of the activator have occurred with dose.

A decline in sensitivity was observed after 3000 Gy, however, which indicates that competing processes are also at work. It is likely that radiation damage in the crystal lattice becomes significant at this dose level. Consequently, radiation-induced local lattice perturbations could act as luminescence killers, decreasing sensitivity. In this interpretation, irradiation still produces charge carriers that are trapped in photostimulable centers, but radiation damage affects the luminescence process. Since the literature related to KCl:Eu^{2+} dosimetry is extremely limited, further research into the nature of sensitivity change with dose is needed. At the very least, sensitivity change with dose history would be manageable by giving a calibration dose prior to beginning the dose measurement session.

A linear response to dose is expected of PSL systems [6, 7]. In theory, the number of PSL active centers is proportional to the locally deposited dose. The data show that the response of KCl:Eu^{2+} dosimeters changes with dose history. It is hypothesized that the supralinear response of fresh or nearly fresh dosimeters is due to deep, non-photostimulable traps present in the material, perhaps as a result of the crude manufacturing process.

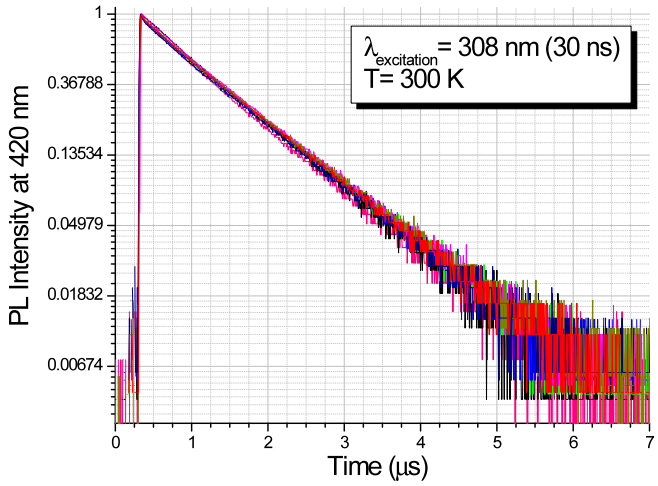

Figure 5.8: Luminescence lifetime with cumulative dose. A 308 nm excimer laser was used to excite KCl:Eu^{2+} PL in dosimeters with dose histories up to 5000 Gy. The PL was sampled during its decay and plotted on a log scale. PL lifetime remains nearly constant at 1.2 microseconds within experimental uncertainty.

These deep traps compete with photostimulable traps for electrons generated during charge separation and result in a reduced signal. At greater cumulated doses, the deep electron traps become filled and more electrons are stored in the photostimulable traps, leading to enhanced photostimulated luminescence signal. Once all of the deep traps are filled, a linear response dominates. If this interpretation is correct, a pre-clinical dose loading protocol would be feasible for ease of calibration. For example, 100 Gy could be given to a fresh dosimeter, the dosimeter optically bleached, and then calibrated for clinical use. This pre-dose should have negligible impact on reusability.

One indication that non-photosimulable traps are responsible for supralinearity may be the sensitivity curve reset after high temperature annealing. After some delocalization temperature, electrons stored in deep traps could be released. It would follow that these traps would once again be available to compete with PSL traps for radiation-generated electrons. High temperature annealing would also provide thermal energy for lattice atoms to move back to equilibrium positions, which would explain the observed recovery of sensitivity.

Since sensitivity recovery is a desirable feature, further systematic studies are necessary to fully understand the effects of annealing and optimize the procedure.

In high speed, two dimensional computed radiography readout systems, a stimulation laser is focused on a single pixel, the information read out, the laser moved to the next pixel, and the process repeated so that the entire imaging panel is read in the matter of seconds. Since similar technology could be applied to KCl:Eu^{2+} dosimetry panels, it is interesting to note that high irradiation does not significantly alter the spectral or temporal properties of the activator in the KCl matrix. Thus, in clinical use, only sensitivity with dose would need to be monitored. Importantly, a change in luminescence lifetime was not detectible outside the uncertainty of the experiment. Thus the readout time as well as the contribution of latent luminescence from neighboring pixels to any given pixel would not change significantly with dose history.

5.5 Conclusion

This chapter has presented the first systematic study of how cumulated dose affects the response of KCl:Eu^{2+}. A supralinear response to dose for fresh dosimeters becomes more linear with dose history. Supralinearity returned after high temperature annealing treatments. Sensitivity increased slightly to 3000 Gy and then decreased to 90% of zero-dose history value at 5000 Gy. There were no significant changes in the signal stability, the PSL stimulation spectra, the PSL emission spectra, the PL emission spectra, or the luminescence lifetime with dose, suggesting that the PSL process, including photo-stimulation, energy transfer, and excitation and relaxation of the activator, remained largely intact even after doses of 5000 Gy. The data presented here support the strong radiation hardness of KCl:Eu^{2+} as well as further investigations of this novel material.

Chapter 6

KCl:Eu^{2+} Panel Dosimeter Developments

Chapters 4 and 5 established KCl:Eu^{2+} as a next-generation dosimetry material. It is shown in this chapter that reducing the thickness of KCl:Eu^{2+} maximizes the water-equivalence of the dose response. Monte Carlo (MC) simulations were performed using BEAMnrcMP and DOSXYZnrc for KCl:Eu^{2+} panels from 1 μm to 1 mm thick. The generation efficiency, W, of prototype KCl:Eu^{2+} was used to estimate the sensitivity of micron-thick dosimeters and determined by comparing the sensitivity of a 150 μm thick KCl:Eu^{2+} two dimensional (2D) panel to a commercial $BaFBr_{0.85}I_{0.15}$:Eu^{2+}-based phosphor with a known W. Dose information was read out on a custom built, high-speed 2D optical scanner. MC simulations demonstrate that micron-thick KCl:Eu^{2+} films have a nearly water-equivalent dose response. W of KCl:Eu^{2+} was determined to be 157 eV/$h\nu$ and sub-millimeter spatial resolution was achieved for films 150 μm thick. It was determined that micron-scale films would generate over $10,000$ photoelectrons at the PMT photocathode for detection and amplification for delivered doses as low as a one cGy dose-to-water. In experiments, PSL was routinely achieved for thin vapor-deposited KCl:Eu^{2+} panels less than 10 μm. Signal stability measurements of thin panels revealed challenges related to moisture protection of this material that may be mitigated through the application of protective coating technologies.

6.1 Importance of Dosimeter Thickness

In radiation therapy it is desirable for a dosimeter to have a waterlike response. That is, the signal resulting from energy deposited in the sensitive volume of the dosimeter should be proportional to the energy deposited in water once the dosimeter is removed. Cavity theories can help illuminate the nature of energy deposition in the sensitive layer of the KCl:Eu^{2+} dosimeter when it is inserted into a medium. According to Burlin's formulation, dose to a cavity, c, can be written as [111]

$$\frac{\bar{D}_c}{D_w} = d \cdot {}_m\bar{S}_w^c + (1-d)\left(\frac{\bar{\mu}_{en}}{\rho}\right)_w^c \tag{6.1}$$

where w is the dosimeter "wall" and d is a thickness dependent parameter relating the degree to which the average cavity fluence equals the equilibrium wall fluence. For the purposes of this discussion, the wall material may be taken as water (e.g., a KCl slab inserted into a waterlike measurement medium). In a perfectly matched dosimeter the mass collision stopping power ratio and the mass energy-absorption coefficient ratio equal unity over all energies. In this case,

$$\frac{\bar{D}_c}{D_w} = 1 \tag{6.2}$$

and the parameter d is eliminated. Since the media are matched, altering the incident radiation spectra does not alter the dosimeter response relative to the medium of interest. However, it is often the case that the sensitive material and the measurement medium are not matched and d becomes an important parameter to consider when designing a dosimeter.

Burlin considered three sizes of cavities, based on the effective cavity diameter, l, and the average range of secondary electrons generated in the cavity, $\langle R \rangle$ [111]:

1. Large Cavity: $l \gg \langle R \rangle$
2. Intermediate Cavity: $l \sim \langle R \rangle$
3. Small Cavity: $l \ll \langle R \rangle$

In case 1, most of the dose is deposited by secondary electrons that are generated inside the cavity and relatively little by secondaries liberated in the surrounding media. The average dose in the cavity delivered by insiders (i.e., $d = 0$) is

$$\frac{\bar{D}_c}{D_w} = \left(\frac{\bar{\mu}_{en}}{\rho}\right)_w^c \tag{6.3}$$

If the cavity material and the wall material are different effective atomic numbers, changing the incident photon spectra will alter the dosimeter response relative to the measurement media. This can be seen from figure 6.1a, which plots the mass energy-absorption coefficient ratio for KCl to water, and, for comparison, BaFBr, which is used in diagnostic radiography, and LiF, a commonly used thermoluminescence dosimetry. This figure suggests that altering the incident radiation spectra will significantly change the response of KCl and BaFBr because more energy is deposited by lower energy photons. This figure also shows a distinct advantage of LiF in that it is more closely matched to water.

For a small cavity (case 3), however, the reverse holds ($d = 1$): the bulk of the dose is deposited by secondaries generated in the surrounding media that cross the cavity. That is, the average dose to the cavity is deposited by electrons generated in the surrounding wall or media of interest (i.e., crossers). In this case,

$$\frac{\bar{D}_c}{D_w} = {}_m\bar{S}_w^c \tag{6.4}$$

For a moderately thick dosimeter (case 2), the situation is more complex. Energy is deposited in the dosimeter by crossers (i.e., secondary electrons completely traversing the cavity), starters (i.e., secondary electrons that start in the cavity and exit), stoppers (i.e., secondary electrons starting in the cavity but stopping in the dosimeter), and insiders (i.e., secondary electrons that start and stop in the sensitive volume of the dosimeter). Hence, the full Burlin equation applies.

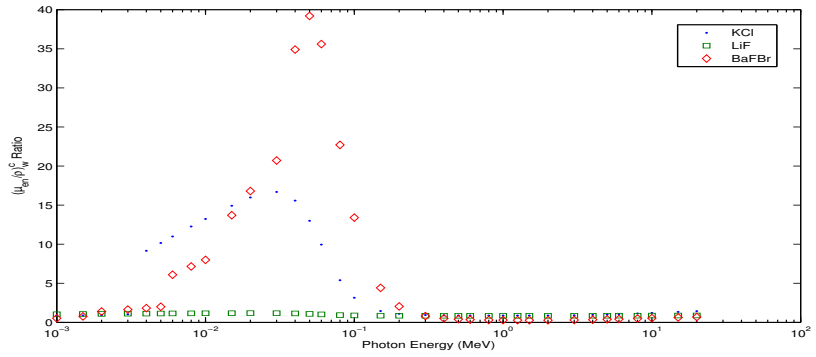

(a) $(\mu_{en}/\rho)^c_w$ Ratio

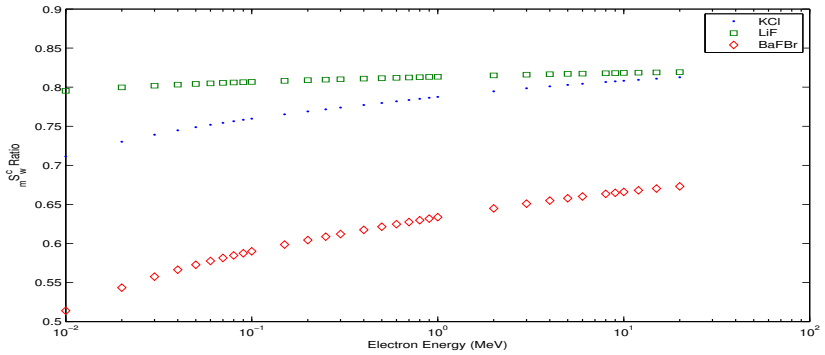

(b) ${}_mS^c_w$ Ratio

Figure 6.1: Approximate (a) mass energy-absorption ratio versus photon energy and (b) mass stopping power ratio versus electron energy relative to liquid water, symbolized by w, for different cavities, symbolized by c: KCl, BaFBr, and LiF. μ_{en}/ρ ratios were calculated from the approximation in equation (7.62) in [111] and data from NIST [122]. ${}_mS$ ratios were calculated from equation (8.13), (8.20), and (8.21a) in [111].

Consider now that a KCl:Eu^{2+} dosimeter inserted into a waterlike medium for measurement of absorbed dose and that it is thin enough so that the average dose deposited in the dosimeter is by electrons generated in the surrounding waterlike medium that cross the cavity. In this case, d in equation 6.1 is equal to unity and the dose to KCl is

$$\frac{\bar{D}_{KCl}}{D_w} = {}_m\bar{S}_w^{KCl} \tag{6.5}$$

As the thickness of the cavity layer is decreased, the average cavity fluence approaches the equilibrium fluence and the dose deposited in KCl relative to water tends towards the ${}_m\bar{S}_w^{KCl}$ ratio. Since the mass stopping power ratio is only weakly dependent on the secondary electron spectrum (figure 6.1b), the KCl:Eu^{2+} dosimeter should have an approximately energy independent dose response.

6.2 Simulation of Panel Dosimeters

The above discussion partly explains why XV film had a reduced over-response to low energy photons compared to $BaFBr_{0.85}I_{0.15}$:Eu^{2+} and KCl:Eu^{2+} (cf. chapter 4). To test whether reducing the thickness of KCl:Eu^{2+} would reduce the energy dependent artifact, thin films of KCl were simulated with EGSnrcMP and DOSXYZnrc [121]. The source model was based on a standard linear accelerator configuration. The phase-space file was used as an input to DOSXYZnrc to simulate the 3D dose distribution in a $40 \times 40 \times 40$ cm^3 solid water phantom both with and without KCl:Eu^{2+} dosimeters.

Figure 6.2 shows that the MC simulated dose distributions agreed well with measured data for the prototype, 1 mm thick dosimeters, at 10×10 cm^2, 20 cm depth, and 100 SSD. Figure 6.3 shows a strong over-response to a 100 μm thick film in the peripheral dose region where low-energy scattered photons are dominant. However, as predicted above, the over-response is removed when film thickness is reduced.

Figure 6.4 shows simulated dose to KCl:Eu^{2+} as a function of dosimeter thickness in a 6 MV, 20×20 cm^2 field at a depth of 10 cm, normalized to that of 1 mm thick dosimeter. The

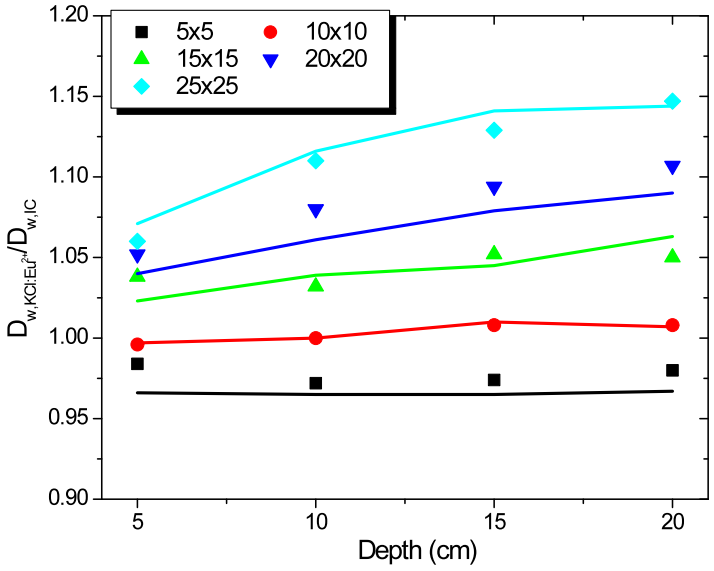

Figure 6.2: Sensitivity of KCl dosimeters as a function of field size and depth, from [121] with permission throughout. Symbols are measured data while lines are simulated data.

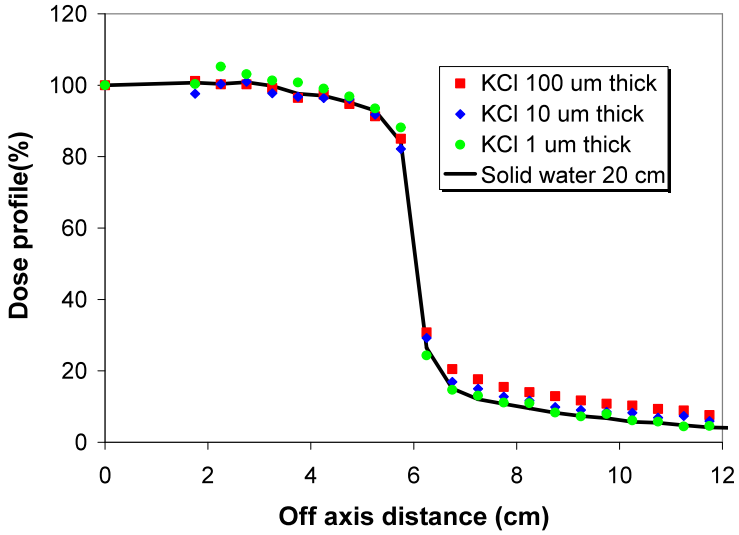

Figure 6.3: MC simulated dose profiles for 1, 10 and 100 μm-thick KCl dosimeters at 20 cm depth, 100 cm SSD, in a 10×10 cm^2 field in a 6 MV beam [121].

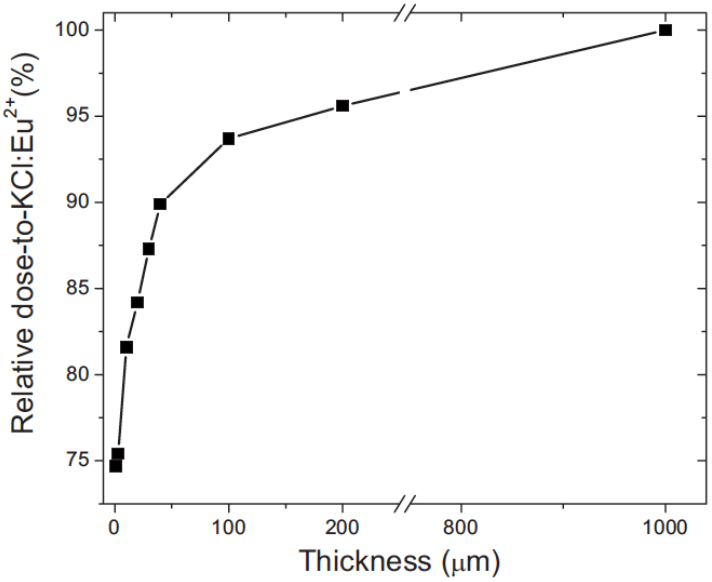

Figure 6.4: MC simulated dose to KCl:Eu^{2+} as a function of dosimeter thickness in a 6 MV, 20×20 cm^2 field at a depth of 10 cm, normalized to that of 1 mm thick dosimeter [121].

dose to a 1 μm film drops to 75% of that of a thick pellet. This ratio agrees nicely with the mass collision stopping power ratio calculated to be between 0.7 and 0.8 between 10 keV and 10 MeV in figure 6.1. Together, figures 6.3 and 6.4 suggest that the theory presented in section 6.1 holds and that the weak dependence of the mass collision stopping power ratio of KCl-to-water on the secondary electron spectrum explains the nearly water-equivalent response of a 1 μm KCl:Eu^{2+} film.

It is worthwhile to ask whether reducing the thickness of a commercial CR plate will also minimize energy-dependent dosimetry artifacts. Figure 6.5 compares a simulated 1 μm thick KCl:Eu^{2+} dosimeter and a simulated 1 μm thick $BaFBr_{0.85}I_{0.15}$:Eu^{2+} dosimeter. It can be seen that the over-response is still present in the commercial material in the peripheral dose regions as low energy photon interactions remain significant in this material even at this thickness.

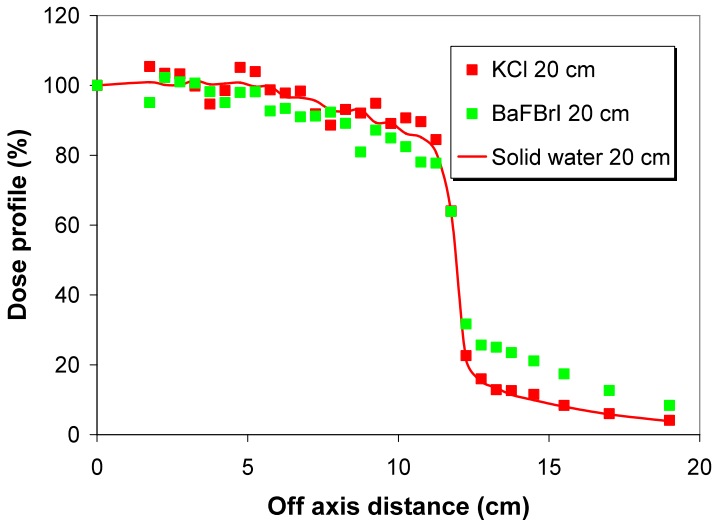

Figure 6.5: MC simulated dose profiles for a 1 μm thick KCl dosimeter and a 1 μm thick $BaFBr_{0.85}I_{0.15}$:Eu^{2+} dosimeter at a depth of 20 cm for a 20×20 cm^2 field at 100 SSD [121].

6.3 Prototype Tape Cast Panel Dosimeters

Preliminary tests in two dimensions were run with inexpensive, tape cast panel dosimeters, utilizing the tape casting system described in section 3.1.3. A thorough study of tape cast KCl:Eu^{2+} dosimeters was outside the scope of this study. Rather, the purpose of each trial recorded in table 6.1 was to generate a prototype film of sufficient quality for preliminary measurements. In each case, polycrystalline KCl:Eu^{2+} was mixed with a polymer binder material and liquid vehicle, cast on a polyethylene terephthalate (PET) substrate, and allowed to dry. FX-419 binder (Coates Screen Inks GMBH, Nuremberg) offered superior adhesion and scratch resistance compared to polyvinyl butyral-based binders. Dispersants had no effect on slip quality, which can be partially attributed to the large particle sizes used in sample preparation. The quality of the dried tape varied considerably and some observations are recorded in table 6.1. However, as figure 6.6 demonstrates, tape casting can be suitable for large area panels greater than 150 μm in thickness.

Table 6.1: Prototype tape cast KCl:Eu^{2+} dosimeters. NS indicates the particle size was not selected. EtOH indicates ethanol; MEK indicates methyl ethyl keytone; PVB indicate polyvinyl butyral formulations (The Tape Casting Warehouse, Yardley, PA). CC59 and PS220 are phosphate esther-based dispersants (Akzo Nobel Surfactants, Chicago, IL). FX-419 is a commercial binder (Coates Screen Inks GMBH, Nuremberg).

Plate	Solids Load (%)	KCl size (μm)	Binder	Liquid Vehicle	Dispersant	Mix Parameters	Observations
A	63	25-45	FX-419	EtOH/MEK	CC59	80 min, 200 rpm	Runny
B	69	25-45	FX-419	EtOH/MEK	PS220	60 min, 150 rpm	Acceptable
C	69	25-45	FX-419	EtOH/MEK		300 min, 150 rpm	Curling, bubbling
D	66	25-45	PVB B79	MEK		80 min, 200 rpm	Runny. Easily scratched
E	66	NS	PVB B98	MEK	PS220	330 min, 150 rpm	Scratch resistant
F	41	25-45	FX-419	EtOH/MEK		360 min, 300 rpm	Agglomerates
G	63	<45	PVB B98	Isop/MEK		21 hr, 100 rpm	Well mixed, runny
H	71	<45	PVB B98	Isop/MEK		24 hr, 150 rpm	Holes visible
I	71	<45	PVB B98	Isop/MEK		24 hr, 200 rpm	Agglomerates
J	69	<45	FX-419	EtOH/MEK		120 min, 400 rpm	Acceptable

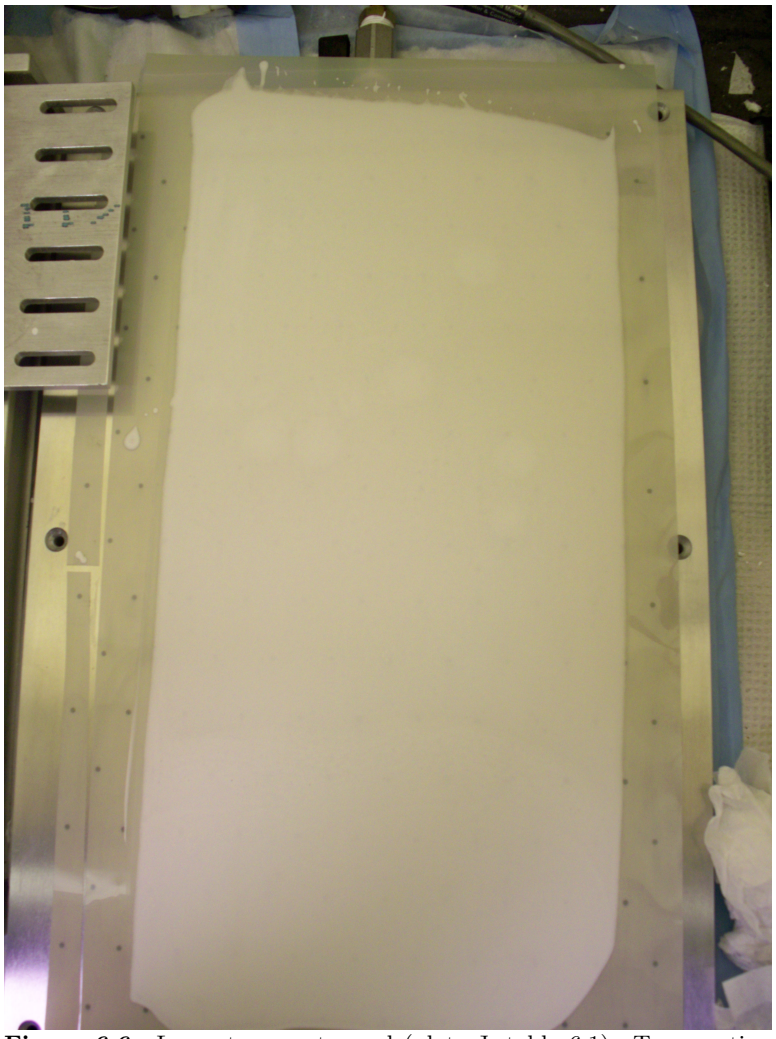

Figure 6.6: Large tape cast panel (plate J, table 6.1). Tape casting can be suitable for large area panels. Shown is an approximately 8×18 in^2 hand cast plate.

6.3.1 Prototype 2D Scanner

Tape cast panel dosimeters were used to run preliminary tests in two dimensions. The dosimeters were read using the setup illustrated in figure 3.12. The stimulation power was supplied by a 594 nm HeNe laser (Melles Griot, Covina, CA). The plate was fixed to a precision tilter and scanned row-by-row in front of the laser, which was blocked with a shutter during the transition to the next row. PSL was directed to a photomultiplier tube (PMT, Hamamatsu, Bridgewater, NJ) which collected and amplified the signals. The system was controlled through a GPIB interface. LabVIEW and Matlab programs were developed to automate the data collection and processing.

6.3.2 Laser Spot Size

In traditional phosphor films, spatial resolution is determined by laser spot size and light scattering in the binder in the phosphor layer. In order to determine the laser spot size, a knife-edge technique was used in which a blade was fixed to the prevision tilter and the blade scanned in front of the laser. The intensity of reflected light was collected during the scan and the edge spread function plotted. The derivative of the edge scan determined the line spread function. The full width at half max (FWHM) of the line spread function was taken as an indicator of laser spot size. Representative scans are shown in figure 6.7. This procedure was repeated while changing the position of the focusing lens with a precision micrometer (see figure 3.11). A minimum spot size of 73 micron was achieved in the current setup (figure 6.8).

6.3.3 Profile

Although thick KCl:Eu^{2+} dosimeters do not have a water equivalent response, the response in the penumbra region of the profile should be improved relative to higher Z $BaFBr_{0.85}I_{0.15}$:Eu^{2+}. This was examined by taking profile scans with the two phosphors and comparing their response to an ionization chamber. While non-uniformities are present

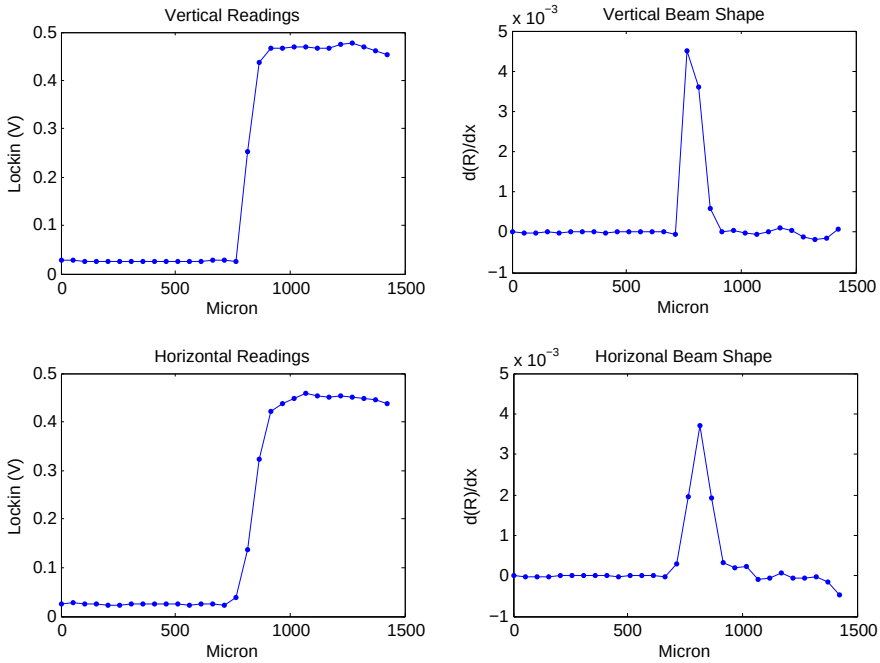

Figure 6.7: Representative beam shape by knife edge technique (see text).

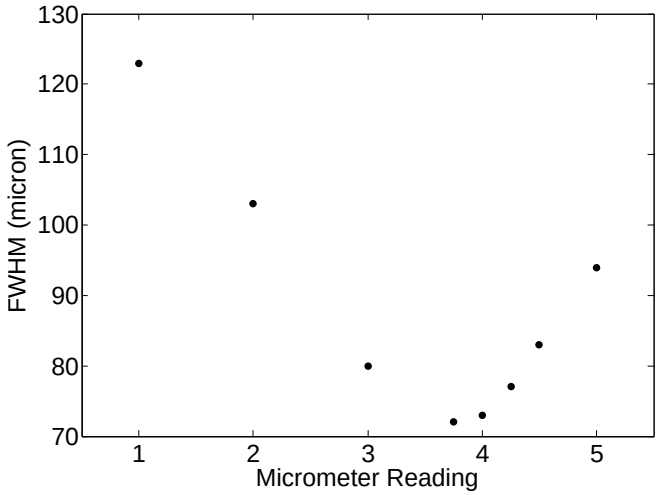

Figure 6.8: Minimum laser spot size in current setup. A focusing lens was adjusted with a precision micrometer and the beam shape was determined by a knife-edge technique.

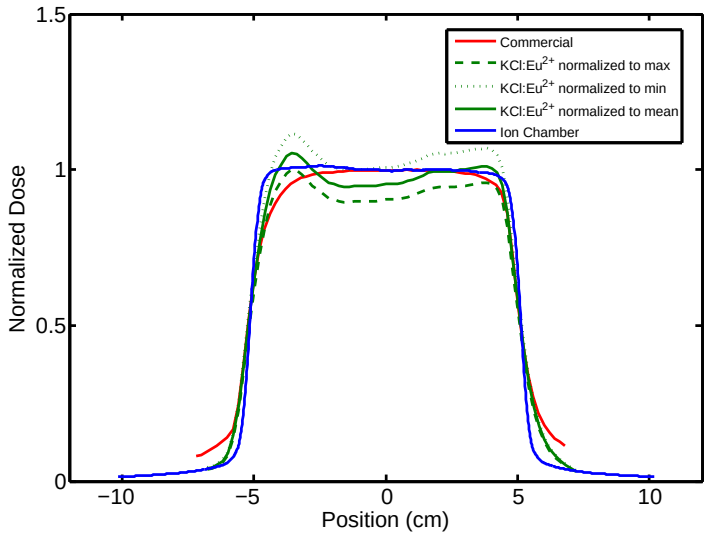

Figure 6.9: Dose profiles for experimental thick KCl:Eu^{2+} panel, $BaFBr_{0.85}I_{0.15}$:Eu^{2+} plate, and ion chamber.

in the prototype KCl:Eu^{2+} dosimeter, the penumbra edge is improved over the commercial phosphor. Future development of tape casting could improve the response uniformity across the profile.

6.3.4 Spatial Resolution

In order to evaluate the spatial resolution of the KCl:Eu^{2+} film and scanner system, a lead pattern irradiation was carried out with a prototype film 150 μm thick. The irradiated film was read out using the 2D scanner (cf. section 6.3.1). Figure 6.10 shows that sub-millimeter spatial resolution is achievable even for the prototype film. It is anticipated that thinner films will have improved spatial resolution and have a uniformity equal to or greater than the tape cast sample.

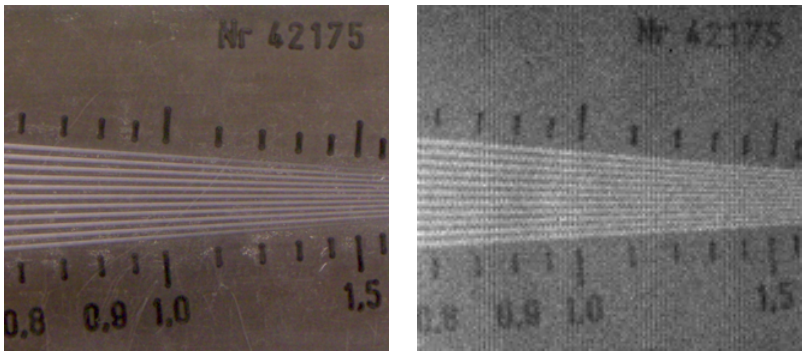

(a) Spatial resolution lead pattern. (b) KCl:Eu^{2+} thick film spatial resolution.

Figure 6.10: Evaluation of the spatial resolution of KCl:Eu^{2+} prototype dosimeters determined by lead pattern irradiation. Units are line pairs per millimeter.

6.4 Generation Efficiency of KCl:Eu^{2+}

A significant question arises as to whether an ultra-thin KCl:Eu^{2+} film, for example, on the order of 1 μm will be sensitive enough for megavoltage photon beam dosimetry. In order to estimate the sensitivity, the generation efficiency, W, must be known. W is defined as the mean energy that must be absorbed by ionizing radiation to produce a PSL photon and was determined to be 160 eV in $BaFBr_{0.85}I_{0.15}$:Eu^{2+} by Li. *et al.* for a Fuji HRIII plate with a thickness of 170 μm in a 6 MV beam [44], a value independent of delivered dose from 1 to 1000 cGy. This information was used in making an estimate of W for KCl:Eu^{2+}.

Polycrystalline KCl:Eu^{2+} with a polymer binder material was tape-cast on a PET substrate with coating weight of 28 mg/cm^2. The coating weight of the $BaFBr_{0.85}I_{0.15}$:Eu^{2+}-based dosimeter was determined to be 53 mg/cm^2 by multiplying the material's physical density of 5.1g/cm^3, filling factor of 61% [17], and film thickness of 170 μm. Both dosimeters were irradiated in a 6 MV beam to 230 MU at a depth of 5 cm and 100 SSD in a 10×10 cm^2 field, which corresponded to a dose of 200 cGy. Dosimeters were read immediately after irradiation. A central axis scan was obtained at 1×1 mm^2 pixel size. The average of

20 pixel values was taken as the reading. The W for KCl:Eu^{2+} was obtained by solving equation 6.6,

$$\frac{PSL_{KCl}}{PSL_{Fuji}} = \frac{M_{KCl}\,(\Delta x)^2\,D_{KCl}/W_{KCl}}{M_{Fuji}\,(\Delta x)^2\,D_{Fuji}/W_{Fuji}} \tag{6.6}$$

where PSL_{KCl} and PSL_{Fuji} are the collected PSL signals, proportional to the number of PSL photons produced through irradiation of the two plates; M is the coating thickness of the plates, in mg/cm^2; $(\Delta x)^2$ is the pixel size, which was the same for both plates; D is the dose delivered to the material (cGy); and W is the generation efficiency (eV/$h\nu$). According to simulations, in a 1 cGy/MU dose-to-water irradiation at 10×10 cm^2 and 5 cm depth, D_{KCl} was approximately 0.9 cGy/MU for a 150 mm thick film and D_{Fuji} was 1.08 cGy/MU. W for the prototype film dosimeter was determined to be 157 eV, nearly the same as the commercial phosphor.

This number was then used to estimate the sensitivity of a micron-thick dosimeters in clinically relevant cases. The energy absorbed in the KCl layer is

$$E_{KCl} = D_{KCl} \cdot \rho \cdot (\Delta x)^2 \cdot d \tag{6.7}$$

where d is the dosimeter thickness and ρ the density. The number of photoelectrons generated at the PMT photocathode can be estimated from

$$N = \frac{E_{KCl}}{W_{KCl}} \cdot \eta \cdot Q_E \tag{6.8}$$

where η is the light collection efficiency and Q_E the PMT quantum efficiency. Estimating the latter two parameters at 30% each, a 1 cGy dose-to-water irradiation for a 1 micron thick panel dosimeter and 0.5×0.5 mm^2 pixel size would nevertheless produce over 1.2×10^4 photoelectrons/pixel at the PMT photocathode for detection [121]. Thus the micron-scale panel dosimeter should have sufficient signal to be usable even to doses down to a few cGy.

In a thin KCl:Eu^{2+} panel, energy deposition is dominated by charged particle interactions. This fact raises a question about the quantum noise of the system. In an imaging system, variance in the number of photons per unit area in a detector gives rise to "quantum mottle," which contributes to noise in the reproduced image. Presumably, in a dosimetry system variance in charged particles per unit area would give rise to a similar quantum noise in the reproduced dose "image." Assume that a thin panel (i.e., thin compared to the range of charged particles crossing the cavity) is inserted into a water-like medium. Furthermore, suppose charged particle equilibrium (CPE) exists and that bremsstrahlung production can be ignored. Megavoltage x ray irradiation of the water medium will produce a statistically large number of electrons emitting a continuous distribution of starting energies. The dose to the KCl panel is

$$D_{KCl}\left(MeV/g\right) = \int_{T_0=0}^{T_{\max}} dT_0 \int_{T=0}^{T_0} \Phi'_e\left(T\right) \left(\frac{dT}{\rho dx}\right)_{col,KCl} dT \tag{6.9}$$

where the differential equilibrium electron fluence as a function of energy, Φ'_e, resulting from a charged particle of starting energy, T_0, is multiplied by the energy-dependent mass stopping power, $\left(\frac{dT}{\rho dx}\right)_{col,KCl}$, and integrated over energy, for all possible starting energies $0 \leqslant T_0 \leqslant T_{\max}$. As a further simplification, assume a monoenergetic electron spectrum at an energy of 0.44 MeV (i.e., the average energy of Compton scattered electrons from a 1 MeV photon). In this case,

$$\bar{D}_{KCl}\left(MeV/g\right) = \Phi_e \cdot \left({}_m\bar{S}^{KCl}\right)_{col} \tag{6.10}$$

where $\left({}_m\bar{S}^{KCl}\right)_{col}$ is the average mass collisional stopping power for KCl. $\left({}_m\bar{S}^{KCl}\right)_{col}$ at this energy is 1.6 (MeV cm^2/g) (calculated from equation (8.13), (8.20), and (8.21a) in [111]).

Thus, for a 1 cGy irradiation,

$$\begin{aligned} \Phi_e(\#/cm^2) &\approx \frac{0.01(Gy)}{1.602 \times 10^{-10}(Gy/MeV/g) \cdot 1.6(MeV \cdot cm^2/g)} \\ \Phi_e(\#/cm^2) &\approx 4 \times 10^7 \end{aligned} \tag{6.11}$$

Changing the pixel size to 0.5 × 0.5 mm^2 gives

$$\Phi^e(\#/mm^2) \approx 1 \times 10^5 \tag{6.12}$$

Assuming the particle fluence can be described by a Poisson distribution, the minimum quantum noise in the simplified system is 0.3%. That is, the variance due to fluctuation in the expected number of particles depositing energy per pixel is 0.3%, which represents the minimum noise attainable in this simplified example. Additionally variance due to x ray absorption will increase the measured variance in a detected signal.

Intuitively, in this analysis quantum noise decreases as dose is increased and decreases as pixel size is increased (e.g., 0.1% for 10 cGy or 0.16% at 1 mm^2 pixel size for 1 cGy). However, this analysis also suggests that increasing the average collisional mass stopping power, for example, by decreasing the average electron energy in the spectrum, would increase the quantum noise. This also makes sense as the number of particles required to deliver a certain average dose would decrease, contributing to pixel-to-pixel variance.

6.5 PVD Development

It is not possible to achieve films on the order of single microns with a tape casting method. For this purpose, a laboratory-scale physical vapor deposition (PVD) unit (Nano38, Kurt J. Lesker, Pittsburgh, PA) was accepted and commissioned during this study and used for prototype thin panel dosimeters. While there are many variables to control in PVD, it was not the purpose of this study to determine the influence of PVD parameters on film

microstructure. Rather, the purpose of this study was to demonstrate that PSL can be achieved from micron-scale panel dosimeters, as suggested by the calculations in section 6.4.

The PVD unit was used to deposit films of various thicknesses onto 1×3 in^2 borosilicate glass substrates, shown in figure 6.11. Mixed powders used as source materials were loaded into tungsten boats and the deposition chamber pumped to 10^{-6} torr. The sources were resistively heated in order to generate a vapor flux. Once the appropriate deposition rate was achieved (as measured by a crystal rate monitor), the source shutter was opened in order to allow deposition onto the substrate. Film thickness was estimated from the measured rate of deposition multiplied by the time of deposition. When the desired thickness was achieved the source shutter was closed and the deposition stopped.

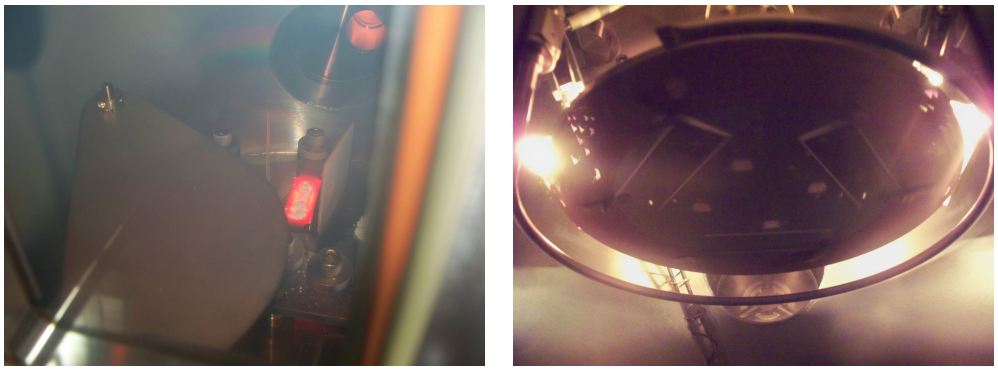

(a) KCl:Eu^{2+}during deposition. (b) Glass substrates during deposition.

Figure 6.11: Physical vapor deposition of KCl:Eu^{2+}. Raw KCl:Eu^{2+} materials are processed and placed into an evaporation chamber. After the chamber is pumped down to 10^{-6} torr, source charges are resistively heated to supply energy for evaporation onto glass substrates.

In preliminary investigations, PSL was achieved regularly in films less than 10 μm. The scanner system was then used to test the signal stability of thin panel dosimeters. A 1×3 in^2 dosimeter was mounted vertically on linear slides and the 2D scanner (cf. section **??**) programmed to take samples along the central line of the dosimeter at regular intervals. In this way, a single point on the dosimeter was read only once. Signal loss to neighboring pixels due to light scattering was determined to be minimal in this setup. A representative signal stability curve is shown in figure 6.12. It was hypothesized that the decrease in stability of

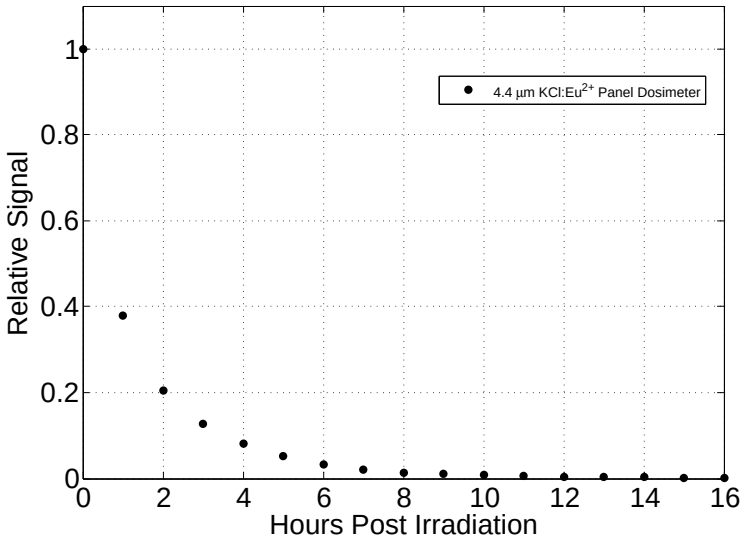

Figure 6.12: Signal stability for 4.4 μm PVD sample.

the thin films compared to the pellet samples is primarily do to KCl deliquescence. Future work will involve the investigation of protective coating technologies [77, 78] in order to mitigate the adverse effects of atmospheric moisture.

6.6 Conclusion

Water-equivalence is a desirable feature of dosimeters used in quantitative radiation therapy dosimetry. While KCl:Eu^{2+} has a lower effective atomic number than diagnostic CR materials, it is still larger than water. Due to the Z^3 dependence of the photoelectric mass attenuation coefficient, KCl:Eu^{2+} will over-respond compared to an ideal water-equivalent dosimeter. However, as suggested in this chapter, the effective atomic number alone does not determine the response of the dosimeter. It is possible to mitigate residual energy dependence by considering the mass collision stopping power ratio, mass energy-absorption coefficient ratio, and thickness in the design of the dosimeter. The simulation data [121] presented above suggest that a KCl:Eu^{2+} film on the order of 1 micron would provide

excellent agreement with water. The few photon interactions in the sensitive volume at this thickness combined with the weak dependence of mass collision stopping power on the secondary electron spectrum may explain the nearly water-equivalent response.

KCl:Eu^{2+} panel dosimeters can be fabricated by tape casting or PVD, however, only PVD is appropriate for films of micron-scale thickness. PVD is appropriate when sources of high crystal symmetry are used. KCl is of a class of compounds whose vapors consist of particles have stoichiometric composition [118]. Thus thin films may be obtained by direct vaporization of this compound. In this preliminary study, PSL was achieved from films less than 5 micron. According to calculations, a micron-scale panel will generate sufficient signal for dose measurements down to a few cGy, which is appropriate for radiation therapy applications. Future work involves the investigation of protective coating technologies to mitigate the adverse effects of atmospheric moisture and provide resistance to abrasion during handling.

Chapter 7

Conclusion

As the complexity of radiation therapy delivery increases, the need for novel devices to measure and monitor the radiation output of sources used in medicine also increases. Yet designing and developing a new dosimeter for radiation therapy is a challenging task, due in part to a unique combination of desirable features, such as water equivalence, high spatial resolution, capability of phantom integration, temporal stability, and reusability. The data presented here support the potential of KCl:Eu^{2+} to advance the state of the art in radiation therapy dosimetry.

KCl:Eu^{2+} dosimeters rely on a complex mechanism of photostimulated luminescence (PSL) to yield dose information. Prototype pellet-style dosimeters exhibited a supralinear response to dose after irradiation by a linear accelerator from 0 to 800 cGy. The dosimeters' signal stabilized to 0.1% signal decrease/h 12 hours after irradiation. There were no dependencies on nominal dose rate from 15-1000 cGy/min or nominal beam energy for 6 to 18 MV x rays or 6 to 20 MeV electrons in these prototype devices. The over-response to low-energy scattered photons was comparable to radiographic film and was reduced by sandwiching the dosimeters between 0.3 mm thick lead foils during irradiation.

The PSL process, however, is complex and can be influenced by materials processing parameters and radiation history. An initially supralinear dose response in KCl:Eu^{2+} became linear over the range of 100 to 700 cGy after cumulated doses of 60 Gy. Furthermore,

linearity did not change significantly in the 5000 Gy dose history spanned in this study. Sensitivity increased out to 3000 Gy history and then decreased to 90% of zero-dose history value at 5000 Gy. The PSL process was examined in detail and found to remain largely intact. The PSL stimulation curve peaked at 560 nm for fresh dosimeters and showed a slight red shift with dose history, possibly due to the creation of large aggregate trap centers. PSL emission remained peaked at 420 nm and agreed well with the photoluminescence (PL) emission spectrum of the europium activator in the material. Luminescence lifetime remained constant at 1.2 μs with dose. These results indicate that the PSL process of irradiation, energy storage, excitation, energy transfer, and excitation and relaxation of the activator remains stable with dose histories up to 5000 Gy and that the material could be reused up to 2500 times at 2 Gy per use, as in, for example, patient-specific quality assurance.

Although KCl:Eu^{2+} has a higher effective atomic number than water (Z=19 compared to 7.5), it was demonstrated from theory that reducing the thickness of KCl:Eu^{2+} maximizes the water-equivalence of the dose response. Monte Carlo (MC) simulations were performed using BEAMnrcMP and DOSXYZnrc for KCl:Eu^{2+} panels from 1 μm to 1 mm thick and the simulation data showed that micron-thick films had a water-equivalent response. It was suggested that the weak dependence of mass collision stopping power on the secondary electron spectrum can explain these results.

The generation efficiency, W, of prototype KCl:Eu^{2+} was used to estimate the sensitivity of micron-thick dosimeters and determined by comparing the sensitivity of a 150 μm thick KCl:Eu^{2+} two dimensional (2D) panel to a commercial $BaFBr_{0.85}I_{0.15}$:Eu^{2+}-based phosphor with a known W. W of KCl:Eu^{2+} was determined to be 157 eV/$h\nu$ and sub-millimeter spatial resolution was achieved for films 150 μm thick. It was determined that micron-scale films would generate over $10,000$ photoelectrons at the PMT photocathode for detection and amplification for delivered doses as low as a one cGy dose-to-water. In experiments, PSL was routinely achieved for thin vapor-deposited KCl:Eu^{2+} panels less than 10 μm.

As research into KCl:Eu^{2+} continues and technology advances, improvements on the

above data are certainly to be expected. One significant area to explore for commercial application of KCl:Eu^{2+} is moisture control and protection. The fabrication process used in this study could easily be incorporated into modern industrial clean room and protected atmosphere systems, which would minimize degradation of sensitive powders during processing. Dosimeters produced in such an environment could be further protected with modern, commercial-grade conformal coating technologies, such as the system developed by AGFA [78]. These changes could significantly reduce the adverse effects of ambient humidity on KCl:Eu^{2+} as well as provide some resistance to abrasion during handling. Furthermore, as processing techniques continue to improve, signal stability may also be optimized. Future pre-clinical studies can then confidently assess in detail other properties of this novel dosimetry material.

Appendix A

Laboratory Procedures

A.1 Standard Powder Production Process

NOTE: containers and equipment should be cleaned before and after use with soap and water. Allow the equipment to dry thoroughly.

1. KCl and europium precursor should be dried in laboratory oven at 125 °C for 24 hours before use.

2. Crush europium precursor with mortar and pestle and sieve to less than 25 micron.

3. Clean 50 mL agate mill jar and 8 large milling balls with water and ethanol. Pry up the Viton o-ring on the milling jar cap and clean with water and ethanol. Note that the Viton ring is sensitive to keytones. Allow the jar and lid to dry in laboratory oven for a few minutes. If the jar had just been used for milling, rinse with tap water thoroughly at least three times and then wipe with ethanol and allow to dry.

4. Weigh about 125-150% of the desired KCl amount (with clean weigh paper) and place in the 50 mL jar.

5. Mill the KCl at 450 rpm for 20 minutes.

6. In a clean 45 micron sieve and base, separate the particles larger than 45 micron and

place these in a clean, labeled container. Place the particles smaller than 45 micron in a separate container.

7. Calculate amount of europium precursor depending on mol % desired.
8. Weigh Eu precursor (less than 25 micron in size) and add it to the sieved KCl.
9. The mixture should be placed in a clean mill jar with two milling balls.
10. Set the ball miller to mix at 350 rpm for 20 minutes.
11. After mixing, remove the sample and place in labeled container.
12. Clean milling jar and lid.

A.2 Standard Pelleting Process

NOTE: Pressing die must be clean before use. When handling hot materials use the oven mitt, taking care not to contaminate the samples. Using this procedure, powdered materials can be used several weeks to make pellets, without regard to process tube cleanliness.

1. Heat powdered material in lab furnace to 350 °C for two hours prior to use (i.e., ramp from 25 to 350 °C in 0.5 hours, then sit at 350 °C for 2 hours)
2. Store heated powder at 100-125 °C in a lab oven during pressing. Store heated powder under high vacuum (e.g., 10^{-7} torr) when not in use.
3. Using oven mitts when necessary, weigh 0.05 g of KCl:Eu^{3+}. Place the powder back in the oven using oven mitt.
4. Put the weighed mixture in the pressing die with the bottom anvil in place.
5. Tap the die several times on the counter, trying to level the powder in the die.
6. Put the top anvil in the die hole and press down firmly.
7. Hook the pellet die to a vacuum line and pump down for a few seconds.

8. *Slowly* press to 1 metric T (=2200 lbs force) and let material rest for 3 minutes.

9. *Slowly* release the pressure release valve—releasing the value too fast will lead to rapid expansion and cracking of pellets.

10. Extract the sample from the die and place in a labeled container.

11. Wipe the anvils with either ethanol or isopropanol and remove large pieces of KCl. If there is residual KCl, use water and then isopropanol and allow to dry. Clean the pressing die sleeve with a tube brush and ethanol or isopropanol and inspect for residual KCl. Allow the sleeve to dry in the laboratory oven.

Appendix B

^{137}Cs Irradiator Isodose Plot

The following isodose plot was obtained from the user's manual for the ^{137}Cs irradiator (J. L. Shepherd and Associates, Mark I Model 25, San Fernando, CA). KCl:Eu^{2+} dosimeters were placed near the center of the irradiation chamber and rotated to mitigate any inverse square dependence on delivered dose.

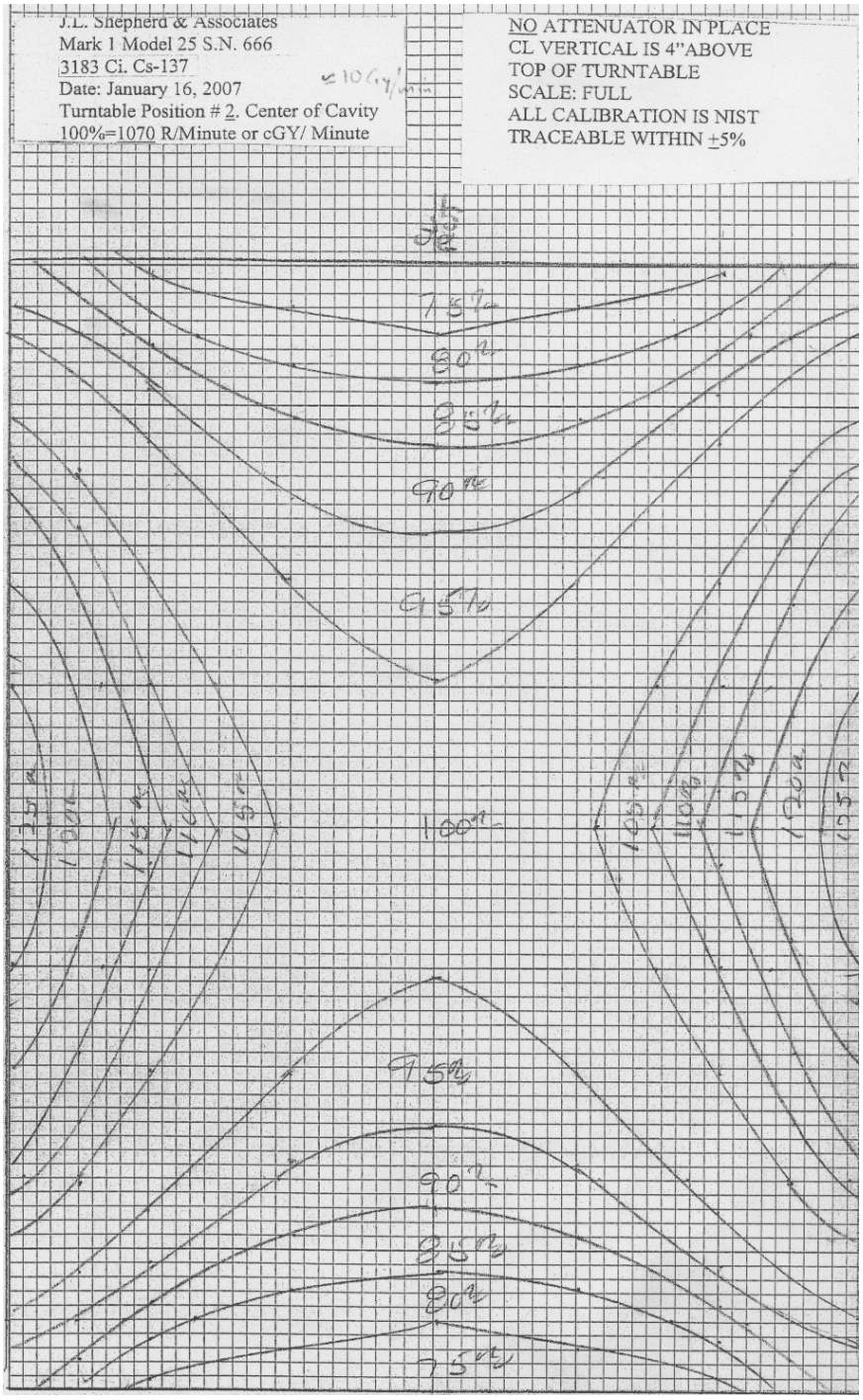
J.L. Shepherd & Associates
Mark 1 Model 25 S.N. 666
3183 Ci. Cs-137
Date: January 16, 2007
Turntable Position # 2. Center of Cavity
100%=1070 R/Minute or cGY/ Minute
NO ATTENUATOR IN PLACE
CL VERTICAL IS 4"ABOVE
TOP OF TURNTABLE
SCALE: FULL
ALL CALIBRATION IS NIST
TRACEABLE WITHIN ±5%

Bibliography

[1] G. A. Ezzell, J. M. Galvin, D. Low, J. R. Palta, I. Rosen, M. B. Sharpe, P. Xia, Y. Xiao, L. Xing, and C. X. Yu, "Guidance document on delivery, treatment planning, and clinical implementation of IMRT: report of the IMRT subcommittee of the AAPM radiation therapy committee," *Medical Physics*, vol. 30, no. 8, pp. 2089–2115, 2003.

[2] J. M. Galvin, G. Ezzell, A. Eisbrauch, C. Yu, B. Butler, Y. Xiao, I. Rosen, J. Rosenman, M. Sharpe, L. Xing, P. Xia, T. Lomax, D. A. Low, and J. Palta, "Implimenting IMRT in clinical practice: a joint docment of the American Society for Therapeutic Radiology and Oncology and the American Association of Physicists in Medicine," *International Journal of Radiation Oncology, Biology, and Physics*, vol. 58, no. 5, pp. 1616–1634, 2004.

[3] R. Nath, P. J. Biggs, F. J. Bova, C. C. Ling, J. A. Purdy, J. van de Geijn, and M. S. Weinhous, "AAPM code of practice for radiotherapy accelerators," *Medical Physics*, vol. 21, no. 7, 1994.

[4] A. J. Olch, "Evaluation of a computed radiography system for megavoltage photon beam dosimetry," *Medical Physics*, vol. 32, no. 9, pp. 2987–2999, 2005.

[5] K. Takahashi, K. Kohda, and J. Miyahara, "Mechanism of photostimulated luminescence in BaFX:Eu^{2+} (X=Cl, Br) phosphors," *Journal of Luminescence*, vol. 31-32, no. 1, pp. 266–268, 1984.

[6] J. A. Seibert, T. M. Bogucki, T. Ciona, W. Huda, A. Karellas, J. R. Mercier, E. Samei, S. J. Shephard, B. K. Stewart, K. J. Strauss, O. H. Suleiman, D. Tucker, R. A. Uzenoff, J. C. Weiser, and C. E. Willis, "Acceptance testing and quality control of photostimulable storage phosphor imaging systems: Report of AAPM task group 10," tech. rep., American Association of Physicists in Medicine, 2006.

[7] J. A. Rowlands, "The physics of computed radiography," *Physics in Medicine and Biology*, vol. 47, pp. R123–R166, 2002.

[8] H. von Seggern, "X-ray storage phosphors: a review of present understanding," *Brazilian Journal of Physics*, vol. 29, no. 2, pp. 254–268, 1999.

[9] H. von Seggern, "X-ray storage phosphors: physical mechanisms and applications," *Crystal Lattice Defects and Amorphous Materials*, vol. 18, pp. 399–417, 1989.

[10] H. von Seggern, "X-ray imaging with photostimulable phosphors," *Nuclear Instruments & Methods in Physics Research A*, vol. 322, no. 3, pp. 467–471, 1992.

[11] K. Takahashi and J. Miyahara, "Photostimulated luminescence (PSL) and color centers in BaFX:Eu^{2+} (X=Cl, Br, I) phosphors," *Journal of the Electrochemical Society*, vol. 132, no. 6, pp. 1492–1494, 1985.

[12] H. Nanto, K. Murayama, T. Usuda, F. Endo, Y. Hirai, S. Taniguchi, and N. Takeuchi, "Laser-stimulable transparent KCl:Eu crystals for erasable and rewritable optical memory utilizing photostumulated luminescence," *Journal of Applied Physics*, vol. 74, no. 2, pp. 1445–1447, 1993.

[13] Z. Han, J. P. Driewer, Y. Zheng, D. A. Low, and H. H. Li, "Quantitative radiation therapy dosimetry with the storage phosphor KCl:Eu^{2+}," *Medical Physics*, vol. 36, no. 8, pp. 3748–3757, 2009.

[14] K. Takahashi, "Progress in science and technology on photostimulable BaFX:Eu^{2+} (X=Cl, Br, I) and imaging plates," *Journal of Luminescence*, vol. 100, pp. 307–315, 2002.

[15] M. Sonoda, M. Takano, J. Miyahara, and H. Kato, "Computed radiography utilizing scanning laser stimulated luminescence," *Radiology*, vol. 148, no. 3, pp. 833–838, 1983.

[16] H. H. Li, E. Epelbaum, M. Batentschuk, and A. Winnacker, "Tape casting of storage phosphor BaFBr:Eu^{2+} for x-ray imaging," *Materials Science and Engineering B*, vol. 96, no. 3, pp. 313–319, 2002.

[17] M. Thoms, "The quantum efficiency of radiographic imaging with image plates," *Nuclear Instruments and Methods in Physics Research A*, vol. 378, pp. 598–611, 1996.

[18] Y. Iwabuchi, C. Umemoto, K. Takahashi, and S. Shionoya, "Photostumulated luminescence process in BaFBr:Eu^{2+} containing F(Br^-) and F(F^-) centers," *Journal of Luminescence*, vol. 48-49, pp. 481–484, 1991.

[19] Y. Iwabuchi, N. Mori, K. Takahashi, T. Matsuda, and S. Shionoya, "Mechanism of photostimulated luminescence process in BaFBr:Eu^{2+} phosphors," *Japanese Journal of Applied Physics*, vol. 33, no. 1A, pp. 178–185, 1994.

[20] H. Li, P. Hackenschmied, E. Epelbaum, and M. Batentschuk, "Imaging performance of polycrystalline BaFBr:Eu^{2+} storage phosphor plates," *Materials Science and Engineering B*, vol. 94, pp. 32–39, 2002.

[21] M. Thoms, D. Myles, and C. Wilkinson, "Neutron detection with imaging plates part I: Image storage and readout," *Nuclear Instruments and Methods in Physics Research A*, vol. 424, pp. 26–33, 1999.

[22] S. Schweizer, "Physics and current understanding of x-ray storage phosphors," *Physica status solidi (a)*, vol. 187, no. 2, pp. 335–393, 2001.

[23] S. Kanekal, A. Sahai, R. E. Jones, and D. Brown, "Storage-phosphor autoradiography: a rapid and highly sensitive method for spatial imaging and quantitation of radioisotopes," *Journal of Pharmacological and Toxicological Methods*, vol. 33, pp. 171–178, 1995.

[24] M. D. Story, E. . A. Mendoza, R. . E. Meyn, and P. J. Tofilon, "Pulsed-field gel electrophoretic analysis of DNA double-strand breaks in mammalian cells using photostimulable storage pulsed-field gel electrophoretic analysis of DNA double-strand breaks in mammalian cells using photostimulable storage phosphor imaging," *International Journal of Radiation Biology*, vol. 65, no. 5, pp. 523–528, 1994.

[25] A. L. Gonzalez, H. Li, M. Mitch, N. Tolk, and D. M. Duggan, "Energy response of an imaging plate exposed to standard beta sources," *Applied Radiation and Isotopes*, vol. 57, pp. 875–882, 2002.

[26] Y. Amemiya and J. Miyahara, "Imaging plate illuminates many fields," *Nature*, vol. 336, pp. 89–90, 1988.

[27] Y. Hayakawa, Y. Amemiya, J. Tada, K. Hosono, and T. Arimoto, "Application of an imaging plate to dose distribution measurement of proton beam," *Nuclear Instruments and Methods in Physics Research A*, vol. 378, pp. 627–628, 1996.

[28] M. Thoms, M. S. Lehmann, and C. Wilkinson, "The optimization of the neutron sensitivity of image plates," *Nuclear Instruments and Methods in Physics Research A*, vol. 384, pp. 457–462, 1997.

[29] M. Thoms, "Neutron detection with imaging plates part II: Detector characteristics," *Nuclear Instruments and Methods in Physics Research A*, vol. 424, pp. 34–39, 1999.

[30] H. Ohuchi, T. Satoh, Y. Eguchi, and K. Mori, "Preliminary study of using imaging plates to map skin dose of patients in interventional radiology procedures," *Radiation Protection Dosimetry*, vol. 117, no. 4, pp. 432–439, 2005.

[31] H. Ohuchi, A. Yamadera, and M. Baba, "Development of a new passive integral dosemeter [*sic*] for gamma ray monitoring using an imaging plate," *Radiation Protection Dosimetry*, vol. 107, no. 4, pp. 239–246, 2003.

[32] E. Ariga, S. Ito, S. Deji, T. Saze, and K. Nishizawa, "Development of dosimetry using detectors of diagnostic digital radiography systems," *Medical Physics*, vol. 34, no. 1, pp. 166–174, 2007.

[33] P. Leblans, L. Struye, and P. Willems, "New needle-crystalline CR detector," *Proceedings of SPIE: Medical Imaging 2001*, vol. 4320, pp. 59–67, 2001.

[34] B. Schmitt, M. Fuchs, E. Hell, W. Knüpfer, P. Hackenschmied, and A. Winnacker, "Structured alkali halides for medical applications," *Nuclear Instruments and Methods in Physics Research B*, vol. 191, pp. 800–804, 2002.

[35] R. Fasbender and R. Schaetzing, "Neue CR-technologien für die digitale radiographie," *Radiologe*, vol. 43, no. 5, pp. 367–373, 2003.

[36] P. Hackenschmied, *Funktion und Herstellung von Speicherleuchtstoffen für die digitale Röntgendiagnostik*. PhD thesis, Universität Erlangen-Nürnberg, 2002.

[37] P. Hackenschmied, G. Zeitler, M. Batentschuk, A. Winnacker, B. Schmitt, M. Fuchs, E. Hell, and W. Knüpfer, "Storage performance of x-ray irradiated doped CsBr," *Nuclear Instruments and Methods in Physics Research B*, vol. 191, pp. 163–167, 2002.

[38] P. Hackenschmied, G. Schierning, M. Batentschuk, and A. Winnacker, "Precipitation-induced photostimulated luminescence in CsBr:Eu^{2+}," *Journal of Applied Physics*, vol. 93, no. 1, pp. 5109–5112, 2003.

[39] J. Zimmermann, S. Hesse, H. von Seggern, M. Fuchs, and W. Knüpfer, "Influence of Li-codoping on the radiation hardness of CsBr:Eu^{2+}," *Journal of Applied Physics*, vol. 101, pp. 113711–7, 2007.

[40] S. Hesse, J. Zimmermann, H. von Seggern, H. Ehrenberg, and H. Fuess, "The role of segregations and oxygen doping in the photostimulation mechanism of CsBr:Eu^{2+}," *Radiation Measurements*, vol. 42, pp. 638–643, 2007.

[41] S. Hesse, J. Zimmermann, H. von Seggern, X. Meng, C. Fasel, and R. Riedel, "Synthesis and functionality of the storage phosphor BaFBr:Eu^{2+}," *Journal of Applied Physics*, vol. 105, p. 063505, 2009.

[42] S. Wirth, M. Treitl, M. F. Feiser, and M. Körner, "Imaging performance with different doses in skeletal radiography: comparison of a needle-structured and a conventional storage phosphor system with a flat-panel detector," *Radiology*, vol. 250, no. 1, pp. 152–160, 2009.

[43] Z. Wang, Q. J. Wu, and C. H. Sibata, "Megavoltage radiation dose response of digital computed radiography," *Proceedings of SPIE*, vol. 4320, pp. 236–243, 2001.

[44] H. H. Li, A. L. Gonzalez, H. Ji, and D. M. Duggan, "Dose response of BaFBrI:Eu^{2+} storage phosphor plates exposed to megavoltage photon beams," *Medical Physics*, vol. 34, no. 1, pp. 103–111, 2007.

[45] H. Nanto, F. Endo, Y. Hirai, S. Nasu, and N. Takeuchi, "Eu-doped KCl storage phosphor for erasable and rewritable optical memory utilizing photostimulated luminescence phenomenon," *Optical Review*, vol. 1, no. 2, pp. 177–179, 1994.

[46] H. Nanto, F. Endo, Y. Hirai, and S. Nasu, "Eu-doped KCl phosphor crystals as a storage material for two-dimensional ultraviolet-ray or x-ray imaging sensors," *Journal of Applied Physics*, vol. 75, no. 11, pp. 7493–7497, 1994.

[47] J. A. Hernandez, F. J. Lopez, H. S. Murrieta, and J. O. Rubio, "Optical absorption, emission, and excitation spectra of Eu^{2+} in the alkali halides," *Journal of the Physical Society of Japan*, vol. 50, no. 1, pp. 225–229, 1981.

[48] H. Nanto, M. Miyazaki, A. Imai, H. Komori, Y. Douguchi, E. Kusano, and A. Kinbara, "New photostimulable phosphor materials for digital radiography," *IEEE Transactions on Nuclear Science*, vol. 47, no. 4, pp. 1620–1624, 2000.

[49] M. Schlapp, M. Hoelzel, R. Gilles, A. Ioffe, T. Brueckel, H. Fuess, and H. von Seggern, "Novel type of neutron image plates based on KCl:Eu^{2+}-LiF," *Physica B*, vol. 350, pp. e861–e864, 2004.

[50] R. Aceves, R. P. Salas, and M. Barboza-Flores, "The role of F centres [*sic*] in the thermoluminescence of low-energy UV- and X-irradiated KCl:Eu^{2+}," *Journal of Physics: Condensed Matter*, vol. 6, no. 10, pp. 10397–10405, 1994.

[51] R. Meléndrez, R. P. Salas, L. P. Pashchenko, R. Aceves, T. M. Piters, and M. Barboza-Flores, "Dosimetric properties of KCl:Eu^{2+} under α, β, γ, x ray, and ultraviolet irradiation," *Applied Physics Letters*, vol. 68, no. 24, pp. 3398–3400, 1996.

[52] L. P. Pashchenko, R. P. Salas, R. Aceves, and M. Barboza-Flores, "Fading and self-irradiation of potassium halide thermoluminescent dosimeters," *Applied Physics Letters*, vol. 66, no. 23, pp. 3126–3127, 1995.

[53] R. Aceves, J. M. Gracia-Jiménez, R. Silva-González, and C. T.-M. noz, "Thermal and photo stimulated luminescence of F-center aggregates in electron and x-ray irradiated KCl:Eu^{2+} polycrystalline films," *Physica status solidi (c)*, vol. 4, no. 3, pp. 1159–1162, 2007.

[54] A. R. Lakshmanan, "Radiation induced defects and photostimulated luminescence process in BaFBr:Eu^{2+}," *Physica status solidi (a)*, vol. 153, no. 1, pp. 1–27, 1996.

[55] C. Kittel, *Introduction to solid state physics*. John Wiley & Sons, Inc., 8th ed., 2005.

[56] M. Thoms, H. von Seggern, and A. Winnacker, "Spatial correlation and photostimulability of defect centers in the x-ray-storage phosphor BaFBr:Eu^{2+}," *Physical Review B*, vol. 44, no. 17, pp. 9240–9247, 1991.

[57] H. von Seggern, T. Voigt, W. Knüpfer, and G. Lange, "Physical model of photostimulated luminescence of x-ray irradiated BaFBr:Eu^{2+}," *Journal of Applied Physics*, vol. 64, no. 3, pp. 1405–1412, 1988.

[58] H. H. Rüter, H. von Seggern, R. Reininger, and V. Saile, "Creation of photostimulable centers in BaFBr:Eu^{2+} single crystals by vacuum-ultraviolet radiation," *Physical Review Letters*, vol. 65, no. 19, pp. 2439–2441, 1990.

[59] N. Itoh, "Creation of lattice defects by electronic excitation in alkali halides," *Advances in Physics*, vol. 5, no. 491-551, 31.

[60] T. Hangleiter, F. K. Koschnick, J.-M. Spaeth, R. H. D. Nuttall, and R. S. Eachus, "Temperature dependence of the photostimulated luminescence of x-irradiated BaFBr:Eu^{2+}," *Journal of Physics: Condensed Matter*, vol. 2, pp. 6837–6846, 1990.

[61] F. K. Koschnick, J.-M. Spaeth, R. S. Eachus, W. G. McDugle, and R. H. D. Nuttall, "Experimental evidence for the aggregation of photostimulable centers in BaFBr:Eu^{2+} single crystals by cross relaxation spectroscopy," *Physical Review Letters*, vol. 67, no. 25, pp. 3571–3574, 1991.

[62] W. Chen and M. Su, "Process of photoluminescence and photostimulated luminescence in BaFBrEu^{2+} phosphors," *Journal of Materials Science and Technology*, vol. 11, no. 5, pp. 388–390, 1995.

[63] A. Harrison, M. T. Harrison, G. P. Keogh, R. H. Templer, and A. S. Wills, "Trapped charge migration in BaFBr:Eu^{2+}: The recuperation of photostimulated luminescence," *Physical Review B*, vol. 53, no. 9, pp. 5039–5042, 1996.

[64] J. Zimmermann, *Untersuchungen zur Strahlenstabilität des Rötgenspeicherleuchtstoffes CsBr:Eu^{2+}*. PhD thesis, Universität Darmstadt, 2005.

[65] Y. Vassilev, M. Karamikhailova, M. Mladenova, and M. Georgiev, "Room temperature investigation of the photostimulated afterglow in KCl:Eu^{2+} crystals," *Physica status solidi (b)*, vol. 100, pp. 463–471, 1980.

[66] E. G. Yukihara and S. W. S. McKeever, "Optically stimulated luminescence (OSL) dosimetry in medicine," *Physics in Medicine and Biology*, vol. 53, pp. R351–R379, 2008.

[67] S. Hesse, J. Zimmermann, H. von Seggern, H. Ehrenberg, H. Fuess, C. Fasel, and R. Riedel, "$CsEuBr_3$: crystal structure and its role in the photostimulation of CsBr:Eu^{2+}," *Journal of Applied Physics*, vol. 100, p. 083506, 2006.

[68] G. A. Appleby, J. Zimmermann, S. Hesse, O. Karg, and H. von Seggern, "Sensitization of the photostimulable x-ray storage-phosphor CsBr:Eu^{2+} following room-temperature hydration," *Journal of Applied Physics*, vol. 105, no. 7, p. 073511, 2009.

[69] P. A. Jursinic, "Characterization of optically stimulated luminescent dosimeters, OSLDs, for clinical dosimetric measurements," *Medical Physics*, vol. 12, no. 4594-4604, 34.

[70] C. S. Reft, R. Runkel-Muller, and L. Myrianthopoulos, "In vivo and phantom measurements of the secondary photon and neutron doses for prostate patients undergoing 18 MV IMRT," *Medical Physics*, vol. 33, no. 10, pp. 3734–3742, 2006.

[71] P. A. Jursinic, "Changes in optically stimulated luminescent dosimeter (OSLD) dosimetric characteristics with accumulated dose," *Medical Physics*, vol. 37, no. 1, pp. 132–140, 2010.

[72] J. Zimmermann, S. Hesse, H. von Seggern, M. Fuchs, and W. Knüpfer, "Radiation hardness of CsBr:Eu^{2+}," *Journal of Luminescence*, vol. 114, pp. 24–30, 2005.

[73] V. P. Savel'ev, V. P. Avdonin, L. D. Dugarova, A. P. Nedashkovskii, and B. T. Plachenov, "Aggregation of Eu^{2+}-V_c^- centers in europium-activated alkali halide crystals," *Soviet Physics: Solid State*, vol. 16, no. 4, pp. 700–702, 1974.

[74] S. Schweizer, U. Rogulis, S. Assmann, and J.-M. Spaeth, "RbBr and CsBr doped with Eu^{2+} as new competitive x-ray storage phosphors," *Radiation Measurements*, vol. 33, pp. 483–486, 2001.

[75] H. Ohuchi and A. Yamadera, "Development of a functional equation to correct fading in imaging plates," *Radiation Measurements*, vol. 35, pp. 135–142, 2002.

[76] Y. Douguchi, H. Nanto, T. Sato, A. Imai, S. Nasu, E. Kusano, and A. Kinbara, "Optically stimulated luminescence in Eu-doped KBr phosphor ceramics," *Radiation Protection Dosimetry*, vol. 84, no. 1-4, pp. 143–148, 1999.

[77] M. Nakazawa, O. Morikawa, M. Nitta, H. Tsuchino, and F. Shimada, "Effect of protective layer on resolution properties of photostimulable phosphor detector for digital radiographic system," *Proceedings of SPIE*, vol. 1231, pp. 350–363, 1990.

[78] P. Leblans, R. V. den Bergh, L. Joly, and L. Struye, "A phosphor panel with good humidity resistance," *European Patent Specification*, no. EP 1 286 364 B1, 2008.

[79] E. Spezi, A. L. Angelini, F. Romani, and A. Ferri, "Characterization of a 2D ion chamber array for the verification of radiotherapy treatments," *Physics in Medicine and Biology*, vol. 50, pp. 3361–3373, 2005.

[80] B. Poppe, A. Blechschmidt, R. Kallhoff, A. Rubach, K. C. Willborn, and D. Harder, "Two-dimensional ionization chamber arrays for IMRT plan verification," *Medical Physics*, vol. 33, no. 4, pp. 1005–1015, 2006.

[81] B. Poppe, A. Djouguela, A. Blechschmidt, K. Willborn, A. Rühmann, and D. Harder, "Spatial resolution of 2D ionization chamber arrays for IMRT dose verification: single-detector size and sampling step width," *Physics in Medicine and Biology*, vol. 52, pp. 2921–2935, 2007.

[82] J. Herzen, M. Todorovic, F. Cremers, V. Platz, D. Albers, A. Bartels, and R. Schmidt, "Dosimetric evaluation of a 2D pixel ionization chamber for implementation in clinical routine," *Physics in Medicine and Biology*, vol. 52, pp. 1197–1208, 2007.

[83] A. V. Esch, C. Clermont, M. Devillers, M. Iori, and D. P. Huyskens, "On-line quality assurance of rotational radiotherapy threatment delivery by means of a 2D ion chamber array and the Octavius phantom," *Medical Physics*, vol. 34, no. 10, pp. 3825–3837, 2007.

[84] S. Devic, M. R. McEwen, and C. G. Orton, "Point/counterpoint: radiochromic film is superior to ion chamber arrays for IMRT quality assurance," *Medical Physics*, vol. 37, no. 3, pp. 959–961, 2010.

[85] J. Esthappan, S. Mutic, W. B. Harms, and J. F. Dempsey, "Dosimetry of therapeutic photon beams using an extended dose range film," *Medical Physics*, vol. 29, no. 10, pp. 2338–2345, 2002.

[86] X. R. Zhu, P. A. Jursinic, D. F. Grimm, F. Lopez, J. J. Rownd, and M. T. Gillin, "Evaluation of Kodak EDR2 film for dose verification of intensity modulated radiation therapy delivered by a static multileaf collimator," *Medical Physics*, vol. 29, no. 8, pp. 1687–1692, 2002.

[87] A. J. Olch, "Dosimetric performance of an enhanced dose range radiographic film for intensity-modulated radiation therapy quality assurance," *Medical Physics*, vol. 29, no. 9, pp. 2159–2169, 2002.

[88] C. Martens, I. Claeys, C. D. Wagter, and W. D. Neve, "The value of radiographic film for the characterization of intensity-modulated beams," *Physics in Medicine and Biology*, vol. 47, pp. 2221–2234, 2002.

[89] I. J. Chetty and P. M. Charland, "Investigation of Kodak extended dose range (EDR) film for megavoltage photon beam dosimetry," *Physics in Medicine and Biology*, no. 3629-3641, 47.

[90] N. Dogan, L. B. Leybovich, and A. Sethi, "Comparative evaluation of Kodak EDR2 and XV2 films for verification of intensity modulated radiation therapy," *Physics in Medicine and Biology*, vol. 47, pp. 4121–4130, 2002.

[91] P. M. Charland, I. J. Chetty, S. Yokoyama, and B. A. Fraass, "Dosimetric comparison of extended dose range film with ionization measurements in water and lung equivalent heterogeneous media exposed to megavoltage photons," *Journal of Applied Clinical Medical Physics*, vol. 4, no. 1, pp. 25–39, 2003.

[92] N. L. Childress, M. Salehpour, L. Dong, C. Bloch, R. A. White, and I. I. Rosen, "Dosimetric accuracy of Kodak EDR2 film for IMRT verifications," *Medical Physics*, vol. 32, no. 2, pp. 539–548, 2005.

[93] S. Pai, I. J. Das, J. F. Dempsey, K. L. Lam, T. J. LoSasso, A. J. Olch, J. R. Palta, L. E. Reinstein, D. Ritt, and E. E. Wilcox, "TG-69: radiographic film for megavoltage beam dosimetry," *Medical Physics*, vol. 34, no. 6, pp. 2228–2258, 2007.

[94] I. J. Yeo, A. Beiki-Ardakani, Y. bin Cho, M. Heydarian, T. Zhang, and M. Islam, "EDR2 film dosimetry for IMRT verification using low-energy photon filters," *Medical Physics*, vol. 31, no. 7, pp. 1960–1963, 2004.

[95] A. Niroomand-Rad, C. R. Blackwell, B. M. Coursey, K. P. Gall, J. M. Galvin, W. L. McLaughlin, A. S. Meigooni, R. Nath, J. E. Rogers, and C. G. Soares, "Radiochromic film dosimetry: recommendations of AAPM radiation therapy committee task group 55," *Medical Physics*, vol. 25, no. 11, pp. 2093–2115, 1998.

[96] C. Fiandra, U. Ricardi, R. Ragona, S. Anglesio, F. R. Giglioli, E. Calamia, and G. Lucio, "Clinical use of EBT model Gafchromic^{TM} film in radiotherapy," *Medical Physics*, vol. 33, no. 11, pp. 4314–4319, 2006.

[97] C. G. Soares, "New development in radiochromic film dosimetry," *Radiation Protection Dosimetry*, vol. 120, no. 1-4, pp. 100–106, 2006.

[98] C. G. Soares, "Radiochromic film dosimetry," *Radiation Measurements*, vol. 41, pp. S100–S116, 2007.

[99] J. F. Dempsey, D. A. Low, S. Mutic, J. Markman, A. S. Kirov, G. H. Nussbaum, and J. F. Williamson, "Validation of a precision radiochromic film dosimetry system for quantitative two-dimensional imaging of acute exposure dose distributions," *Medical Physics*, vol. 27, no. 10, pp. 2462–2474, 2000.

[100] O. A. Zeidan, S. A. L. Stephenson, S. L. Meeks, T. H. Wagner, T. R. Willoughby, P. A. Kupelian, and K. M. Langen, "Characterization and use of EBT radiochromic film for IMRT dose verification," *Medical Physics*, vol. 33, no. 11, pp. 4064–4072, 2006.

[101] B. Hartmann, M. Martišíková, and O. Jäkel, "Technical note: Homogeneity of Gafchromic® EBT2," *Medical Physics*, vol. 37, no. 4, pp. 1753–1756, 2010.

[102] W. van Elmpt, L. McDermott, S. Nijsten, M. Wendling, P. Lambin, and B. Mijnheer, "A literature review of electronic portal imaging for radiotherapy dosimetry," *Radiotherapy and Oncology*, vol. 88, pp. 289–309, 2008.

[103] K. L. Pasma, M. L. P. Dirkx, M. Kroonwijk, A. G. Visser, and B. J. M. Heijmen, "Dosimetric verification of intensity modulated beams produced with dynamic multileaf collimation using an electronic portal imaging device," *Medical Physics*, vol. 26, no. 11, pp. 2373–2378, 1999.

[104] L. N. McDermott, M. Wendling, B. van Asselen, J. Stroom, J.-J. Sonke, M. van Herk, and B. J. Mijnheer, "Clinical experience with EPID dosimetry for prostate IMRT pretreatment dose verification," *Medical Physics*, vol. 33, no. 10, pp. 3921–3930, 2006.

[105] L. E. Antonuk, "Electronic portal imaging devices: a review and historical perspective of contemporary technologies and research," *Physics in Medicine and Biology*, vol. 47, pp. R31–R65, 2002.

[106] A. V. Esch, T. Depuydt, and D. P. Huyskens, "The use of an aSi-based EPID for routine absolute dosimetric pre-treatment verification of dynamic IMRT fields," *Radiotherapy and Oncology*, vol. 71, pp. 223–234, 2004.

[107] L. J. Schreiner, "Review of Fricke gel dosimeters," *Journal of Physics: Conference Series*, vol. 3, pp. 9–21, 2004.

[108] C. Baldock, Y. D. Deene, S. Doran, G. Ibbott, A. Jirasek, M. Lepage, K. B. McAuley, M. Oldham, and L. J. Schreiner, "Polymer gel dosimetry," *Physics in Medicine and Biology*, vol. 55, pp. R1–R63, 2010.

[109] P. Y. Guo, J. A. Adamovics, and M. Oldham, "Characterization of a new radiochromic three-dimensional dosimeter," *Medical Physics*, vol. 33, no. 5, pp. 1338–1345, 2006.

[110] H. S. Sakhalkar, J. Adamovics, G. Ibbott, and M. Oldham, "A comprehensive evaluation of the PRESAGE/optical-CT 3D dosimetry system," *Medical Physics*, vol. 36, no. 1, pp. 71–82, 2008.

[111] F. H. Attix, *Introduction to radiological physics and radiation dosimetry*. Wiley-VCH, reprint ed., 2004.

[112] C. S. Reft, "The energy dependence and dose response of a commercial optically stimulated luminescent detector for kilovoltage photon, megavoltage photon, and electron, proton, and carbon beams," *Medical Physics*, vol. 36, no. 5, pp. 1690–1699, 2009.

[113] A. Viamonte, L. A. R. da Rosa, L. A. Buckley, A. Cherpak, and J. E. Cygler, "Radiotherapy dosimetry using a commercial OSL system," *Medical Physics*, vol. 35, no. 4, pp. 1261–1266, 2008.

[114] L. Bøtter-Jensen, S. W. S. McKeever, and A. G. Wintle, *Optically stimulated luminescence dosimetry*. Elsevier, 2003.

[115] V. Schembri and B. J. M. Heijmen, "Optically stimulated luminescence (OSL) of carbon-doped aluminum oxide (Al_2O_3:C) for film dosimetry in radiotherapy," *Medical Physics*, vol. 34, no. 6, pp. 2113–2118, 2007.

[116] W. D. Callister, *Materials science and engineering: an introduction*. John Wiley & Sons, Inc., 6th ed., 2003.

[117] R. E. Mistler, *Tape casting: theory and practice*. Wiley-American, 2000.

[118] J. E. Mahan, *Physical vapor deposition of thin films*. John Wiley & Sons, Inc., 2000.

[119] P. R. Almond, P. J. Biggs, B. M. Coursey, W. F. Hanson, M. S. Huq, R. Nath, and D. W. O. Rogers, "AAPM's TG-51 protocol for clinical reference dosimetry of high-energy photon and electron beams," *Medical Physics*, vol. 26, no. 9, pp. 1847–1870, 1999.

[120] J. R. Taylor, *An introduction to error analysis: the study of uncertainties in physical measurements*. University Science Books, 1982.

[121] Y. Zheng, Z. Han, J. P. Driewer, D. A. Low, and H. H. Li, "Theoretical and empirical investigations of KCl:Eu^{2+} for nearly water-equivalent radiotherapy dosimetry," *Medical Physics*, vol. 37, no. 1, pp. 146–153, 2010.

[122] J. H. Hubbell and S. M. Seltzer, "Tables of x-ray mass attenuation coefficients and mass energy-absorption coefficients," Tech. Rep. NISTIR 5632, National Institute of Standards and Technology, April 2009.

VITA

Joe Driewer grew up in western Nebraska and attended Sidney High School, graduating in 1995. His parents modeled a love for learning and raised him to find everything interesting. Consequently, in college and graduate school, he made an effort to explore a multitude of topics, along the way picking up a bachelor of science degree from Washington University (St. Louis, MO), a bachelor of arts from Hastings College (Hastings, NE), a master of divinity from Covenant Theological Seminary (St. Louis, MO), and a master of science from the University of Missouri, Columbia. During his time at Covenant Seminary, he met his bride, Nicole. They married in 2002. Together they have four intelligent and creative daughters: Margaret, Isabelle, Lucille, and Lydia.